DEVELOPMENT OF INORGANIC POLYPHOSPHATE-BASED NANOPARTICLES FOR DRUG DELIVERY INTO ARTICULAR CARTILAGE

by

Jordan Nhan

Thesis submitted in partial fulfillment of the requirements for the degree of

Master of Applied Science in Chemical Engineering

Department of Chemical and Biological Engineering

Faculty of Engineering

University of Ottawa

ABSTRACT

Osteoarthritis is a degenerative joint disease which affects the entire joint; however, one of its hallmarks is the progressive degeneration of the articular cartilage layer. Patients suffering from osteoarthritis exhibit chronic pain, stiffness, and a decreased range of motion, greatly affecting their quality of life. No drugs have been approved to stop the progression of osteoarthritis and focus solely on the management of symptoms. This is partly due to the challenges in delivering drugs to afflicted joints, and specifically to cartilage due to its lack of vasculature. While intra-articular injection holds promise for the local administration of drugs, small molecules are rapidly cleared from the synovial fluid. As a result, there is a need to develop effective drug delivery strategies to improve residence times in the joint to elicit a sustained therapeutic effect. Previous studies identified polyphosphate as a pro-anabolic molecule, promoting glycosaminoglycan and collagen accumulation in cartilage constructs. Therefore, polyphosphate may be a therapeutic of interest to address the degeneration of articular cartilage in patients suffering from osteoarthritis. In this study, calcium-polyphosphate and strontium-polyphosphate particles were synthesized and characterized as a potential drug carrier into articular cartilage. Physicochemical characterization revealed that the particles exhibit a spherical morphology, have a negative zeta potential, and are nanoscale in size. Biological characterization in chondrocytes confirmed cellular uptake of the particles and demonstrated a size and concentration-dependent cytotoxicity at high concentrations. Furthermore, treatment of chondrocytes with these particles resulted in a reduction in metabolic activity and cell proliferation, confirming biological effects. Preliminary studies using cartilage explants suggest that the particles can penetrate and be retained in cartilage tissue. Therefore, from the results obtained within this study, the polyphosphate-based particles may be a potential drug delivery strategy for delivery into articular cartilage.

RÉSUMÉ

L'arthrose est une maladie articulaire dégénérative qui touche l'ensemble de l'articulation, caractérisée principalement par la détérioration progressive de la couche de cartilage articulaire. Les patients souffrant d'arthrose présentent des douleurs chroniques, des raideurs articulaires et une diminution de l'amplitude de leurs mouvements, affectant considérablement leur qualité de vie. Aucun médicament n'a été approuvé pour arrêter la progression de l'arthrose et la gestion des symptômes. Cela est causé en partie par les difficultés rencontrées durant l'administration des médicaments aux articulations touchées, plus particulièrement aux tissus cartilagineux, en raison de l'absence de vascularisation. Alors que l'injection intra-articulaire est prometteuse pour une administration locale de traitement, les molécules thérapeutiques sont toutefois rapidement éliminées du liquide synovial. En conséquence, il est nécessaire de développer des stratégies efficaces pour l'administration de ces médicaments question d'améliorer les temps de rétention dans l'articulation pour un effet thérapeutique soutenu. Des études antérieures ont identifié le polyphosphate comme une molécule pro-anabolique favorisant l'accumulation de glycosaminoglycane et de collagène dans les constructions cartilagineuses. Par conséquent, le polyphosphate peut être une thérapie d'intérêt pour traiter la dégénérescence du cartilage articulaire. Dans le cadre de cette étude, des particules de polyphosphate de calcium et de polyphosphate de strontium ont été synthétisées et caractérisées comme transporteurs potentiels de médicament dans le cartilage articulaire. La caractérisation physicochimique de ces particules a révélé une morphologie sphérique, un potentiel zêta négatif et une taille de ces particules à l'échelle du nanomètre. La caractérisation biologique dans les chondrocytes a confirmé l'absorption cellulaire des particules et a su démontrer une cytotoxicité dépendante de leur taille et de leur concentration, et ce, lorsqu'administrés à des concentrations élevées. De plus, le traitement

des chondrocytes avec ces particules a entraîné une réduction de l'activité métabolique et de la prolifération cellulaire, confirmant les effets biologiques désirés. Des études préliminaires utilisant des explants de cartilage suggèrent que les particules peuvent pénétrer et être retenues dans le tissu cartilagineux. Par conséquent, d'après les résultats obtenus en accord avec l'étude présente, les particules à base de polyphosphate pourraient constituer une stratégie potentielle d'administration de médicament dans le cartilage articulaire.

ACKNOWLEDGEMENTS

I would like to express my deepest gratitude to my supervisor, Dr. Jean-Philippe St-Pierre, for his unwavering support throughout the entirety of my thesis project. I have learned so much from his expertise and guidance and I am very fortunate to have been given so many opportunities to grow and develop my skills during my studies. He has been instrumental in the completion of this thesis, and I cannot thank him enough for everything that he has done for me. I truly could not have asked for a better thesis supervisor.

I am sincerely thankful to my fellow colleagues in the St-Pierre Lab for all their support. To all the past and present labmates (Janani Mahendran, Denis Viera Rey, Dayna Zunder, Abrie Girgis, Noor Ghadie, Sietske Barnes, Luisa Metzler, Michael Mulholland, Rayehe Ghofrani, and Wendy Wu) – it has always been a pleasure to work in such a collaborative environment with all of you. I would like to extend my appreciation to my students, Khushnouma Virah Sawmy, Nicolas Strebel, and Jordan Yin, who have all been of great assistance in completing this project, as well as to Hannah Prazak for her assistance on a collaborative project with the NRC. I would also like to thank Dr. Xudong Cao for graciously sharing his laboratory space and equipment with us. I would like to thank Dr. David Taylor, Dr. Andrew Sowinski, and Dr. Clémence Fauteux-Lefebvre for being wonderful supervisors during my teaching assistantships under them – I am grateful for their trust and support. Lastly, I would like to thank all my previous research supervisors (Dr. Marc Ekker, Dr. John Pezacki, and Dr. Xudong Cao) for giving me the wonderful opportunities to work in their labs and gain an introduction to research during my undergraduate studies, as well as my past student mentors (Megan Jung, Tyler Shaw, Shuying Li, and Denis Viera Rey) for all the lab techniques and research skills that they have taught me. I would not be as passionate and driven towards research without their guidance.

TABLE OF CONTENTS

LIST OF TABLES

LIST OF FIGURES

LIST OF ABBREVIATIONS

AC	articular cartilage
ACI	autologous chondrocyte implantation
ADAMTS	a disintegrin and metalloproteinase with thrombospondin motifs
AFM	atomic force microscopy
ANOVA	analysis of variance
ATP	adenosine triphosphate
ATR	attenuated total reflectance
BSA	bovine serum albumin
calcein-AM	calcein acetoxymethyl ester
COX-2	cyclooxygenase-2
CTAB	cetyltrimethylammonium bromide
CuAAC	copper (I)-catalyzed azide-alkyne cycloaddition
DAPI	4’,6-diamidino-2-phenylindole
diH_2O	deionized water
DLS	dynamic light scattering
DLVO	Derjaguin-Landau-Verwey-Overbeek
DMEM	Dulbecco’s modified Eagle’s medium
DMMB	1,9-dimethylmethylene blue
DMOAD	disease-modifying osteoarthritis drug
DMSO	dimethyl sulfoxide
DNA	deoxyribonucleic acid
dsDNA	double stranded deoxyribonucleic acid
ECM	extracellular matrix
EDAC	1-ethyl-3-(3-dimethylaminopropyl)carbodiimide
EDTA	ethylenediaminetetraacetic acid
EdU	5-ethynyl-2’-deoxyuridine
EDX	energy dispersive x-ray spectroscopy
EthD-1	ethidium homodimer-1
FBS	fetal bovine serum

FGF18	fibroblast growth factor 18
FTIR	Fourier-transform infrared
GAG	glycosaminoglycan
GFP	green fluorescent protein
HBSS	Hanks' balanced salt solution
IGF-1	insulin-like growth factor 1
IL-1	interleukin-1
IL-1α	interleukin-1α
IL-1β	interleukin-1β
IL-1R	interleukin-1 receptor
IL-6	interleukin-6
LRP1	low density lipoprotein receptor-related protein 1
MACI	matrix-induced autologous chondrocyte implantation
MMP	matrix metalloproteinase
MTT	3-(4,5-dimethylthiazol-2-yl)-2,5-diphenyltetrazolium bromide
MW	molecular weight
NF-κB	nuclear factor-κB
NMR	nuclear magnetic resonance
NSAID	nonsteroidal anti-inflammatory drug
OA	osteoarthritis
PAMAM	polyamidoamine
PBAE	poly(β-amino ester)
PBS	phosphate buffered saline
PCLA	poly(ε-caprolactone-co-lactide)
PDI	polydispersity index
PEG	poly(ethylene glycol)
PEI	polyethyleneimine
pHEMA	poly(2-hydroxyethyl methacrylate)
PLGA	poly(lactic-co-glycolic acid)
polyP	polyphosphate

PSD	particle size distribution
SEM	scanning electron microscopy
sGAG	sulfated glycosaminoglycan
TEM	transmission electron microscopy
TGFβ	transforming growth factor-β
TNF	tumour necrosis factor
Tukey's HSD	Tukey's honestly significant difference
XRD	X-ray diffraction

STATEMENT OF CONTRIBUTION

The overall conception and design of the project was performed by Dr. Jean-Philippe St-Pierre, and the design of the experiments presented within this thesis was performed by Dr. Jean-Philippe St-Pierre and Jordan Nhan. Preliminary work was performed by Janani Mahendran, Justin Quan, Eran Ittah, and Abrie Girgis.

All experiments presented within this thesis were performed by or were conducted under the direct supervision of Jordan Nhan. Khushnouma Virah Sawmy assisted in the synthesis of the nanoparticles and optimization of the synthesis protocol. Khushnouma Virah Sawmy, Jordan Yin, and Nicolas Strebel assisted in the physical characterization of the nanoparticles and evaluation of cationic surface coatings. SEM imaging and EDX analysis of nanoparticle samples was performed by Dr. Jianqun Wang (Nano Imaging Facility, Carleton University). Raman spectroscopy was performed by Michael Mulholland. Nicolas Strebel assisted in the live-dead, MTT, DNA, and EdU cell proliferation assays. Cartilage tissue explants utilized in the tissue penetration and retention experiments were dissected by Dr. Jean-Philippe St-Pierre. Data analysis was performed by Jordan Nhan.

This thesis was written by Jordan Nhan. Nicolas Strebel and Danielle Abdul Nour assisted in the translation of the abstract to French. Nicolas Strebel assisted in the literature review process and editing. Dr. Jean-Philippe St-Pierre greatly contributed towards the editing of the thesis.

CHAPTER 1: INTRODUCTION

1.1 Purpose and Objectives

Articular cartilage (AC) is the connective tissue responsible for the transmission of mechanical forces and allows for smooth articulation of the joint. As AC has poor regenerative capabilities, this makes clinical interventions necessary upon damage or disease. For example, osteoarthritis (OA) is a degenerative joint disease affecting almost 5 million Canadians, and while the disease affects the entire joint, one of its hallmarks is the progressive degeneration of AC. Patients suffering from OA experience chronic pain, stiffness, and a decreased range of motion, which can greatly affect their quality of life. Currently, no therapies have been approved to stop or reverse the progression of OA, with current strategies focusing solely on the management of symptoms. While surgical interventions exist, these typically provide limited and temporary relief, and a total joint replacement may ultimately be required once the disease has progressed towards its end-stage. The lack of effective drug therapies is in part due to the many challenges in the delivery of drugs to afflicted joints, and specifically to articular cartilage due to its lack of vasculature. While intra-articular injection can be effective for the local administration of drugs, small molecules are rapidly cleared from the synovial fluid, often in a matter of hours to days. This scale of joint residence time is at odds with the timeframe for disease progression of years to decades. Therefore, there is a need to develop disease-modifying OA drugs which can stop or reverse the progression of OA, that can also be sufficiently maintained in the joint at therapeutic concentrations to exert both a positive and sustained effect. This may be achieved by nanoparticle-based carriers, which are small enough in size to penetrate into the cartilage tissue to effectively deliver the drug, while also being shielded from clearance. Previous studies identified polyphosphate (polyP) as a pro-

anabolic molecule, promoting extracellular matrix accumulation in chondrocytes. Therefore, polyP may be of interest as a potential therapeutic molecule to reverse the degeneration of AC in patients suffering from OA.

In this study, calcium-polyphosphate (Ca-polyP) and strontium-polyphosphate (Sr-polyP) particles were synthesized and characterized as a potential drug delivery strategy to help carry and retain polyP into AC. This thesis will discuss work related to five main objectives:

1. Synthesis and physicochemical characterization of polyphosphate-based particles
2. Determination of the effects of environmental factors on particles
3. Identification of cationic surface coatings to induce a positive surface charge
4. Biological characterization of interactions between the particles and chondrocytes, as well as cartilage tissue explants
5. Evaluation of polyphosphate-based particles for cartilage tissue engineering

1.2 Organization of Thesis

This thesis is divided into six chapters. *Chapter 2* will provide a review of the relevant literature pertaining to drug delivery strategies into the joint. *Chapter 3* highlights all the relevant methods utilized within the project. *Chapter 4* presents all the results obtained within this study, followed by a discussion with comparisons to previous studies. *Chapter 5* provides the key conclusions obtained from the study and discusses both ongoing and potential future directions for the improvement and continuation of this project. Finally, *Chapter 6* briefly highlights additional work performed in collaboration with other groups during the completion of this thesis.

CHAPTER 2: LITERATURE REVIEW

2.1 Articular Cartilage

Articular cartilage (AC) is the connective tissue that covers the articulating ends of bones. It is responsible for the transmission of mechanical loads, and provides a smooth, lubricated surface to facilitate movement of the joint. Importantly, AC is an aneural and avascular tissue, and processes such as nutrient uptake and communication with other tissues through signaling molecules would rely on diffusion but may also facilitated by compressive forces that act on AC [1].

2.1.1 Composition

AC is comprised of a dense extracellular matrix (ECM) composed primarily of both collagens and proteoglycans, in addition to non-collagen proteins and water. Chondrocytes are the resident cell type in AC, and account for about 1 – 5% of the volume of AC depending on age and location [2]. The primary function of chondrocytes is in the maintenance of cartilage tissue, through synthesis and remodelling of the ECM to withstand the mechanical forces exerted on the tissue, as well as to adapt to changing demands of the tissue [3].

Collagen accounts for approximately 60 – 70% of the dry weight of AC. Collagen type II, IX, and XI are cartilage-specific [4], with type II being the most abundant in AC, constituting about 90 – 95% of the collagens in the ECM [1]. In addition, numerous other minor collagens are also present in healthy AC, including types III, IV, V, VI, IX, X, XI, XII, XIII, XIV, XVI, XXII, and XXVII [1,5–8]. Collagen type II self-assembles into crosslinked, fibrillar networks which provides the framework of the ECM and endows the tissue a high tensile strength [9].

Proteoglycans account for approximately 30% of the dry weight of AC. Aggrecan is the predominant proteoglycan in AC, occurring as proteoglycan aggregates within the interfibrillar space of the ECM, where numerous aggrecan molecules interact directly with a central hyaluronic acid via a link protein. The core protein of aggrecan is decorated with many glycosaminoglycan (GAG) chains, including keratin sulfate and chondroitin sulfate [10]. These GAGs are negatively charged, which provides AC with a highly fixed negative charge. Of importance, GAGs induce a large osmotic swelling pressure due to the abundance of cations such as Na^+, which balance the negative charge of GAGs. As these proteoglycan aggregates are embedded within the matrix, this causes water to be drawn into the tissue, resulting in swelling which contributes to its high resistance to compressive loads [11]. Meanwhile, the collagen networks counteract this swelling effect through elastic forces [12]. As a result, cartilage tissue has a high water content with the fluid phase accounting for about 80% of the total wet weight [1].

2.1.2 Zonal Organization

AC is an anisotropic tissue consisting of a depth-dependent, zonal architecture that may be divided into four main zones – the superficial zone, mid zone, deep zone, and the zone of calcified cartilage. The collagen fibre orientation varies in each zone and contributes to the mechanical properties required for the function of cartilage tissue. In the superficial zone, the fibers are aligned parallel to the surface which enhances its resistance to shear stress, while the fibers are oriented more randomly in the mid zone and perpendicular to the tissue surface in the deep zone, which allows for the tissue to withstand compressive forces [13,14]. Additionally, proteoglycan content increases at greater depths, however due to an increase in collagen fibre thickness at greater depths, this also leads to lower water content [1].

Chondrocytes also exhibit different depth-dependent phenotypes [15]. In the superficial zone, chondrocytes are elongated, oriented parallel to the surface, and are most densely populated. These cells produce lubricin, a proteoglycan which aids in lubrication and contributes to smooth articulation at the surface [16]. Meanwhile, the mid zone cells are spherical and more sparsely populated. Both the superficial and mid zone chondrocytes are responsible for synthesizing ECM [17]. Lastly, deep zone chondrocytes typically exist in clusters, forming columns perpendicular to the surface and parallel to the collagen fibre orientation. These chondrocytes are terminally differentiated, actively synthesizing collagen X and play a role in modulating calcification of cartilage at the interface with subchondral bone [17,18].

2.1.3 Extracellular Matrix Metabolism

Chondrocytes are presented with numerous challenges related to ECM synthesis and deposition. As AC lacks vasculature, this creates an environment with reduced access to nutrients and oxygen required for metabolic processes. Furthermore, the low cellularity of the tissue limits the amount of ECM that may be synthesized in a tissue. In fact, the half-life of GAGs can be over 2 years [19], while proteoglycan turnover may take up to 25 years [20]. Meanwhile the half-life of collagen type II is estimated to be between 100 – 400 years [20]. Therefore, chondrocytes must be able to maintain a fine balance of both anabolic and catabolic processes for supporting the long-term integrity of cartilage tissue.

2.2 Osteoarthritis

Osteoarthritis (OA) is a degenerative joint disease that involves changes in AC, the subchondral bone, synovial capsule, synovium, ligaments, and periarticular muscles, and is estimated to affect

250 million people worldwide [21]. While OA afflicts all tissues of the joint, one of the major hallmarks of OA is the progressive degeneration of AC, causing patients suffering from OA to experience chronic pain, stiffness, and a decreased range of motion, which can greatly affect their quality of life. The most prominent risk factors include age and obesity, but may involve a combination of factors including sex, genetics, and joint trauma [21]. Therefore, OA is considered to be both a multi-factorial and heterogeneous disease, with multiple underlying issues capable of leading to degeneration of the overall joint (Figure 2.1). The pathogenesis of OA has been revealed to be very complex, and consequently, early events of OA have yet to be well established fully, resulting in difficulties in early detection and interventions at points where disease progression may potentially be stopped or even reversed.

2.2.1 Dysregulated Metabolism in Articular Cartilage

Early observations of OA-afflicted AC include fibrillation of the superficial zone, swelling, and thickening of cartilage tissue [22]. Pathological signals from aging, inflammation, or trauma, result in an altered chondrocyte phenotype, whereby they form clusters of cells through proliferation and become hypertrophic. This negatively alters the amount and composition of ECM synthesized, resulting in ECM of poorer quality. In OA, proteoglycan content is markedly reduced through catabolic enzymatic activity, resulting in a decrease in the compressive strength of cartilage tissue, which alters the mechanical cues experienced by chondrocytes [23,24]. Furthermore, denaturation and loss of collagen type II is also observed in OA. In an attempt to repair the cartilage tissue, both proteoglycan and collagen synthesis is upregulated by chondrocytes in early stages of OA, but these new ECM components fail to appropriately repair the tissue [25]. Furthermore, while collagen synthesis increases, the composition of collagen also differs. Collagen type II is the native

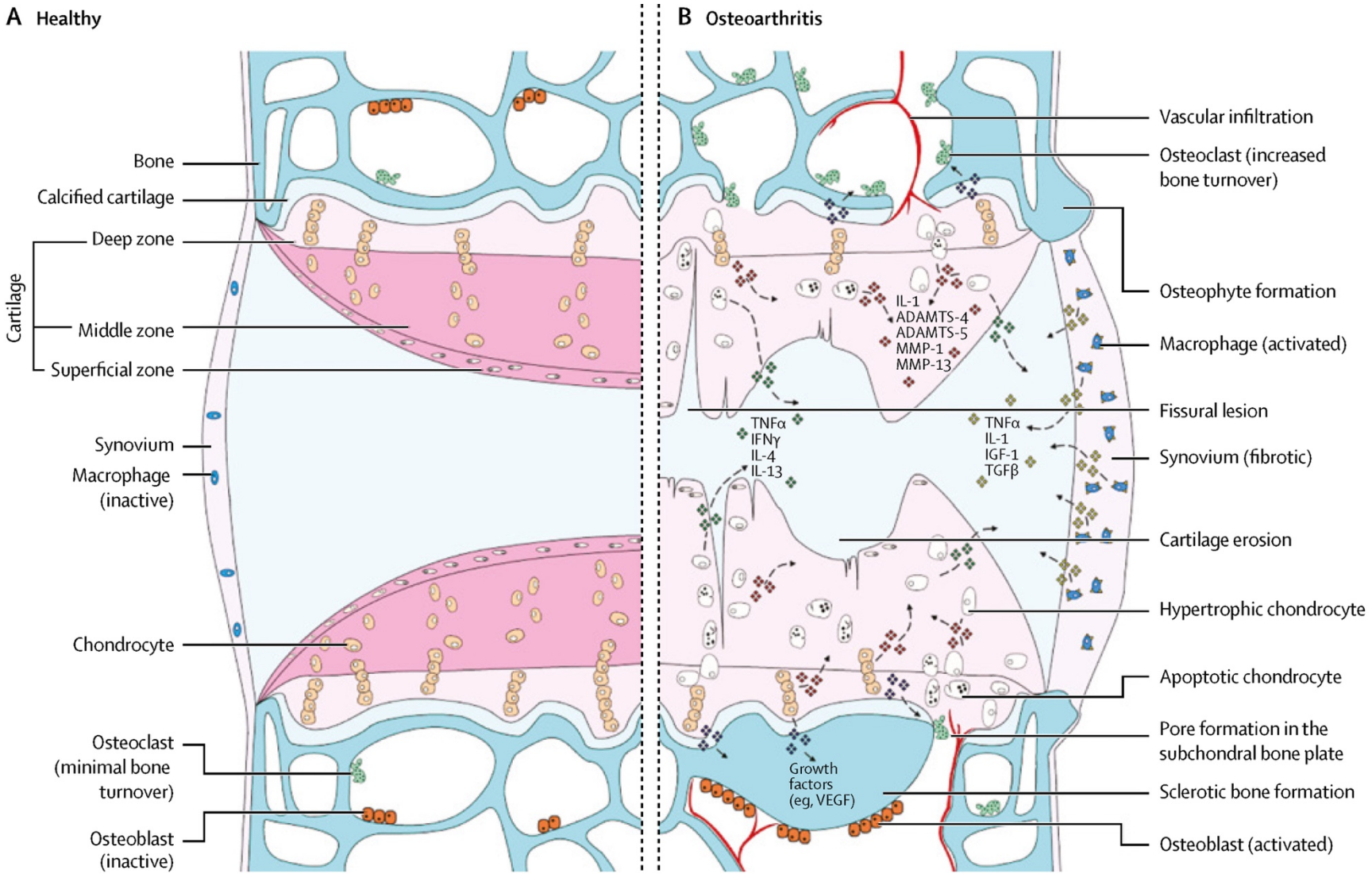

Figure 2.1 – Pathological changes in osteoarthritis. Dysregulation of biological pathways in osteoarthritis ultimately leads to structural changes of the joint, including the degeneration of cartilage, tissue hypertrophy, vascular invasion, and bone remodeling. Figure obtained from Hunter and Bierma-Zeinstra (2019) [21].

and major form of collagen in cartilage, but it becomes increasingly replaced with collagen type I, which is not normally present in healthy cartilage and is a factor associated with OA [26]. In fact, collagen type II contains higher levels of moieties that mediate interactions with proteoglycans, and the loss of collagen type II for type I disrupts the overall ECM network [23,24]. Along with the loss of proteoglycan content, these changes in the structure and composition of the ECM further facilitate degradation of the tissue due to a loss of mechanical integrity leading to an inability to properly sustain mechanical loads.

In addition to changes in anabolic processes, catabolic processes are also dysregulated in OA. The progression of OA can be linked to inflammation of the joint. Interleukin-1β (IL-1β) and tumour necrosis factor (TNF) are key proinflammatory cytokines involved in OA, with IL-1β being implicated in cartilage degradation and TNF driving the inflammatory response. Both of these cytokines are upregulated in OA, and result in the dysregulated expression and activity of matrix metalloproteinases (MMPs) and a disintegrin and metalloproteinase with thrombospondin motifs (ADAMTSs), which are proteases involved in the catabolism of ECM [27]. Major MMPs of interest include MMP-1, MMP-3, and MMP-13, however MMP-13 is the most highly expressed in OA and is primarily responsible for the degradation of the collagen networks, and in particular collagen type II [28]. Likewise, ADAMTS-4 and ADAMTS-5 are aggrecanases that are induced by these cytokines [27,29].

2.2.2 Surgical Treatments

Due to the avascular nature of AC, its self-repair properties are very poor. Superficial lesions, such as fibrillations of the superficial zone observed in OA, will not heal spontaneously and instead will become increasingly damaged over time [30]. However, spontaneous repair may occur if the lesion

reaches into the subchondral bone, a type of damage termed as a full-thickness defect, where bone marrow-derived cells are able to populate the defect and form a fibrocartilage clot [30]. While AC is a specialized form of hyaline cartilage enriched with collagen type II, fibrocartilage is composed primarily of collagen type I and has a lower proteoglycan content, making it both mechanically and functionally inferior. Current surgical strategies focus on repairing small defects to reduce further degeneration of the tissue (Figure 2.2, a). Due to these limitations, early interventions are required. However, once the disease progresses towards its end-stage, total joint replacement will ultimately be required for successful outcomes.

To induce spontaneous repair, the defect is debrided followed by the removal of the calcified cartilage tissue (Figure 2.2, b). Microfracture is then performed, in which perforations are created on the subchondral plate, leading to the formation of a blood clot inside the cartilage defect and enhancing the migration of mesenchymal stem cells from bone marrow to the site of injury (Figure 2.2, c) [31,32]. As discussed, this leads to the formation of mechanically inferior fibrocartilage. While good clinical outcomes are observed in the short term, treatment is expected to fail for many patients after 5 years post-operation [33].

Osteochondral autografts may also be performed, where osteochondral plugs are harvested from the low weight-bearing distal femur. Due to using mature tissues, these grafts are capable of bearing loads early in the postoperative stage, leading to faster recovery. However, with limited availability of graft sites, this option is reserved for very small defects [32]. Meanwhile, allografts can be of great interest, given that cartilage is considered to exhibit immune privilege due to its lack of vasculature. However, bone is also transferred which is not immune privileged, and issues with disease transmission may exist. Nonetheless, allografts circumvent the restrictions in using autologous tissue due to minimal donor tissue availability and would require only a single surgery

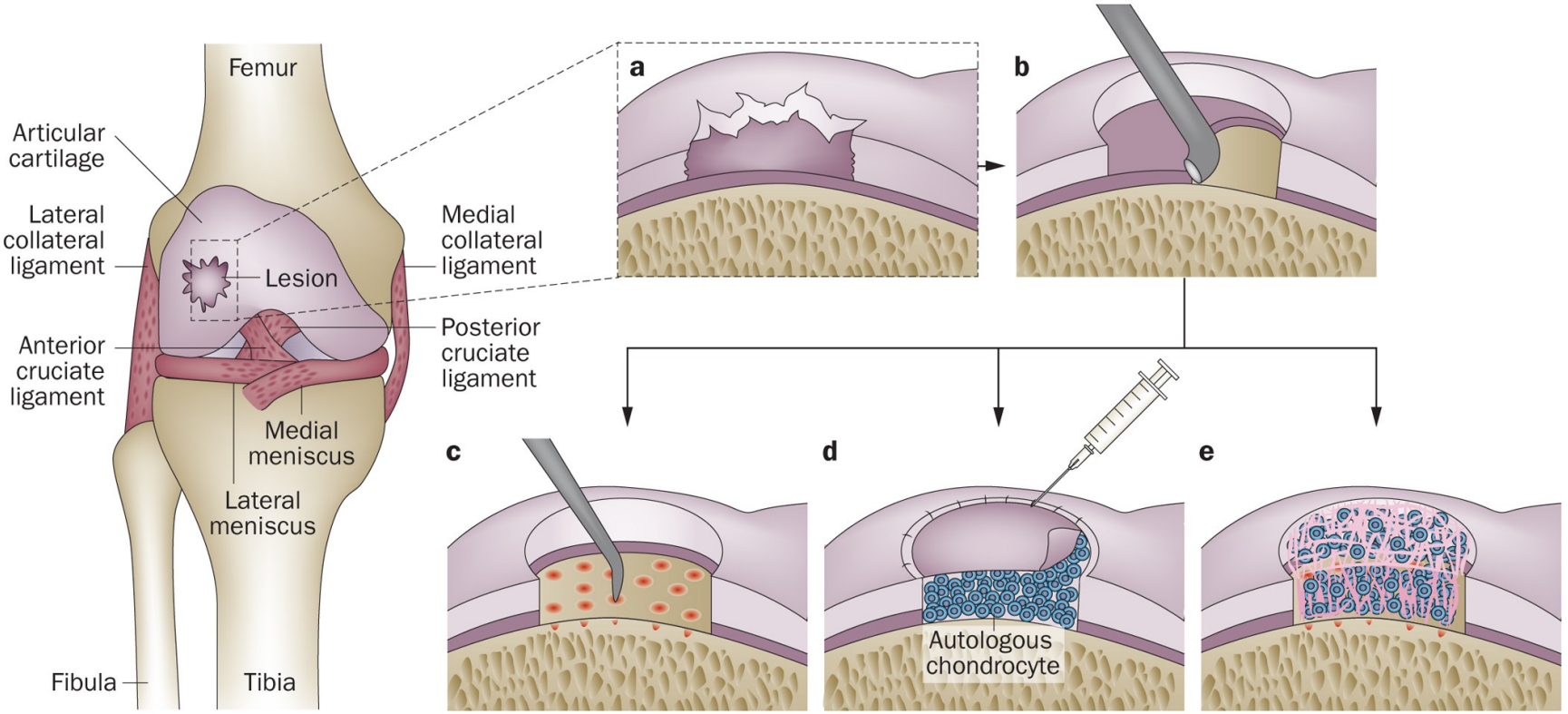

Figure 2.2 – Cartilage regeneration techniques. (A) Full thickness cartilage defects undergo **(B)** debridement to facilitate integration of new tissue. This may be followed by techniques including **(C)** microfracture, **(D)** autologous chondrocyte implantation, or **(E)** matrix-induced autologous chondrocyte implantation to repair the cartilage lesion. Figure obtained from Makris et al. (2014) [31].

[34]. Osteochondral autografts exhibited successful outcomes in 72% of patients after a mean follow-up of 10.2 years [35], while allografts similarly had a survival rate of about 79% at 10 years [36].

Tissue engineering strategies may also be applied for the repair of AC lesions. Autologous chondrocyte implantation (ACI) is a cell-based technique in which healthy chondrocytes from the patient are harvested from a low weight-bearing region of AC and propagated in vitro. These cells may then be reimplanted in the debrided lesion and covered by a membrane (Figure 2.2, d). ACI can be preferred to osteochondral autografts due to requiring less tissue from the donor site [31]. Similarly, matrix-induced autologous chondrocyte implantation (MACI) instead cultures the cells onto a collagen-based membrane which may then be implanted (Figure 2.2, e), offering benefits such as more ease of use, and reducing dedifferentiation of the chondrocytes due to 3D culture conditions [31]. However, both of these methods are quite costly due to the multi-step process, especially with laboratory cell culture requirements for chondrocyte propagation. Furthermore, the outcomes of ACI are comparable to microfracture for small defects, while MACI may be superior for larger defects [31].

2.2.3 Pharmacological Therapeutics

Ideally, OA could be treated prior to necessitating the use of invasive surgical treatments to induce tissue repair and ultimately avoid total joint replacement. However, there are currently no disease-modifying OA drugs (DMOADs) that have been approved for use in the clinic, and this is likely in part due to the complexities and multifactorial nature of OA, leading to an incomplete understanding of the pathogenesis of the disease. As a result, current pharmacological treatments focus solely on the management of symptoms to improve the quality of life, in particular by

reducing pain and inflammation of the joint. This is often achieved by analgesics such as acetaminophen (and rarely opioids such as tramadol), as well as nonsteroidal anti-inflammatory drugs (NSAIDs) including ibuprofen, naproxen, diclofenac, and celecoxib [37]. Duloxetine, a serotonin-norepinephrine reuptake inhibitor, is also used as a second-line treatment for pain relief in OA [38]. These pharmacological treatments are often administered along with conservative treatment recommendations, which may include weight loss and exercise regimens. Meanwhile, efforts are being made for the development of DMOADs, of which there are many potential targets, including cartilage metabolism, bone remodelling, and the synovial inflammation. Of particular interest is the inhibition of ECM proteases, such as MMP-13 and ADAMTS-5 via small-molecule inhibitors or neutralizing antibodies. Conversely, studies have also been performed to stimulate cartilage repair by delivery of fibroblast growth factor 18 (FGF18) and transforming growth factor-β (TGFβ) [38].

2.3 Drug Delivery Strategies

As AC is an avascular tissue, the systemic administration of drugs is ineffective for treatments that target specifically this tissue, as it relies solely on entry from the capillaries of the synovium into the joint. These capillaries are fenestrated, allowing small molecules to exit freely, but diffusion into the joint is mainly impeded by the ECM of the synovium. Meanwhile, the endothelial lining acts as a sieve, limiting the rate of passage for larger molecules [39]. Consequently, local administration of drugs into the joint would circumvent these mass transfer limitations and allow for an increase in bioavailability of the therapeutic. Of note, avoiding systemic exposure also reduces the possibility of off-target and adverse effects, as well as a decrease in total drug costs [39,40]. This may be accomplished by intra-articular injection into the joint, which is currently

used for the administration of therapies including corticosteroids, hyaluronic acid (also known as viscosupplementation), and platelet-rich plasma [41,42].

While intra-articular injection allows for efficient delivery of drugs in the joint, maintaining the drug at therapeutic concentrations to elicit a positive effect poses another challenge. Small molecules are rapidly cleared from the joint by synovial capillaries, while larger macromolecules are cleared by the lymphatic system [39]. In fact, the half-life of various drugs such as NSAIDs administered via intra-articular injection is around 1 – 5 hours [43]. Of course, this short duration is insufficient for the treatment of a chronic condition such as OA, which progresses over years to decades, likely requiring regular intra-articular injections for a prolonged effect, with implications for increased healthcare cost and resource utilization.

Furthermore, the dense ECM of AC, primarily composed of self-assembled networks of collagens and proteoglycans, acts as a physical barrier for the entry and diffusion of drugs into the tissue. In fact, the spacing between collagen fibrils is estimated to be between 60 – 200 nm [44–46]. These collagen networks entrap proteoglycan aggregates, adding to an already dense ECM arrangement. Within these proteoglycan aggregates, adjacent aggrecan proteins linked to hyaluronic acid are estimated to be 20 – 50 nm apart [44], while the chondroitin sulfate and keratin sulfate chains that are bound to aggrecan are only 2 – 4 nm in distance between each other [45,46]. These networks present substantial steric hindrance for the delivery of drug carriers targeting AC via penetration into the tissue, requiring them to be in the nano- or at least submicron range. However, due to the anisotropic zonal organization of AC, ensuring that these drug carriers may access the deeper zones of cartilage may be of great importance. As the density of GAGs increases throughout the depth of cartilage, this additionally reduces the pore size and permeability into the tissue [9,45], making drug delivery into the middle and deep zones, which contains a majority of

the overall chondrocyte population, a challenge. In addition, due to the high abundance of GAGs, cartilage tissue has a highly fixed negative charge, with an average fixed charged density of -170.0 mM [47]. This can act as an additional barrier of entry as a result of electrostatic repulsive forces, depending on the surface charge of the molecules or carriers.

As a result of the degeneration of AC as seen in OA, the permeability of drug carriers into cartilage tissue is increased due to an increase in the effective pore size, enabling faster uptake at higher concentrations (Figure 2.3) [48]. While these beneficial effects may be observed in moderate to severe cases of OA, this may not be exploited during the early stages of the disease where the structural integrity of the tissue has not yet been substantially compromised. Early interventions may be key in stopping or reversing disease progression, and therefore there is a need to develop drug delivery strategies that allow for effective and sustained delivery of therapeutics into affected cartilage tissue by taking into consideration as many of these barriers as possible. A variety of delivery platforms are currently being assessed for this application, including carrier molecules, hydrogels, microparticles, and nanoparticles.

2.3.1 Carrier Molecules

Carrier molecules, such as peptides, proteins, and polymers, may be utilized to facilitate the entry of drugs into cartilage tissue. These carriers are often covalently conjugated to a drug, forming a pro-drug, whereby cleavage of the bond releases the active molecule to exert a therapeutic effect. For example, the highly fixed negative charge of AC caused by its high GAG content may be exploited to facilitate penetration and retention of positively charged drug carriers within the tissue [45,47]. Cook Sangar et al. (2020) identified cystine-dense peptides that accumulate in cartilage tissue due to a positively charged surface. Conjugation of these peptides with the corticosteroid,

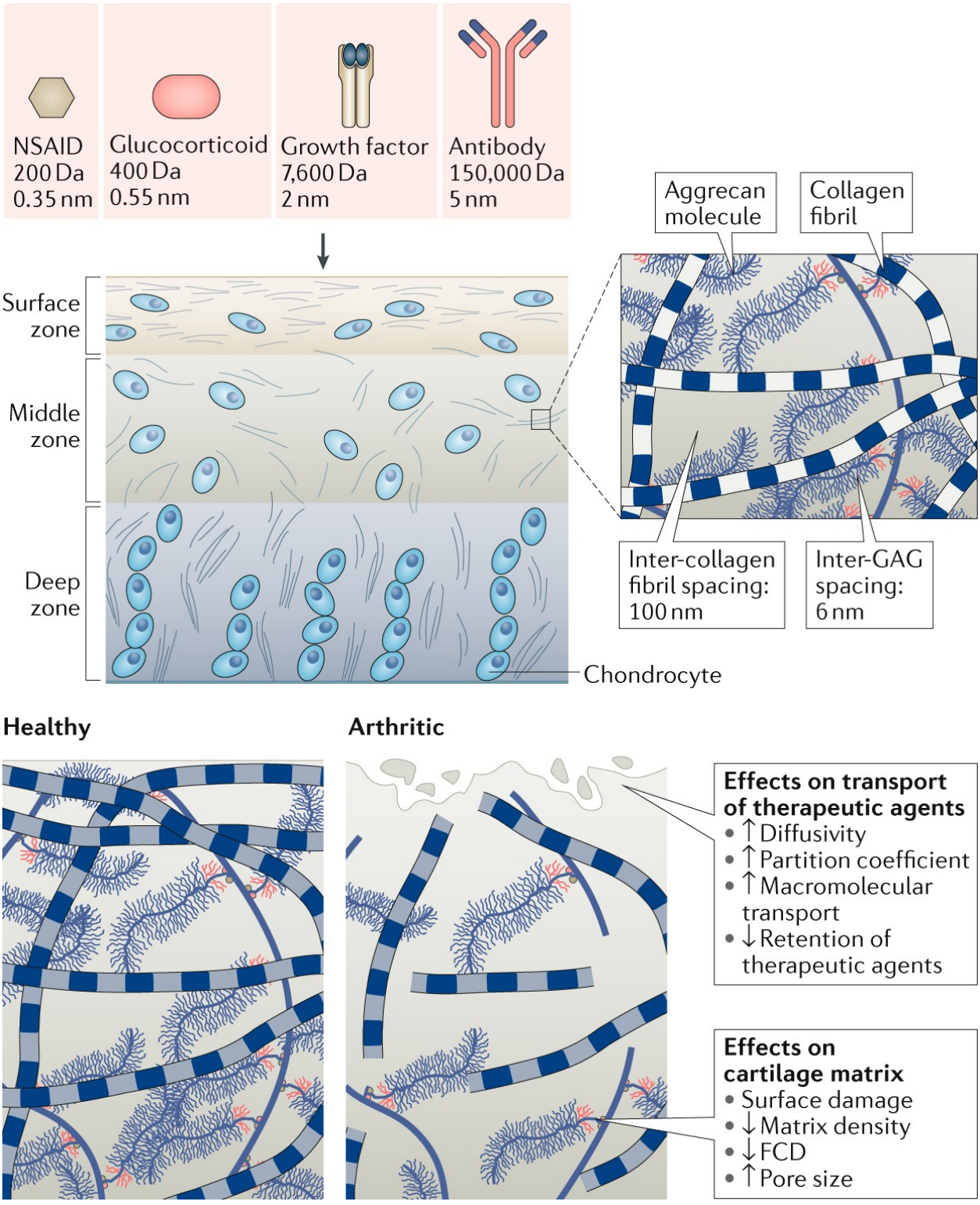

Figure 2.3 – Molecular transport of potential therapeutics in healthy and arthritic cartilage. Figures obtained from DiDomenico et al. (2018) [48].

triamcinolone acetonide, successfully alleviated joint inflammation of an arthritic rat model [49]. Vedadghavami et al. (2022) conjugated insulin-like growth factor 1 (IGF-1), which plays an important role in ECM anabolism, with a cationic peptide carrier enriched with arginine residues. This peptide-conjugated IGF-1 penetrated and was retained in cartilage explants, and suppressed the catabolic effects induced by interleukin-1α (IL-1α) [50]. Similar work was also performed using proteins as carrier molecules. Conjugation of the glucocorticoid dexamethasone with the positively charged protein avidin successfully rescued cartilage explants treated with IL-1α [51,52]. However, it is important to note that an increased positive charge does not necessarily equate to improved penetration into the negatively charged cartilage tissue. For instance, Krishnan et al. (2018) studied engineered green fluorescent protein (GFP) with varying net positive charges as potential drug carriers. GFP with a net charge of +9 and +15 had significantly higher uptake ratios in cartilage than GFPs with a +25 and +36 net charge, which may be explained by stronger binding interactions with GAGs in the tissue that prevent migration into the deeper zones [53].

Polymer-based carriers have also been developed following similar principles. Perni and Prokopovich (2017) used poly(β-amino ester) (PBAE) conjugated to dexamethasone through a hydrolysable ester link. The PBAE-dexamethasone enhanced retention in the tissue and the release kinetics may be controlled by the choice of linker between the drug and carrier [54]. Further work optimized the PBAE polymers through modulation of the amine, acrylate, and end-capping groups for dexamethasone delivery, which was able to suppress IL-1α-induced catabolism [55]. Geiger et al. (2018) utilized amine terminal polyamidoamine (PAMAM) dendrimers as a carrier for IGF-1. The dendrimers were end-functionalized with poly(ethylene glycol) (PEG) to control the surface charge. Optimal PEGylation improved human chondrocyte viability while maintaining relatively high tissue uptake, and improved retention in rat knees by 10-fold and for up to 30 days, compared

to IGF-1 alone. Furthermore, the dendrimer-IGF-1 delivery system reduced cartilage degeneration and osteophyte burden in surgically induced OA in rats [56]. Meanwhile, Formica et al. (2019) conjugated dexamethasone to chitosan which was shown to improve tissue penetration, reduce cyclooxygenase-2 (COX-2), interleukin-6 (IL-6), and MMP-13 levels in chondrocytes, and reduce GAG depletion in cartilage explants following IL-1β treatment [57].

Aside from targeting cartilage via electrostatic interactions with GAGs, other strategies have also been explored. Rothenfluh et al. (2008) identified a peptide sequence, WYRGRL, which specifically binds to collagen type II [58]. This peptide has been exploited as a targeted carrier for drug delivery into cartilage tissue. Similarly with chitosan, Formica et al. (2019) also conjugated dexamethasone with the WYRGRL peptide to improve cartilage uptake and retention. Treatment of WYRGRL-dexamethasone reduced NF-κB activity in lipopolysaccharide-stimulated M1-like macrophages, confirming an anti-inflammatory response. Furthermore, the pro-drug successfully prevented GAG loss following IL-1β treatment of cartilage explants [57]. Hulme et al. (2017) engineered high affinity and selective avimers that bind to collagen type II and fused it with an IL-1 receptor (IL-1R) antagonist. Intra-articular pre-treatment into the knee joints of rats with the avimer-antagonist complex one week prior to IL-1β treatment inhibited the production of IL-6. Meanwhile, pre-treatment with the IL-1R antagonist alone did not elicit a protective effect, which demonstrates that incorporation of the avimer improved residence times within the joint to allow for a more sustained effect [59].

2.3.2 Hydrogels

Hydrogels consist of a crosslinked, polymeric networks characterized by a high water content. As a result of these properties, hydrogels offer a great potential for the entrapment of therapeutics and

cells for drug delivery and tissue regeneration applications respectively [60]. While 3D hydrogel scaffolds may be implanted into the joint for either of these purposes, the focus of this section will be on injectable hydrogels which allow for a non-invasive procedure for drug delivery. Ideally, the solubility and gelation of these injectable hydrogels can occur under physiological conditions to allow for the sustained release of the therapeutic over a long term, and at a suitable rate for clinical practice [61].

Natural hydrogels are often utilized for these purposes due to their high biocompatibility, biodegradability, and similarities to ECM components. Tanaka et al. (2019) used a simvastatin-conjugated gelatin hydrogel, which has been demonstrated to have chondroprotective effects. This hydrogel, after application in an OA-induced mice model, exhibited lower grades of OA and also had higher collagen type II and lower MMP-13, ADAMTS-5, and IL-1β expression as determined by immunohistochemistry [62]. García-Fernández et al. (2020) developed a hydrogel drug delivery system using oxidized dextran, gelatin, and hyaluronic acid loaded with naproxen or dexamethasone. While the naproxen-loaded gels exhibited degradation by 16 days and released the majority of naproxen within 4 hours, the dexamethasone-loaded gels maintained integrity for up to 30 days and released 22% of its drug content in 5 days. Intra-articular injection of the naproxen and dexamethasone-loaded hydrogels in OA-induced rabbit knees prevented OA progression, while dexamethasone-loaded hydrogels additionally improved cartilage regeneration [63]. Mou et al. (2021) synthesized a chitosan-based hydrogel via crosslinking of N-carboxyethyl chitosan, adipic acid dihydrazide, and hyaluronic acid aldehyde. Here, the therapeutic was the hydrogel itself, as chitosan offers anti-inflammatory properties. Intra-articular injection of the hydrogel into the knees of OA-induced rats reduced the expression of inflammatory cytokines in synovial fluid and cartilage, and alleviated cartilage degeneration. Behavioural studies in the rats

also suggest potential pain relief as a result of hydrogel treatment, based on an increase in weight-bearing capacity compared to the untreated control group [64].

Synthetic hydrogels may also be preferable due to having improved mechanical properties. Furthermore, the use of synthetic hydrogels allows for modulation of the properties of the polymer. Petit et al. (2014) synthesized thermo-responsive acetyl-capped PCLA-PEG-PCLA which gels at 37°C. Intra-articular injection into the knee of rats indicated sustained levels of celecoxib in serum for 4 to 8 weeks, suggesting long term release to the joint [65]. Similarly, Wang et al. (2019) used PLGA-PEG-PLGA thermogels containing kartogenin, which has been previously demonstrated to enhance cartilage regeneration. In vitro studies indicated sustained release of kartogenin from the thermogel over 20 days. Intra-articular injection into OA-induced rabbit knees demonstrated a protective effect of the kartogenin-loaded thermogel, with shallow fissuring, and only partial and localized loss of proteoglycans and collagen type II compared to the control and thermogel alone [66]. Ha et al. (2021) used a pseudopolyrotaxane synthesized from PEG, attapulgite mineral, and α-cyclodextrin, for the sustained release of diclofenac. Intra-articular injection of the fluorescent dye-loaded hydrogel in the plantar region of rats demonstrated fluorescence up to 7 days. Further, the diclofenac-loaded hydrogel exhibited anti-inflammatory effects at 7 days post-injection in a rat model for acute inflammatory paw edema, while pathological changes were observed in diclofenac alone [64].

2.3.3 Microparticles and Nanoparticles

Particle-based drug delivery systems have also been of interest for cartilage tissue applications and may be broadly classified as either microparticles or nanoparticles based on the size of the carrier. Due to the larger size, particle-based drug carriers are not easily cleared from the synovial fluid as

compared to soluble molecules. As demonstrated by Singh et al. (2014), intra-articular injection of varying sizes of BSA-complexed pHEMA-pyridine particles in the stifle joint of rats resulted in differing half-lives. Soluble BSA was rapidly cleared from the joint, having a half-life of 0.63 days, while the 500 nm and 900 nm particles had half-lives of 1.9 and 2.5 days respectively [67]. Meanwhile, in vivo injection into murine joints of poly(propylene sulphide) particles conjugated to WYRGRL demonstrated penetration of 38 nm particles into the cartilage tissue, however the larger 96 nm particles were unable to effectively advance past the superficial zone [58]. Therefore, particle size is a major consideration in determining appropriate strategies for drug delivery. While larger particles will be retained within the synovial fluid for a longer period of time, they may not effectively penetrate into cartilage tissue and instead would rely on sustained release. Conversely, smaller particles are rapidly cleared from the joint, but have an improved capability to penetrate deeper into the cartilage tissue, allowing for a more targeted drug delivery approach. Either of the cases may also exploit surface-binding to the cartilage tissue for improving retention in the joint.

Zhu et al. (2015) encapsulated an inhibitor of Rac1, a GTPase implicated to be involved in OA development, in chitosan microparticles of around 100 μm in size. Weekly injections of these chitosan microparticles via hyaluronic acid in OA-induced mice 10 days post-surgery resulted in decreased cartilage degeneration and lower OA grades at 4, 6, and 8 weeks of treatment, indicating a protective effect in delaying OA development [68]. Rudnik-Janssen et al. (2017) used amino acid-based polyester amide microspheres having an average size of 22.4 μm and loaded with the corticosteroid triamcinolone acetonide. Following intra-articular injection in the knees of rats with or without OA induction, a gradual decline in signal was observed over 70 days. Interestingly, no clear differences were observed in retention between OA-afflicted and healthy control knees. While no differences were observed between treatment with the microspheres and triamcinolone

acetonide alone for cartilage degeneration, the drug-loaded microspheres were more effective in reducing synovitis [69]. Dhanabalan et al. (2020) utilized PLGA microparticles approximately 1 μm in size, and loaded with rapamycin which has been shown to delay degeneration of AC. Using larger molecular weight (MW) PLGA improved the sustained release of rapamycin. In vitro studies demonstrated that these rapamycin-loaded microparticles prevented chondrocyte senescence and sustained sGAG production during genomic and oxidative stresses. Furthermore, intra-articular injection of fluorescently-labelled PLGA microparticles into mouse knee joints indicated longer residence times with detectable levels after 30 days, while localization of the microparticles in various tissues of the knee joint was confirmed at 19 days post-injection [70].

Deloney et al. (2020) synthesized a hollow nanoparticle system capable of increased drug loading compared to solid nanoparticles. These were utilized to load an anti-inflammatory peptide as cargo, and successfully reduced IL-6 production in IL-1β treated chondrocytes in vitro. In vivo experiments confirmed that these hollow nanoparticles could be retained in the joint of mice for 7 days following intra-articular injection [71]. Wei et al. (2021) loaded micellular nanoparticles with an inhibitor of phospholipase A_2, an inflammatory mediator involved in OA development. These 10 nm nanoparticles accumulated and penetrated into the deep zone of cartilage explants. Fluorescently-labelled nanoparticles were used to evaluate in vivo retention in healthy and early OA knee joints of mice, which demonstrated an improved retention over 28 days compared to the free fluorophore, and in OA compared to healthy joints, potentially due to synovial thickening. Furthermore, biweekly injections of the drug-loaded nanoparticles following OA induction in mice improved the overall morphology of the AC, with no proteoglycan loss after 4 months unlike with free phosphatase A_2 inhibitor [72]. In another study, Wei et al. (2021) successfully utilized these

micellular nanoparticles for delivery of TGFα, which similarly attenuated cartilage degeneration in an OA model [73].

2.4 Polyphosphate

Polyphosphate (polyP) is an inorganic polymer comprised of repeating orthophosphate units. In fact, previous studies have identified pro-anabolic effects of polyP in chondrocytes. St-Pierre et al. (2012) demonstrated that treatment of chondrocytes with 1 mM of soluble polyP resulted in a significant increase in sGAG content (normalized to DNA) at 2 and 4 weeks of culture, as well as a significant increase in collagen content (normalized to DNA) by 4 weeks of culture using in vitro tissue cultures [74]. Ex vivo cultures of cartilage explants also demonstrated a significant increase in sGAG content by approximately ~45%, as well as an increase in collagen by ~30% after 1 week of treatment with 2 mM of polyP [74]. These results identify polyP as a molecule of interest for cartilage tissue engineering and regenerative medicine applications. Further studies have also demonstrated that this anabolic response is mediated by calcium signaling in chondrocytes [75]. Wang et al. (2016) developed a bio-matrix coating composed of hyaluronic acid and Mg-polyP. Chondrocytes that were cultured on these matrix-coated slides exhibited significant upregulation of chondrogenic genes SOX9 and COL3A1 after 21 days of culture, compared to the controls, as well as compared to hyaluronic acid or Na-polyP alone [76].

Therefore, it is postulated that polyP may be a therapeutic of interest for the regeneration of AC due to its pro-anabolic effects in chondrocytes, giving it the potential to stop or reverse the degeneration of AC in OA. However, drug delivery systems need to be established to effectively deliver and retain polyP within afflicted joints, allowing for improved residence times. Previous work by others have developed ionically crosslinked inorganic polyP-based particles [76–86],

which may be utilized as a drug delivery system into the joint to improve residence times. While other alternatives have been discussed, it is thought that nanoparticles offer a great compromise, typically having longer residence times than hydrogels while also exhibiting a greater capability to penetrate into the dense ECM network of AC compared to microparticles [87]. Combinatorial strategies for particle-based drug delivery systems may be performed, such as inclusion of carrier molecules to facilitate targeted drug delivery [58,88–93], and delivery within a hydrogel network to enhance sustained release [94–99], making particle-based strategies an attractive option. Herein, we aim to develop, optimize, and characterize these polyP-based particles for use in cartilage tissue engineering and drug delivery.

CHAPTER 3: MATERIALS AND METHODS

3.1 Materials

Sodium polyphosphate (Na-polyP; average chain length of 40 orthophosphate units) was a kind gift from Budenheim, Germany. Details of the procurement of other materials will be provided as they appear in the methods.

3.2 Polyphosphate-Based Particle Synthesis

Calcium polyphosphate (Ca-polyP) and strontium polyphosphate (Sr-polyP) particles were prepared by dropwise addition of Na-polyP solution into the corresponding crosslinking bath. Briefly, 5 mL of 4% w/v Na-polyP in deionized water (diH_2O) at pH = 10 was added at a rate of 60 mL/h using a syringe pump to 5 mL of 0.762 M $CaCl_2$ or $SrCl_2$ in diH_2O at pH = 10, respectively. Concurrently, 2 mL of 1 M NaOH in diH_2O was added dropwise at a rate of 25 mL/h using a syringe pump to maintain the pH of the solution at or above 10. The solution was stirred continuously at 300 rpm through the addition step (5 min) and for a total of 3 hours. Particles were then washed by centrifuging for 2 min at 2000 rcf, removal of supernatant, and resuspending in diH_2O. Washes were repeated five times. Following the final wash, particles were resuspended in 70% ethanol to a total volume of 10 mL and stored at –20°C until further use.

3.3 Particle Dispersion by Probe Sonication

Sonication was performed using a Q500 Sonicator (Qsonica) equipped with a microtip probe with a 1.6 mm tip diameter (#4417, Qsonica). Ca-polyP or Sr-polyP particles were diluted to an

appropriate particle concentration in diH_2O, and sonication was performed on ice at an amplitude of 50% for 30 seconds on and 30 seconds off, repeated for a total of 10 cycles.

3.4 Synovial Fluid Collection and Preparation

Synovial fluid was aspirated aseptically from the metacarpophalangeal joints of 2 to 4 year old cows sourced from a local abattoir (Tom Henderson Meats and Abattoir Inc.) within 24 hours of death, and frozen at -80°C until further use. Hyaluronidase (0.02 M phosphate buffer, 77 mM NaCl, 0.01% bovine serum albumin (BSA; VWR), pH = 7; Sigma-Aldrich) was added to the synovial fluid at a final concentration of 0.01 wt% and incubated for 30 minutes at 37°C on an orbital rocker. Following enzymatic digestion, the synovial fluid was centrifuged at 2000 rcf for 10 minutes, and the supernatant was filtered with a 0.20 μm cellulose acetate syringe filter (VWR) to remove cell debris and protein aggregates.

3.5 Particle Size and Surface Charge Characterization

For particle size and surface charge characterization, washed Ca-polyP and Sr-polyP particles were diluted 1:100 by volume in diH_2O unless otherwise stated and sonicated as described previously. Particle size distributions were measured by dynamic light scattering (DLS) at daily intervals over the course of 4 days, and the zeta potential was measured in folded capillary zeta cells (Malvern Panalytical) by electrophoretic mobility measurements. DLS and zeta potential measurements were performed using the Zetasizer Nano ZS (Malvern Panalytical) at a temperature of 25°C and a final particle dilution of 1:200.

In comparing size distributions of the as synthesized or sonicated particles over time as described previously, the particles were stored in diH_2O. For the pH experiment, particles were

instead sonicated and incubated in 8 mM Tris-HCl at the corresponding pH. For the osmolarity experiment, sonicated particles were stored at varying concentrations of NaCl. For the experiments in Dulbecco's modified Eagle's medium (DMEM; Corning), the particles were stored in low glucose DMEM (1 g/L glucose) supplemented with 3.7 g/L $NaHCO_3$, and 100 units/mL penicillin, 100 units/mL streptomycin, and 250 ng/mL amphotericin B (1X antibiotic-antimycotic; Gibco), with or without 10% fetal bovine serum (FBS; VWR) and incubated at 37℃ over the 4 days. For the cationic surface coatings, sonicated particles were incubated at varying concentrations of cetyltrimethylammonium bromide (CTAB; Sigma-Aldrich), chitosan (0.2 M acetic acid, pH = 6.5, ≥75% deacetylated; Sigma-Aldrich), linear polyethyleneimine (PEI) (MW ~60,000; Alfa Aesar), or branched polyethyleneimine (MW ~600, ~2000, or ~10,000; Thermo Fisher Scientific). For the synovial fluid experiment, the particles were stored in 10% synovial fluid with 1X antibiotic-antimycotic and incubated at 37℃ over the 4 days. The data of sonicated particles stored in diH_2O was replicated for the osmolarity and cationic surface coating experiments as the control sample which contains no NaCl or cationic molecules.

3.6 Scanning Electron Microscopy (SEM) and Elemental Analysis

Particles were sonicated in diH_2O and dried directly on aluminum stubs for imaging, while the as synthesized particles were dried on conductive tape for elemental analysis. Samples were sputter coated with gold using a Q150T ES (Quorum Technologies) at a thickness below 10 nm and imaged using a VEGA-II XMU Scanning Electron Microscope (TESCAN) equipped with an INCA Energy X-Act (Oxford Instruments) spectroscope for energy dispersive X-ray spectroscopy (EDX) operating at 20.00 kV. Particle diameters were measured manually from SEM images using ImageJ (NIH; version 1.51).

3.7 Fourier-Transform Infrared (FTIR) Spectroscopy

Ca-polyP and Sr-polyP particles were dried, and FTIR was performed using a Cary 630 FTIR Spectrophotometer with attenuated total reflectance (ATR) sampling module (Agilent) at a spectral range of 650 – 4000 cm^{-1} and a resolution of 2 cm^{-1}. Spectra were compared to Na-polyP starting material and hydroxyapatite nanoparticles (Sigma-Aldrich). Spectral analysis consisted of boxcar smoothing using ResolutionsPro (Agilent; version 5.2.0).

3.8 Raman Spectroscopy

Raman spectroscopy was performed on Na-polyP starting material and hydroxyapatite using an alpha300 RS Raman-SNOM Microscope (WITec) equipped with a 532 nm He-Ne laser (WITec) and EC Epiplan 20x/0.4 M27 objective (Zeiss). Spectral reads were performed at an integration time of 10 seconds with 10 accumulations. Spectral analysis consisted of Savitzky-Golay smoothing, asymmetric least squares baseline subtraction, and z-score normalization using OriginPro 2018 (OriginLab; version 9.5.1.195).

3.9 Cartilage Tissue Extraction and Chondrocyte Isolation

Full thickness articular cartilage (AC) was extracted aseptically from the metacarpophalangeal joints of 2 to 4 year old cows sourced from a local abattoir (Tom Henderson Meats and Abattoir Inc.) within 24 hours of death. The excised cartilage was maintained in high glucose DMEM (4.5 g/L glucose) supplemented with 1X antibiotic-antimycotic for 3 days in a cell incubator kept at 37°C, 95% relative humidity and 5% CO_2. The cartilage tissue was first digested with 0.2% w/v Pronase protease (EMD Millipore) in high glucose DMEM for 2 hours, followed by 3 washes in DMEM. The tissues were subsequently digested with 0.1% w/v collagenase (Sigma-Aldrich) in

high glucose DMEM for 1 or 2 days in a cell incubator. Following digestion, the cell suspension was passed through a 100 μm cell strainer and centrifuged at 500 rcf for 5 min to pellet the cells, and the supernatant was removed. Chondrocytes were resuspended in fresh DMEM, and the washing steps were repeated a second time, at which point cells were counted using a haemocytometer. Finally, the cells were washed once more and resuspended in Ham's F12 medium with L-glutamine (Corning) supplemented with 5% FBS and 1X antibiotic-antimycotic to an appropriate concentration for each experiment.

For tissue penetration and retention experiments, the excised cartilage was punched into 6 mm diameter full thickness discs with biopsy punches (Integra). The wet weight of each cartilage explant was measured, and the tissues were briefly maintained in phosphate buffered saline (PBS; Sigma-Aldrich) until further use.

3.10 Determination of Cellular Particle Uptake

Ca-polyP and Sr-polyP particles were diluted to 2 mg/mL in diH_2O and incubated with 0.1 mg/mL of 4',6-diamidino-2-phenylindole (DAPI) overnight. The binding of DAPI to polyP causes a shift in its fluorescence emission peak, permitting the visualization of the particles in the yellow-green spectrum rather than the blue spectrum associated with nucleic acids or GAGs [100]. DAPI-stained particles were then washed five times as previously described in sterile diH_2O. Chondrocytes were seeded onto 24-well tissue culture plates at 400,000 cells/well in Ham's F-12 medium with L-glutamine supplemented with 5% FBS and 1X antibiotic-antimycotic. After 24 hours, the medium was replaced with 2 mL of low glucose DMEM supplemented with 3.7 g/L $NaHCO_3$, 1X antibiotic-antimycotic, 10% FBS, and 100 μg/mL of DAPI-stained particles. After 24 hours of treatment, cells were washed three times with Hanks' Balanced Salt Solution (HBSS; Wisent

Bioproducts). Finally, trypan blue was added to a final concentration of 0.1% w/v for 1 minute. Trypan blue has been demonstrated to quench green fluorescence and is unable to pass through the cell membrane of viable cells, allowing for the visualization of DAPI-stained particles localized intracellularly [101,102]. Fluorescent microscopy was performed using an Axio Observer 7 (Zeiss).

3.11 Live-Dead Assay

Chondrocytes were seeded onto 24-well tissue culture plates at 25,000 cells/well in 1 mL of low glucose DMEM supplemented with 3.7 g/L $NaHCO_3$, 1X antibiotic-antimycotic, and 10% heat-inactivated FBS. Following 1 day of cell attachment, the culture medium was replaced with 1 mL of fresh medium containing 0 – 100 μg/mL of Ca-polyP or Sr-polyP, as synthesized or sonicated as described previously. After 1 day of treatment, cells were stained with 2 μM of calcein acetoxymethyl ester (calcein-AM; Life Technologies) and 4 μM of ethidium homodimer-1 (EthD-1; Sigma-Aldrich) in culture medium and incubated at 37℃ for 30 minutes. Calcein-AM may be hydrolyzed by intracellular esterases that are present in viable cells, forming calcein which is fluorescent and impermeable to the cell membrane, allowing for staining of live cells. Meanwhile, EthD-1 is a cell impermeant dye that strongly binds to nucleic acids, passing through compromised cell membranes of non-viable cells [103]. Five images were taken for each condition using the Axio Observer 7, and live and dead cells were counted using ImageJ.

Similarly, this was repeated in 48-well tissue culture plates at 80,000 cells/well in 400 μL of low glucose DMEM supplemented with 3.7 g/L $NaHCO_3$, 1X antibiotic-antimycotic, and 10% heat-inactivated FBS to match the culture and particle exposure conditions used for the MTT, DNA, and EdU assays.

3.12 EdU Cell Proliferation Assay

Chondrocytes were seeded onto 48-well tissue culture plates at 80,000 cells/well in 400 μL of low glucose DMEM supplemented with 3.7 g/L $NaHCO_3$, 1X antibiotic-antimycotic, and 10% heat-inactivated FBS. Following 1 day of cell attachment, the culture medium was replaced with 400 μL of fresh medium containing 0 – 100 μg/mL of Ca-polyP or Sr-polyP, as synthesized or sonicated as described previously.

After 1 day of treatment with the particles, 300 μL of medium in each well was removed and replaced with 100 μL of fresh medium without particles containing 20 μM of 5-ethynyl-2'-deoxyuridine (EdU) in DMSO and incubated for 4 hours. As EdU is a nucleoside analogue of thymidine, it can be incorporated into the DNA of proliferating cells undergoing DNA replication. After labelling proliferating cells with EdU, the cells were fixed in 3.7% formaldehyde in PBS for 15 minutes and washed twice in 3% BSA in PBS. The cells were then permeabilized in 0.5% Triton X-100 in PBS for 20 minutes on an orbital rocker, followed by two washes in 3% BSA in PBS. EdU detection was performed using the Click-iT EdU Cell Proliferation Kit for Imaging (Invitrogen) as per the manufacturer's protocol using an Alexa Fluor 488 azide via the copper (I)-catalyzed azide-alkyne cycloaddition (CuAAC) click reaction to covalently couple with the alkyne moiety of EdU, forming a stable triazole ring and labelling proliferating cells [104]. The cells were then washed once more in 3% BSA in PBS, followed by another wash in PBS. Nuclear staining was then performed using 5 μg/mL of Hoechst 33342 in PBS for 30 minutes on an orbital rocker, protected from light. The cells were washed twice in PBS prior to imaging with the Axio Observer 7. Five images were taken for each condition, and both proliferating and total cells were counted using ImageJ. Total cell numbers were additionally quantified by imaging the entire surface of the well with the Axio Observer 7 by counting the total number of nuclei using ImageJ.

3.13 MTT and DNA Assay

Chondrocytes were seeded onto 48-well tissue culture plates at 80,000 cells/well in 400 μL of low glucose DMEM supplemented with 3.7 g/L $NaHCO_3$, 1X antibiotic-antimycotic, and 10% heat-inactivated FBS in triplicate wells for each condition. Following 1 day of cell attachment, the culture medium was replaced with 400 μL of fresh medium containing 0 – 100 μg/mL of Ca-polyP or Sr-polyP, as synthesized or sonicated as described previously.

For the MTT assay, after 1 day of treatment with the particles, the medium was replaced with 100 μL of fresh medium without particles. Subsequently, 10 μL of 12 mM 3-(4,5-dimethylthiazol-2-yl)-2,5-diphenyltetrazolium bromide (MTT; Calbiochem) in sterile PBS was added to each well. As MTT may be reduced in the cell into insoluble, purple formazan crystals by mitochondrial activity, the amount of formazan produced can correspond to a measure of metabolic activity [105]. The cells were incubated for 4 hours, after which 220 μL of dimethyl sulfoxide (DMSO) was added and incubated for an additional 10 minutes at 37°C. Each well was then thoroughly mixed and 100 μL was added to 96-well plates in triplicates and absorbance was read at 540 nm using a Synergy H1 Microplate Reader (BioTek).

For the DNA assay, after 1 day of treatment with the particles, the medium was replaced with 200 μL of diH_2O. The plates were frozen at -80°C and underwent three freeze-thaw cycles to facilitate cell lysis. To each well, 200 μL of 80 μg/mL of papain (Sigma-Aldrich) in 10 mM of cysteine-HCl and 10 mM of ethylenediaminetetraacetic acid (EDTA) dissolved in PBS was added. The cell lysates were transferred to microtubes and digested at 65°C for 24 hours. DNA quantification was performed using the Quant-iT PicoGreen dsDNA Assay Kit (Invitrogen) as per the manufacturer's instructions using a Synergy H1 Microplate Reader.

3.14 ATP Assay

Chondrocytes were seeded onto 48-well tissue culture plates at 80,000 cells/well in 400 μL of low glucose DMEM supplemented with 3.7 g/L $NaHCO_3$, 1X antibiotic-antimycotic, and 10% heat-inactivated FBS. Following 1 day of cell attachment, the culture medium was replaced with 400 μL of fresh medium containing 0 or 100 μg/mL of Ca-polyP or Sr-polyP, as synthesized or sonicated as described previously.

After 1 day of treatment with the particles, ATP was quantified using CellTiter-Glo 2.0 Reagent (Promega) based on the manufacturer's instructions. Briefly, the culture plate was equilibrated to room temperature for 30 minutes, and 300 μL of medium in each well was transferred to 1.5 mL microtubes. One volume of CellTiter-Glo 2.0 reagent was added to each well and mixed thoroughly to facilitate cell lysis for the measurement of intracellular ATP levels. Similarly, one volume of CellTiter-Glo 2.0 reagent was added to the corresponding media for the measurement of extracellular ATP levels. After 10 minutes in room temperature, 150 μL of each solution was transferred to a white and opaque 96-well plate. Luminescence was measured using a Synergy H1 Microplate Reader (BioTek).

3.15 Evaluation of Cartilage Tissue Penetration and Retention

Circular full thickness cartilage discs were rinsed in PBS and incubated in 400 μL of fresh PBS supplemented with 10% heat-inactivated FBS and 100 μg/mL of DAPI-stained particles for 3 days on an orbital rocker at 37°C. The fluorescence of the solution was then measured at 415 nm excitation and 485 nm emission using a Synergy H1 Microplate Reader and the fluorescence was compared to the corresponding solution incubated without cartilage tissue (control). Similarly, PBS supplemented with 10% heat-inactivated FBS incubated with and without the cartilage

explants were used as respective blanks. Some of the cartilage explants were briefly rinsed in PBS and subsequently cut into thin slices using a custom-made device comprising a number 22 scalpel blade and a cryotome blade and tissue fluorescence was observed using an Axio Observer 7. Fluorescent profiles of the cartilage cross-sections were measured using ZEN software (Zeiss; version 3.2). Meanwhile, all remaining cartilage explants were briefly rinsed in PBS, transferred to 400 µL of fresh PBS supplemented with 10% heat-inactivated FBS, and incubated for an additional 3 days on an orbital rocker at 37°C to assess retention of the particles within the tissue. Fluorescence of the solution was measured as previously described and compared to the initial fluorescent particle solution incubated without cartilage tissue.

3.16 3D Tissue Culture

Millicell cell culture inserts (EMD Millipore; diameter = 12 mm, hydrophilic PTFE membrane, pore size = 0.4 µm) were coated with 50 µg of collagen type II from chicken sternal cartilage (Sigma-Aldrich) dissolved in 0.1 N acetic acid and allowed to dry sterilely overnight in a biosafety cabinet. The inserts were subsequently subjected to UV irradiation for 15 minutes. Chondrocytes were seeded at 1,000,000 cells per insert. The preculture medium utilized was comprised of Ham's F12 medium with L-glutamine supplemented with 5% FBS or heat-inactivated FBS depending on the culture medium used following preculture, and 1X antibiotic-antimycotic. Tissues were precultured for 5 days, and the medium outside the insert was changed with fresh preculture medium on day 2 of preculture.

After 5 days of preculture (which corresponds to day 0 of culture), the medium outside the insert was replaced with 500 µL of fresh culture medium, while the medium inside the insert was replaced with 500 µL of particle addition medium. Four different culture media were tested, all of

which were supplemented with 1X antibiotic-antimycotic and 100 µg/mL of ascorbic acid: (1) high glucose DMEM with pyruvate and L-glutamine, supplemented with 10% FBS, (2) high glucose DMEM with pyruvate and L-glutamine, supplemented with 10% heat-inactivated FBS, (3) high glucose DMEM without pyruvate and L-glutamine (Gibco), supplemented with 10% heat-inactivated FBS, and (4) Ham's F12 with L-glutamine, supplemented with 10% heat-inactivated FBS. Particle addition medium was always composed of high glucose DMEM without pyruvate and L-glutamine supplemented with 10% of the corresponding FBS, 1X antibiotic-antimycotic, 100 µg/mL of ascorbic acid, and 200 µg of sonicated Ca-polyP or Sr-polyP particles, or without polyP-based particles as the control. After 24 hours of particle addition, the inserts were fully submerged by addition of 1 mL of the corresponding culture medium. Media changes were performed twice a week (after 2 and 4 days of particle addition), and particle addition was repeated weekly (at days 7, 14, and 21) for a total of 4 applications over the 28-day culture period.

3.17 Biochemical Characterization of In Vitro Tissues

Tissues were cut out from the Millicell cell culture inserts and briefly rinsed in PBS. Excess liquid was removed gently with absorbing paper, and the wet weight of each tissue was measured. The tissues were frozen at -80℃ and lyophilized in a FreeZone Plus 6 Liter Cascade Console Freeze Dry System (Labconco) overnight. The dry weight of the lyophilized tissues was measured, and subsequently digested in 40 µg/mL of papain (Sigma-Aldrich) in PBS containing 5 mM cysteine-HCl and 5 mM EDTA at 65℃ for 2 days.

Sulfated glycosaminoglycan (sGAG) content was quantified using 1,9-dimethylmethylene blue (DMMB). Briefly, 10 µL of tissue digest appropriately diluted in PBS was added to a 96-well plate, followed by 200 µL of DMMB solution (16 µg/mL DMMB, 40 mM glycine, 40 mM NaCl,

pH = 1.5) in technical triplicates. Chondroitin sulfate was utilized as the standard. Absorbance was read at 525 and 590 nm using a Synergy H1 Microplate Reader, and the A_{525}/A_{590} ratio was correlated to the sGAG content in each sample.

Collagen content was estimated by quantification of hydroxyproline. Tissue digests were subjected to acid hydrolysis to release free hydroxyproline from collagen. Briefly, 100 µL of tissue digest was combined with 100 µL of 6 N HCl in a Pyrex tube and heated to 110°C for 18 hours. Samples were cooled on ice, briefly centrifuged, and neutralized by addition of 100 µL of 5.7 N NaOH. Samples were appropriately diluted and aliquoted to a final volume of 120 µL in diH_2O, and to each of these samples, 60 µL of 0.05 N chloramine-T prepared in 20% v/v diH_2O, 30% v/v 2-methoxyethanol, and 50% v/v assay buffer (0.05 g/mL citric acid, 0.12% v/v glacial acetic acid, 72.3 mg/mL sodium acetate, pH = 6) was added and allowed to stand for 20 minutes. Next, 60 µL of 3.15 N perchloric acid was added to each sample for 5 minutes. Lastly, 60 µL of 0.2 g/mL of p-dimethylaminobenzaldehyde in 2-methoxyethanol was added, mixed, and incubated at 60°C for 20 minutes. Samples were briefly cooled in a water bath, and 100 µL of sample was added to a 96-well plate in technical duplicates. Absorbance was measured at 560 nm using a Synergy H1 Microplate Reader and compared to L-hydroxyproline standards. In determining collagen content, it was assumed that all hydroxyproline is attributed to collagen, and that collagen contains 13 wt% of hydroxyproline.

DNA content was quantified using the Quant-iT PicoGreen dsDNA Assay Kit (Invitrogen) as per the manufacturer's instructions using a Synergy H1 Microplate Reader.

3.18 Statistical Analysis

Data are presented as means ± standard deviation unless otherwise stated. Statistical analyses were performed with SPSS (IBM; version 28.0.1.1). Statistical differences between groups were evaluated by univariate multi-way analysis of variance (ANOVA). Pairwise comparisons were performed within groups using one-way ANOVA with post-hoc Tukey's HSD. The level of significance was set at $p < 0.05$ (*), $p < 0.01$ (**), $p < 0.001$ (***), and $p < 0.0001$ (****).

CHAPTER 4: RESULTS AND DISCUSSION

4.1 Physicochemical Characterization of Polyphosphate-Based Particles

4.1.1 DLS and Zeta Potential

Ca-polyP and Sr-polyP particles were synthesized by drop-wise addition of polyP into respective cation baths. In this study, Ca^{2+} and Sr^{2+} were selected as the ionic crosslinkers of polyP to compare potential differences in biological activity as a result of the counterion. The choice of calcium is mainly attributed to the fact that Ca-polyP have been studied in other cell types by others [77–80,82,83,85,86]. Furthermore, it has been proposed that calcium may stimulate the synthesis of proteoglycans in cartilage [106]. Importantly, the anabolic effects of polyP in chondrocytes have been attributed to calcium signalling [75], suggesting a synergistic effect of Ca-polyP particles for cartilage tissue engineering. Meanwhile, strontium has been demonstrated to stimulate proteoglycan and collagen synthesis in chondrocytes in vitro [107–109]. Additionally, strontium promotes chondrogenesis in adipose-derived dedifferentiated fat cells and mesenchymal stem cells [110–112]. In vivo studies have also confirmed a pro-anabolic effect, with strontium upregulating anabolic pathways [112], as well as inhibiting key proteases and IL-1β, reducing the progression of OA [113]. Results obtained from clinical studies and reviews have also suggested positive outcomes of strontium ranelate on reducing the progression of OA in patients [114–116].

To assess the particle size stability of Ca-polyP and Sr-polyP, both the as synthesized and sonicated particles were stored in diH_2O, and DLS was performed daily over the course of 4 days (Figure 4.1, A – B). Three-way ANOVA indicates a significant effect of cation type ($p < 0.0001$) and time ($p < 0.0001$) on the particle size. However, probe sonication successfully reduced the size

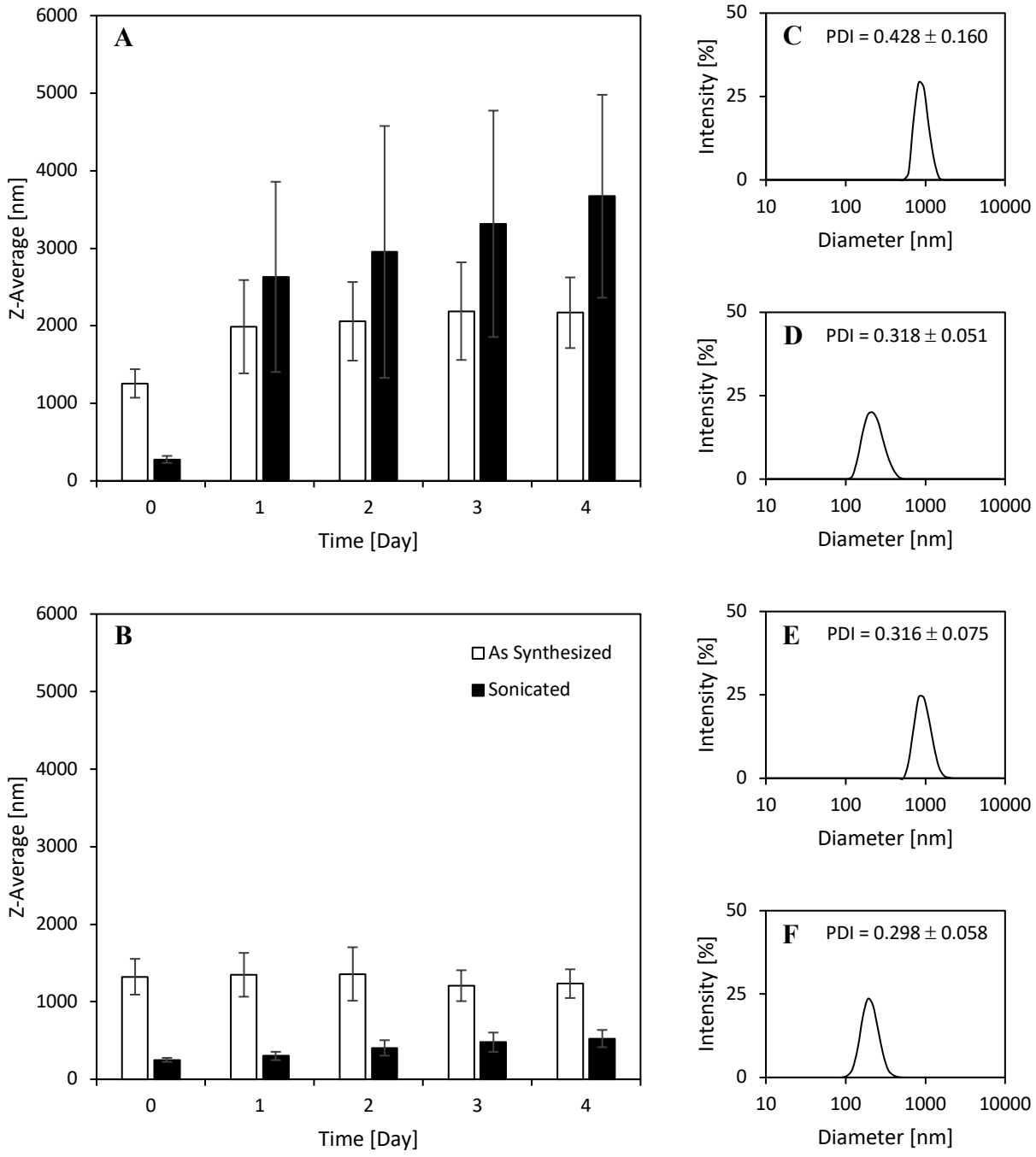

Figure 4.1 – Size of polyP-based particles in deionized water. PolyP-based particle size was measured by DLS in deionized water for **(A)** Ca-polyP and **(B)** Sr-polyP particles. Measurements were performed every day for 4 days to assess size stability. Representative particle size distributions and the average PDI for **(C)** Ca-polyP particles as synthesized or **(D)** sonicated and **(E)** Sr-polyP particles as synthesized or **(F)** sonicated obtained from Day 0 measurements are indicated. Data are presented as averages ± standard deviation for $n \geq 4$ experiments.

of particle agglomerates of Ca-polyP from 1257 ± 184 nm to 277.7 ± 45.0 nm ($p < 0.0001$) and Sr-polyP from 1322 ± 231 nm to 250.7 ± 25.9 nm ($p < 0.0001$), bringing the size of the particles to a submicron scale. Interestingly, particles in the range of 100 to 300 nm in size have been reported to selectively enter OA cartilage but not healthy cartilage [117,118], suggesting that these particles may be feasible for our applications. As can be seen in the particle size distributions (PSD) of Ca-polyP and Sr-polyP (Figure 4.1, C – F), the particle population for all conditions exhibit a unimodal distribution that is moderately polydisperse based on the average polydispersity index (PDI) [119,120]. Furthermore, as the PDI of the sonicated Ca-polyP and Sr-polyP are below 0.4, the particle population is considered to be sufficiently uniform in size, making them feasible for biomedical applications [121].

While the size of Ca-polyP and Sr-polyP are quite similar, it is evident that Ca-polyP exhibits much poorer size stability compared to Sr-polyP. Comparing the particles as synthesized, Ca-polyP particles increase in size after 1 day of incubation ($p < 0.05$), however the particle size remains quite stable thereafter, with a 1.7-fold increase by day 4. Meanwhile, Sr-polyP particles remain similar in size throughout the entire 4 days, with no significant differences in the size between all timepoints. These trends in size stability are also observed for the sonicated polyP-based particles. The sonicated Ca-polyP particles rapidly agglomerate following sonication, with a significant increase between the Z-average of day 0 and day 1 ($p < 0.01$), even exceeding the size of the as synthesized Ca-polyP particles, with an over 13-fold increase by day 4. In contrast, Sr-polyP particles agglomerate at a slower rate, with a statistically significant increase beginning between day 0 and day 2 ($p < 0.01$) but overall, the Z-average remains much smaller than the as synthesized Sr-polyP throughout the entire 4 days, with an over 2-fold increase by day 4. Of note,

sonication of agglomerates formed after incubating sonicated particles for 4 days in diH_2O allowed to recover their initial size following sonication (data not shown).

The mechanism causing the improved size stability of Sr-polyP is unknown. The zeta potential of Ca-polyP and Sr-polyP in diH_2O was measured to be -22.7 ± 3.2 mV and -21.5 ± 2.6 mV respectively, indicating negligible differences in the surface charge. Therefore, the stability of Sr-polyP is not likely attributed to increases in the electrostatic repulsive forces between individual particles. While calcium and strontium ions contain many similarities, their chemistry and interactions with other molecules may differ drastically. For example, the ionic radii of strontium ions are slightly larger than calcium ions, which may affect its bonding and crosslinking with polyP due to potential changes in the crystallinity, lattice parameters, crystal size, morphology, solubility, and stability of the material [122]. Through XRD analysis, Qiu et al. (2006) observed a monoclinic crystal system in Ca-polyP and a rhombohedral crystal system in Sr-polyP [123]. Low substitution of Ca-polyP scaffolds with strontium does not alter the crystal structure [123–126], however at higher strontium substitutions above 50%, the crystal structure of the Sr/Ca-polyP scaffolds switch from monoclinic to rhombohedral [123]. It is plausible that these differences in crystal structure may also be present between our Ca-polyP and Sr-polyP particles. As crystallinity may influence the size stability of nanoparticles [127], this may be a contributing factor in the improved size stability of Sr-polyP.

4.1.2 SEM and EDX Analysis

SEM was performed on both sonicated Ca-polyP and Sr-polyP particles, which revealed that the particles exhibit a spherical morphology (Figure 4.2, A – B). Importantly, SEM was performed on the as synthesized Ca-polyP and Sr-polyP particles, which indicated similar morphologies in all

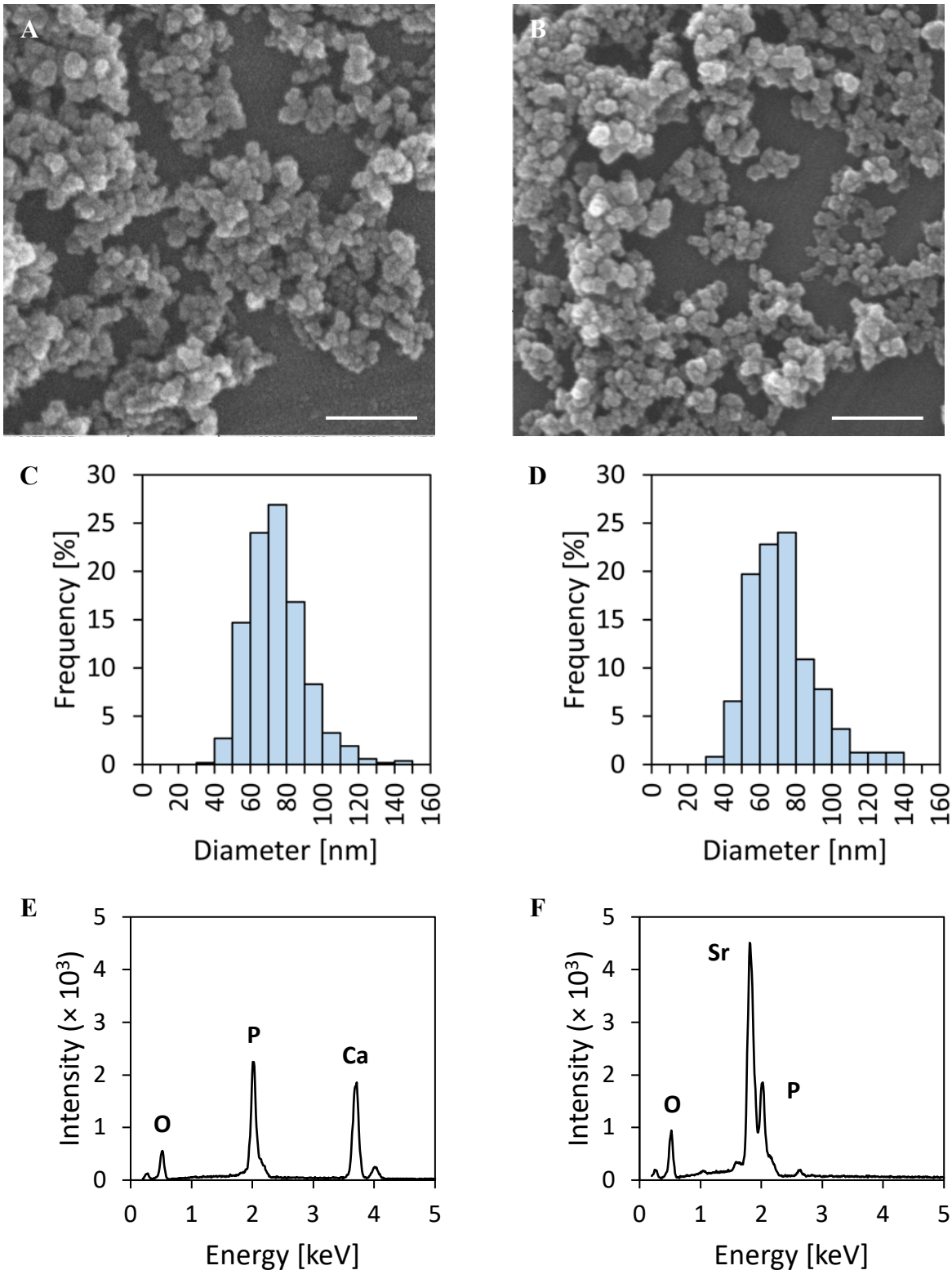

Figure 4.2 – PolyP-based particle morphology and composition. SEM images of **(A)** Ca-polyP and **(B)** Sr-polyP particles along with estimated particle size distributions of **(C)** Ca-polyP and **(D)** Sr-polyP particles. EDX spectra of **(E)** Ca-polyP and **(F)** Sr-polyP particles. Scale bar = 500 nm.

samples (data not shown). This confirms that sonication merely breaks up agglomerates of particles, as opposed to forming smaller particles. Interestingly, having a spherical morphology can be beneficial in terms of biocompatibility. For instance, Zhao et al. (2013) found that both spherical and rod-shaped hydroxyapatite nanoparticles exhibited less cytotoxicity than needle or plate-like hydroxyapatite nanoparticles. Additionally, both needle and plate-like nanoparticles induced inflammatory signals due to an increase in IL-6 production, which was absent in the spherical and rod-shaped particles [128].

The average particle diameter measured directly from SEM imaging is estimated to be approximately 74 ± 16 nm (n = 517 particles) and 72 ± 18 nm (n = 487 particles) for Ca-polyP and Sr-polyP respectively (Figure 4.2, C – D). While this measurement may not be very accurate, it does suggest that DLS measurements may overestimate the actual size of the individual polyP-based particles. This discrepancy in measurements can be partially explained due to the difference in size definition. DLS is an indirect method which provides the Z-average based on an intensity average of the hydrodynamic diameter dependent on the diffusion coefficient of particles undergoing Brownian motion, as measured by the scattering intensity [129]. As the scattering intensity is proportional to the square of size, DLS results are biased towards large particles [129]. Meanwhile, SEM allows for a direct measurement of the geometric size of a particle [130].

Importantly, the SEM results suggests that the particles are within a nanoscale range, and therefore may be feasible for cartilage tissue applications. However, these conclusions rely on the assumption that ultrasonication is sufficient to break up the particle agglomerates into individual spherical particles. It is possible that the particles are stable as aggregates of multiple particles in solution even after sonication, leading to the larger sizes as measured in DLS. From the SEM imaging, it is not possible to discern whether the particles were individual particles that aggregated

due to the drying process, or if the particles were initially in an aggregated form in solution even after sonication. While individual particles were visualized under some areas using SEM (data not shown), further work is required to validate the dimensions of these polyP-based particles. This can be facilitated by imaging using less particles. Additional size characterization methods such as transmission electron microscopy (TEM) and atomic force microscopy (AFM) [131] to supplement DLS and SEM measurements would also be highly beneficial.

EDX analysis was also performed on the particles (Figure 2, E – F), confirming that the particles are composed of calcium or strontium, phosphate, and oxygen. This also confirms that the particle preparation was mostly clean, with minimal impurities of sodium and chloride ions present during the synthesis. EDX suggests an approximate 1:1 atomic ratio of Ca:P and Sr:P for Ca-polyP and Sr-polyP respectively. Meanwhile, similar materials such as hydroxyapatite are characterized by a theoretical Ca/P ratio of 1.67, while the Ca/P ratio in a calcium polyP scaffold was found to be 0.45 [132].

4.1.3 FTIR Spectroscopy

Fourier-transform infrared spectroscopy was performed on dried Ca-polyP and Sr-polyP particles and compared to both the Na-polyP starting material as well as hydroxyapatite nanoparticles as a control (Figure 4.3). The spectra observed for Na-polyP closely matches that as reported by others [76,77,81,84,133–135]. Meanwhile, similar spectra were obtained for Ca-polyP [76,77,80,84] and Sr-polyP [81] as previously reported. Importantly, the spectral shift of Na-polyP to two main peaks at approximately 908 cm^{-1} and 1107 cm^{-1} in both Ca-polyP and Sr-polyP can be attributed to ionic crosslinking of polyP with the divalent cations, which crosslinks the free oxygen of the phosphate groups in polyP and increases interacting bond strengths between polyP chains [76]. Meanwhile,

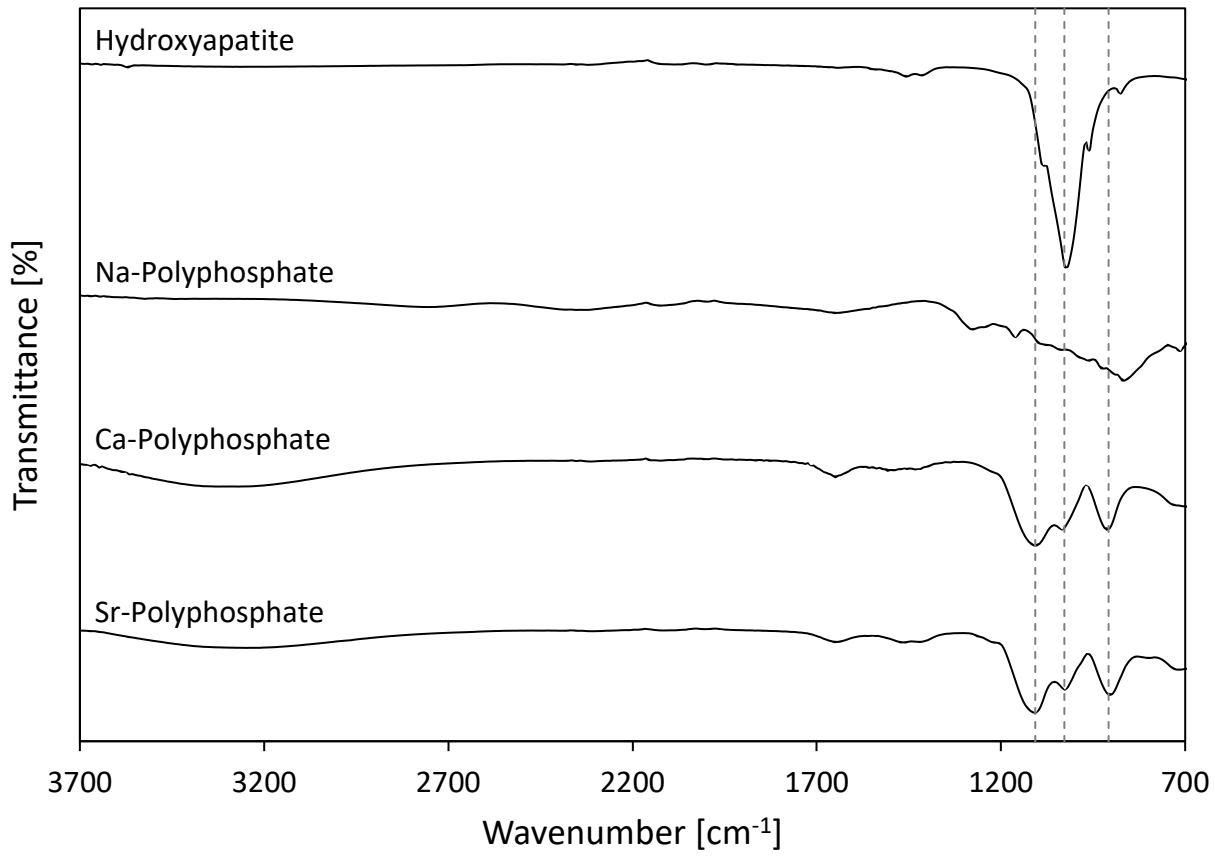

Figure 4.3 – FTIR spectra of polyP-based particles. The peaks at approximately 908 cm^{-1} and 1107 cm^{-1} are both characteristic of polyP, representing P–O–P and PO_3^{2-} respectively. Meanwhile, the 1028 cm^{-1} peak represents PO_4^{-} as observed in hydroxyapatite.

the peak at approximately 3259 cm^{-1} may be attributed to the hydroxyl end-groups of polyP [133,136] or water that may be adsorbed to the sample [76].

Of possible concern is the matching phosphate peak observed in the spectra for Ca-polyP, Sr-polyP, and hydroxyapatite at approximately 1028 cm^{-1}, which may suggest partial hydrolysis of polyP into free phosphate groups. While peaks are found around this wavenumber in previously reported spectra [76,77,80], the peak observed in our samples are notably much larger. A possible explanation for this result is the drying process required for FTIR analysis, which leads to a prolonged exposure to moisture. A preliminary test comparing drying overnight or by heating at 50°C indicated no differences in the phosphate peak (data not shown). Additionally, given that the particle washing step was done in diH_2O, this may also facilitate hydrolysis. However, washing in 95% ethanol also failed to remove this peak (data not shown). It can also be ruled out that the Na-polyP utilized in the experiment was degraded due to the absence of this peak in the Na-polyP spectra. Additional validation was performed on the Na-polyP starting material compared to hydroxyapatite by Raman spectroscopy, which also illustrates the absence of a phosphate peak in Na-polyP (Supplementary Figure 1). Therefore, it appears that polyP degradation occurs during the synthesis process, and further optimization of the synthesis procedure would be required to minimize degradation of the base polymer.

4.1.4 Effect of pH

As polyP is a highly ionizable inorganic polymer, the effect of pH on the size stability and surface charge was explored. Both Ca-polyP and Sr-polyP were sonicated in 8 mM Tris at pH values between 7.0 – 11.5, and DLS was performed over 4 days to assess size stability (Figure 4.4, A – B). The particles were maintained in 8 mM Tris to ensure that the pH remained stable throughout

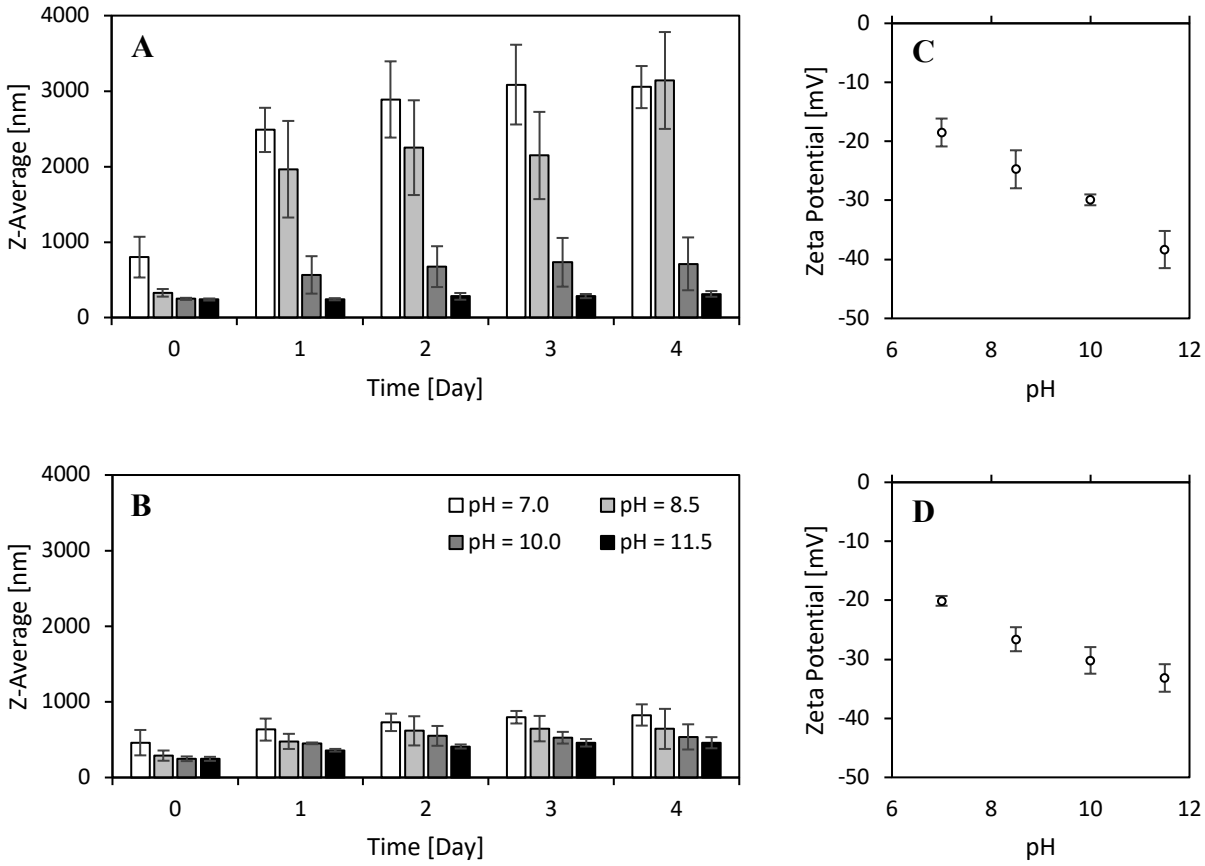

Figure 4.4 – Effect of pH on polyP-based particle size and surface charge. Sonicated polyP-based particle size was measured by DLS in 8 mM Tris for **(A)** Ca-polyP and **(B)** Sr-polyP particles at varying pH values. Measurements were performed every day for 4 days to assess size stability. Zeta potential was also measured for sonicated **(C)** Ca-polyP and **(D)** Sr-polyP particles at varying pH. Data are presented as averages ± standard deviation for n = 3 experiments.

the entire experiment. Three-way ANOVA using cation type, pH, and time indicates a significant effect on particle size for each factor ($p < 0.0001$). As observed from the data, pH has a notable effect on size stability, especially for the Ca-polyP particles. While similar trends are observed in Sr-polyP, due to the inherently higher stability of these particles, the Z-averages at all pH values are quite similar to each other. Zeta potential measurements were also performed at day 0 (Figure 4.4, C – D), and two-way ANOVA suggests a significant effect of pH on the zeta potential ($p < 0.0001$). Logically, the surface charge of the particles would be affected by pH due to changing the degree of ionization of the phosphate groups of polyP. As the pH is increased, the zeta potential measured increasingly becomes more negative. This explains the improved size stability at more alkaline pH, as this results in increased electrostatic repulsive forces between individual particles, which hinders particle agglomeration. A zeta potential greater than +30 mV or less than -30 mV is generally considered to be sufficient for a stable colloid system [137,138].

Each phosphate subunit within a polyP chain contains a strongly acidic hydrogen, having a pK_a of approximately 0 – 3. Meanwhile, the terminal phosphates of polyP each contain one weakly acidic hydrogen, having a pK_a of approximately 7 – 9 [136]. As an estimate, the degree of ionization was calculated using the Henderson-Hasselbalch equation with the pH values utilized in this experiment and the estimated pK_a range, with the assumption that all groups behave as a weak acid (Supplementary Table 1). As can be seen from these estimates, it is expected that the degree of ionization for each strongly acidic hydrogen would not change, given that all values are essentially equal to 1, suggesting complete ionization. However, there would be a large effect of pH within the range investigated on the ionization status of the weakly acidic hydrogen present on the end-groups. As a result, it is thought that the increasingly negative zeta potential at more alkaline pH may be attributed to increased ionization of the end-groups. Interestingly, the polyP

utilized in the experiment has an average length of ~40 orthophosphate subunits, and with one subunit on each terminal end of the polymer containing a weakly acidic hydrogen, the contribution of the end-groups to the overall charge is expected to be 2/42, or under 5%. Despite this, the zeta potential decreases significantly between pH = 7.0 to 11.5 for Ca-polyP ($p < 0.0001$) and Sr-polyP ($p < 0.001$). Therefore, it is thought that the end-groups are enriched at the surface of the particles, possibly due to the preferred orientation of the polyP molecules when crosslinked with the divalent cations, resulting in a large contribution towards the surface charge. However, further work would be required to confirm this. One strategy can involve end-group titration which exploits the different pK_a of the terminal ends, allowing for quantification of the end-group concentration [136,139]. By quantifying the end-group concentration at the surface, it may then be compared to the overall polyP or end-group concentration of the bulk material. However, this heavily relies on the assumption that only the surface of the particle may participate in the titration, which may not be valid. Another possible strategy involves the use of ^{31}P NMR, which is able to distinguish the terminal, penultimate, and core phosphate groups of polyP from one another [136,140,141]. Solid-state ^{31}P NMR has been used to deduce core-shell structures and surface chemistry of nanoparticles [142,143], potentially allowing for the quantification of terminal phosphates at the surface relative to the bulk.

Of course, as the goal is to utilize these polyP-based particles for in vitro experiments and eventually for biomedical applications, the pH of the environment would be the physiological pH. The pH of synovial fluid has been reported to be 7.43 ± 0.02 [144] or weakly basic at approximately 7.77 ± 0.05 [145] in normal joints. Measurements performed on the synovial fluid of osteoarthritic (OA) joints have indicated a weakly basic pH of 7.55 ± 0.04 [145] or 7.78 ± 0.38 [146]. Meanwhile, cartilage tissue itself is weakly acidic, having a depth-dependent pH ranging

from 7.3 at the surface of the superficial zone down to 6.9 in the deep zone [147]. In a study, the average pH of grade 0 (normal) cartilage surfaces was reported to be 7.1 ± 0.4, with increasing acidity observed in OA with a pH of 6.2 ± 0.9, 5.7 ± 1.0, and 5.5 ± 1.0 for OA grades of 1 to 3 respectively [148]. Therefore, further work to explore the size stability and zeta potential at more acidic pH values may be beneficial to better understand the particle behaviour under pathological conditions, where drug delivery applications would be more relevant. From the results obtained, it is expected that particle stability would decrease at more acidic pH due to a decrease in the absolute value of the zeta potential. This also provides the potential for incorporating pH-responsive strategies to facilitate drug delivery in OA-afflicted cartilage.

4.1.5 Effect of Ionic Strength

The effect of ionic strength on the particle size stability was also evaluated. Both Ca-polyP and Sr-polyP were incubated in varying concentrations of NaCl, and DLS was performed to assess size stability over time (Figure 4.5, A – B). The concentration of 0.9% w/v NaCl, also known as normal saline solution, is at a physiological osmolarity, and was selected as the highest salt concentration as it is reflective of in vitro and physiological environments. Three-way ANOVA with cation type, NaCl concentration, and time indicates a significant effect on particle size for each factor ($p < 0.0001$). It is observed that increasing salt concentration results in a decrease in particle size stability, which is similarly reported by others [149–151]. This can be explained from the classical Derjaguin-Landau-Verwey-Overbeek (DLVO) theory, which presents a mathematical model to predict the stability of colloidal systems based on the attractive van der Waals forces and the repulsive forces due to the electrical double layer [152,153]. According to the DLVO theory, an increase in the ionic strength results in screening of the electrostatic interactions by reducing the

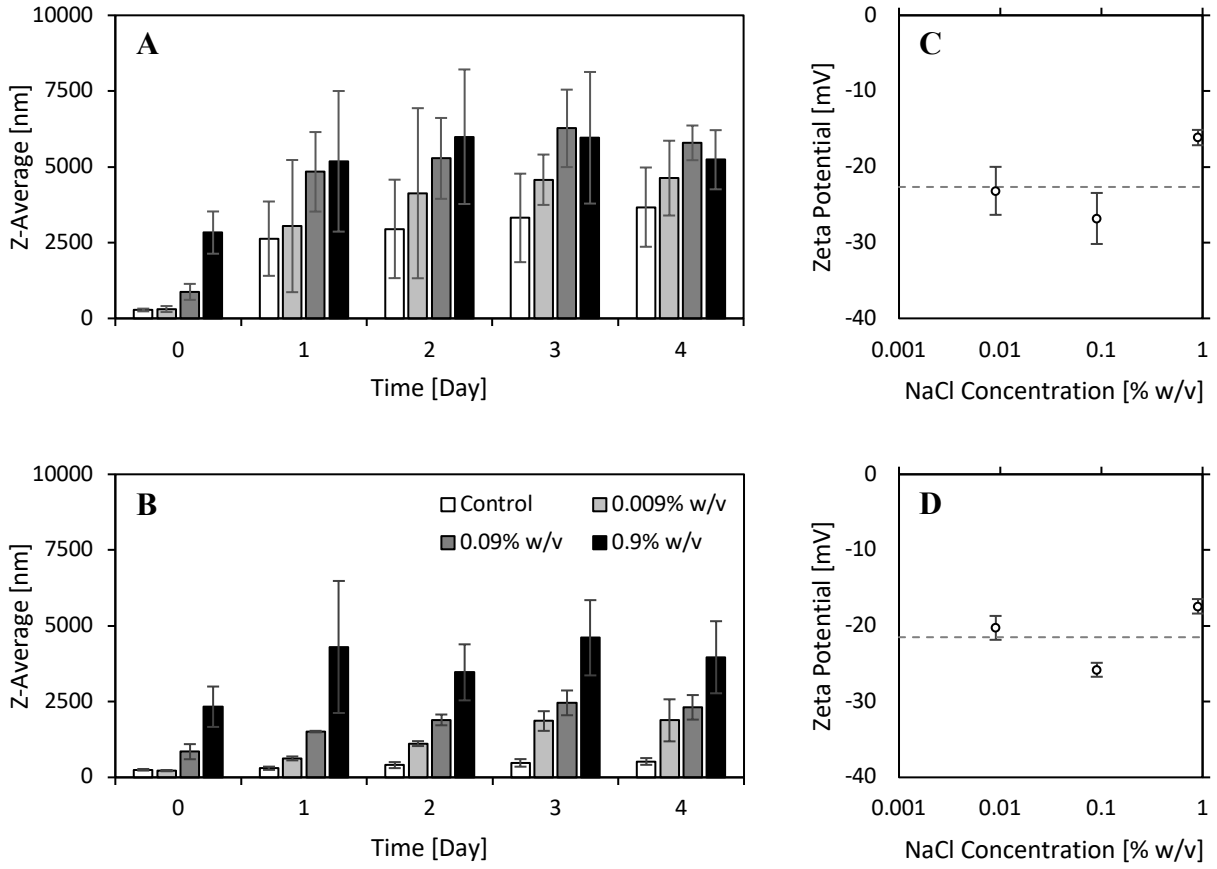

Figure 4.5 – Effect of ionic strength on polyP-based particle size and surface charge. Sonicated polyP-based particle size was measured by DLS in varying concentrations of sodium chloride for **(A)** Ca-polyP and **(B)** Sr-polyP particles. Measurements were performed every day for 4 days to assess size stability. Zeta potential was also measured for sonicated **(C)** Ca-polyP and **(D)** Sr-polyP particles at varying osmolarities. Dotted lines represent the average zeta potential measured in deionized water. Data are presented as averages ± standard deviation for n = 3 experiments.

double layer thickness. This reduces the energy barrier preventing coagulation, thereby facilitating particle agglomeration.

Similarly, the zeta potential as a function of ionic strength was characterized (Figure 4.5, C – D). Two-way ANOVA indicates a significant effect on zeta potential for NaCl concentration ($p < 0.0001$). However, as can be observed, there is no clear trend with increasing NaCl concentration. Based on classical DLVO theory, one would expect a decrease in the surface charge of the particle due to the screening effect, which has been reported by others with different particles [154–156]. While no trend is observed, this can explain the increase in zeta potential observed at 0.9% w/v NaCl for both Ca-polyP and Sr-polyP. Interestingly, despite the lack of data points to confirm these claims, it does appear that the zeta potential has a parabolic trend as a function of salt concentration, in which a potential minimum (or maximum absolute value) is present around 0.09% w/v NaCl for both Ca-polyP and Sr-polyP. Many studies have also reported observing an ionic strength-dependent maximum zeta potential [157–160], and this phenomenon has been determined to be system-dependent [161]. Currently, there are three main interpretations used to explain these maxima, and of these, multiple factors may even be considered: (i) there is specific ionic adsorption at the interface; (ii) the particles are covered with flexible chains containing ionic groups repelled from the particle surface, known as the "hairy layer model"; and (iii) an anomalous change of surface conductivity [161]. With regards to the polyP-based particles, all explanations may be plausible, especially as the results of the pH experiment suggested enrichment of terminal phosphate groups of polyP at the particle surface. While not confirmed, this may support the hairy layer model hypothesis whereby polyP chains are surrounding the particle.

The zeta potentials of the particles were also measured in PBS, which reflects a high ionic strength at a physiological pH. As expected, the absolute value of the zeta potential drops towards

a more neutral surface charge within the same range as normal saline solution due to their similar ionic strengths, at -13.7 ± 1.6 mV and -14.9 ± 3.8 mV for Ca-polyP and Sr-polyP respectively. In contrast, Müller et al. (2018) measured a zeta potential of -33.6 ± 2.3 mV for Ca-polyP in PBS [82], however this discrepancy may be explained due to differences in the particle synthesis procedures.

4.1.6 In Vitro and In Vivo Environment

As the goal is to apply these polyP-based particles for in vitro experiments, the particles were characterized in cell culture medium to replicate the in vitro environment, which also better resembles a physiological environment in the synovial joint. As synthesized and sonicated Ca-polyP and Sr-polyP particles were stored in DMEM with or without 10% FBS supplementation, incubated at 37°C, and DLS was performed over 4 days (Figure 4.6, A – D). Four-way ANOVA indicates a significant effect of FBS ($p < 0.0001$) and time ($p < 0.001$) on particle size. Evidently, all particles agglomerated immediately when added to DMEM, which matches our previous observations with normal saline solution given its similar ionic strength to that of DMEM. However, for the particles added to DMEM with 10% FBS, the size remained essentially constant throughout the 4 days. It has been well established that proteins readily adsorb onto the surfaces of particles to form a protein corona, which is dependent on the particle composition, size, shape, surface charge and chemistry, as well as environmental factors [162–164]. Similar studies have also demonstrated an improved colloidal stability in serum-supplemented media [165–171]. In contrast, Cohen et al. (2013) demonstrated that supplementation of 10% FBS destabilized nanoparticles exhibiting a negative zeta potential in RPMI medium, but stabilized nanoparticles with a positive zeta potential [172]. Furthermore, Chern et al. (1999) have also indicated differing

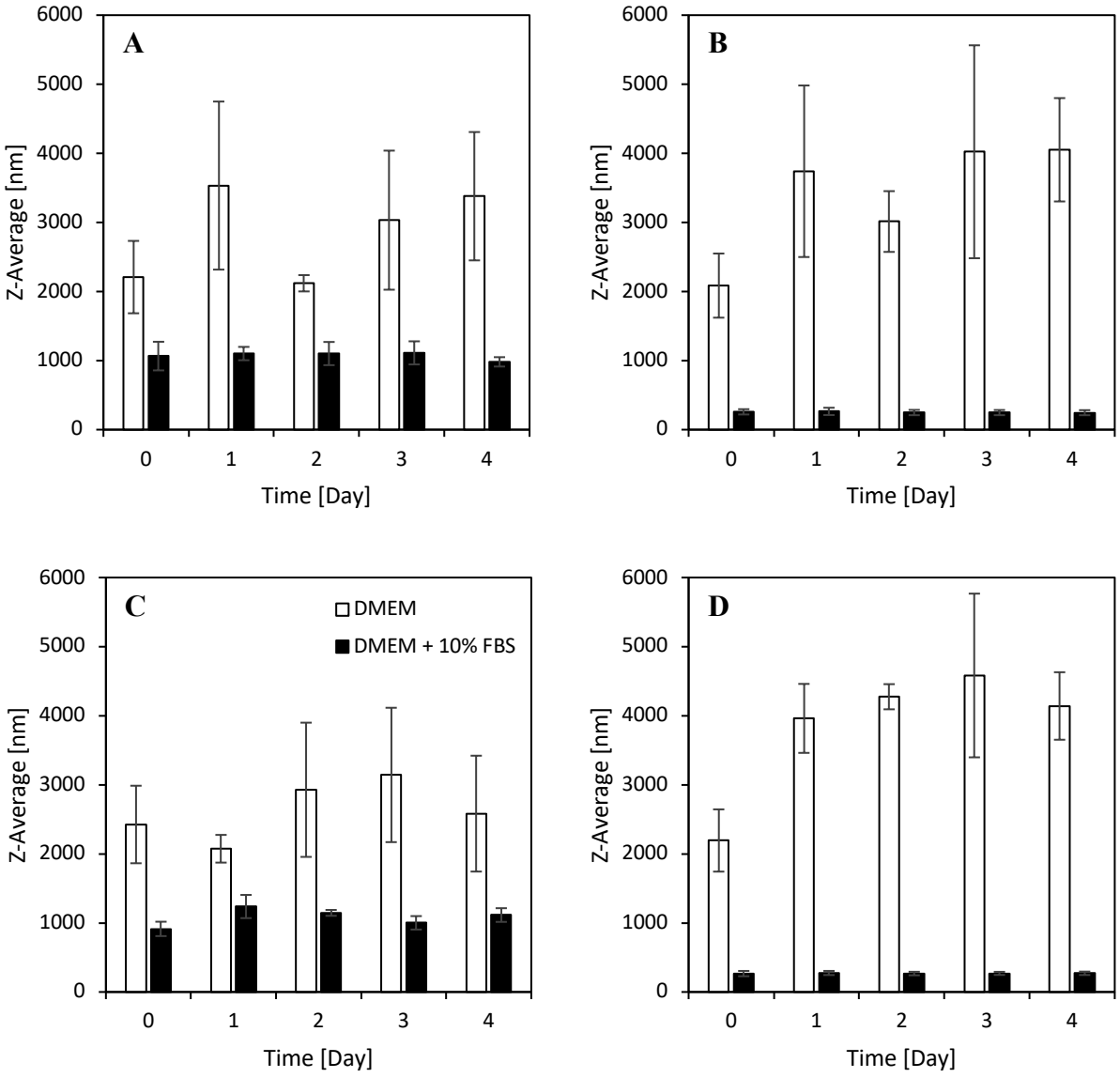

Figure 4.6 – Size of polyP-based particles in cell culture medium with and without FBS. PolyP-based particle size was measured by DLS in low glucose DMEM with or without 10% FBS supplementation for **(A)** Ca-polyP as synthesized or **(B)** sonicated and **(C)** Sr-polyP as synthesized or **(D)** sonicated. The particles were incubated at 37°C, and measurements were performed every day for 4 days to assess size stability. Data are presented as averages ± standard deviation for n = 3 experiments.

results, with chitosan latex particles losing their positive charge in the presence of BSA, resulting in destabilization. However, increasing the BSA concentration eventually restabilizes the particles by induction of a negative charge instead [173]. Adsorption of proteins typically leads to steric stabilization by preventing attractive van der Waals forces between particles through osmotic pressure and elastic recoil effects [174].

Zeta potential measurements were also compared in different media (Table 4.1). As also observed in normal saline solution and PBS, there is a decrease in the magnitude of the zeta potential in DMEM as compared to diH_2O, which is in agreement with observations in previous reports with various cell culture media [171,175,176]. This can similarly be explained by screening due to the increase in ionic strength. Despite having similar osmolarities, there does appear to be additional screening effects in DMEM as there is a greater decrease in the absolute value of the zeta potential. This can be partially explained by the presence of multivalent ions in DMEM. Based on DLVO theory, the Schulze-Hardy rule states that increasing ion valency increases the electrostatic screening effect [174,177], resulting in a more neutral zeta potential compared to normal saline solution and PBS which contains only monovalent ions. However, other factors can also be at play due to the many compositional differences between these solutions.

For particles with a negative zeta potential, addition of serum proteins results in a reduction in the absolute of the zeta potential [165,178–180]. While a slight decrease may be observed from our results, with a zeta potential of -12.0 ± 0.5 mV and -12.1 ± 1.5 mV for Ca-polyP and Sr-polyP respectively, there is no significant difference between DMEM compared to DMEM supplemented with 10% FBS, which has also been similarly reported by others [171]. Importantly, Müller et al. (2018) corroborates our results, demonstrating that the zeta potential of Ca-polyP significantly decreases towards a more neutral surface charge in DMEM with 10% FBS, and is comparable to

Table 4.1 – Zeta potential of sonicated polyP-based particles in various media. Data are presented as averages ± standard deviation for n ≥ 3 experiments.

Medium	Zeta Potential [mV]	
	Ca-PolyP	**Sr-PolyP**
diH_2O	-22.7 ± 3.2	-21.5 ± 2.6
Normal Saline Solution	-16.1 ± 1.0	-17.4 ± 1.0
PBS	-13.7 ± 1.6	-14.9 ± 3.8
DMEM	-13.2 ± 2.5	-12.9 ± 0.8
DMEM + 10% FBS	-12.0 ± 0.5	-12.1 ± 1.5
10% Synovial Fluid	-21.8 ± 0.5	-19.9 ± 1.1

the values observed for our particles [82]. To confirm the effect of serum protein adsorption on the zeta potential, it would be necessary to perform readings in diH_2O supplemented with 10% FBS to minimize the already established effects of ionic strength on zeta potential as seen in normal saline solution, PBS, and DMEM. However, this would not necessarily lead to results independent of ionic strength, given that FBS is also an isosmotic solution. A 10% FBS solution in diH_2O would have a similar osmolarity to 0.09% w/v NaCl (or 0.1X normal saline solution), which was found to be sufficient enough to affect the zeta potential (Figure 4.5, C – D). Another alternative would be to utilize a serum protein such as BSA, which is abundant in FBS and can be prepared in the absence of ions. Regardless, it may be stated that FBS supplementation has negligible effects on the zeta potential when used in the presence of cell culture medium such as DMEM.

Müller et al. (2018) also demonstrated that Ca-polyP particles may be transformed into a coacervate state in the presence of serum, observed through a significant decrease in the absolute value of the zeta potential similar to that measured of Ca-polyP coacervate after 10 and 30 minutes of incubation in DMEM with 10% FBS [82]. However, it has been established that our polyP-based particles behave differently, as observed from the notable difference in the zeta potential. Furthermore, the size stability of the particles in DMEM with 10% FBS does not suggest a loss of particles into a coacervate phase. To verify this, a preliminary test was performed to measure the zeta potential of Ca-polyP and Sr-polyP following a much longer incubation of 24 hours in DMEM supplemented with 10% FBS at 37°C, which better reflects the amount of time the particles are in the culture media during in vitro cell culture experiments. No observable differences in the zeta potential were measured from this study (data not shown), suggesting that Ca-polyP and Sr-polyP remain as particles in the presence of serum. Again, this difference in behaviour is likely attributed to differences in the particle synthesis protocols.

Synovial fluid is rich in proteins, containing approximately 19 to 28 mg/mL in humans [181]. Comparatively, DMEM with 10% FBS supplementation has a much lower protein content, containing between 3 to 4.5 mg/mL [174]. Furthermore, serum albumin is the primary protein in both synovial fluid and FBS, each containing approximately 12 mg/mL [181] and 3.3 mg/mL [174] respectively. While synovial fluid has been reported to be hyperosmolar, having an osmolality of 404 ± 57 mmol/kg in healthy patients at rest [182,183], more typical osmolality values (comparable to blood serum) are reported in patients suffering from OA at 297 ± 17 mmol/kg [182] and post-exercise at 301 ± 19 mmol/kg [183]. These differences in osmolarity and composition may impact the stability and charge of the particles.

To verify the feasibility of these particles in a more physiologically relevant environment, characterization was performed in synovial fluid. However, manipulation of synovial fluid is technically challenging due to its high viscosity, and particulates within the synovial fluid may interfere with DLS measurements. Therefore, synovial fluid was first digested with hyaluronidase, which breaks down the dense hyaluronic acid network, allowing for more ease of use [184]. Subsequent clarification was then performed by centrifugation and filtration to remove cell debris and protein aggregates. As synthesized and sonicated Ca-polyP and Sr-polyP particles were stored in 10% synovial fluid, incubated at 37°C, and DLS was performed over 4 days (Supplementary Figure 2). The results suggest that the particles may be unstable under these conditions given that the size of sonicated particles increase, while the size of as synthesized particles decrease over time. However, it is possible that digestion by hyaluronidase may affect these results, given that hyaluronic acid is highly abundant in synovial fluid at 1 – 4 mg/mL [185]. Therefore, any possible interactions between hyaluronic acid and the particles will be hidden. It is also possible that the viscosity affects interactions between the particles and synovial fluid. Furthermore, depending on

its affinity and interactions with the particle surface, the addition of hyaluronidase may influence the results. However, more work needs to be done to characterize the stability of these particles in synovial fluid to confirm size stability following intra-articular injection into the joint.

4.1.7 Physicochemical Characterization Summary

Both Ca-polyP and Sr-polyP particles have been characterized to be within a nanoscale size and exhibit a negative surface charge. Interestingly, the pH of the solution has been found to have a profound effect on particle size stability and zeta potential. However, these polyP-based particles have poor size stability under physiologically relevant conditions, agglomerating in cell culture medium as a result of the high ionic strength. Supplementation with 10% FBS successfully allows for improved colloidal stability, likely as a result of protein adsorption onto the particle surface which prevents agglomeration. As a result, these particles may be applied for in vitro cell culture experiments.

4.2 Identification of Cationic Molecules as Potential Surface Coatings

As AC has a highly fixed negative charge due to the abundance of GAGs, it has been proposed that positively charged particles would facilitate drug delivery into AC [45]. PolyP-based particles were incubated in varying concentrations of CTAB (Figure 4.7), chitosan (Figure 4.8), linear PEI (Figure 4.9), and branched PEI of different MW (Figures 4.10 and 4.11), and both the size stability and zeta potential were evaluated. These data show that the cationic surface coatings generally improve the size stability of both Ca-polyP and Sr-polyP. All cationic molecules reduced agglomeration of Ca-polyP, with the exception of the low and medium MW branched PEIs. This was also observed with Sr-polyP, with the addition of chitosan also failing to improve the size

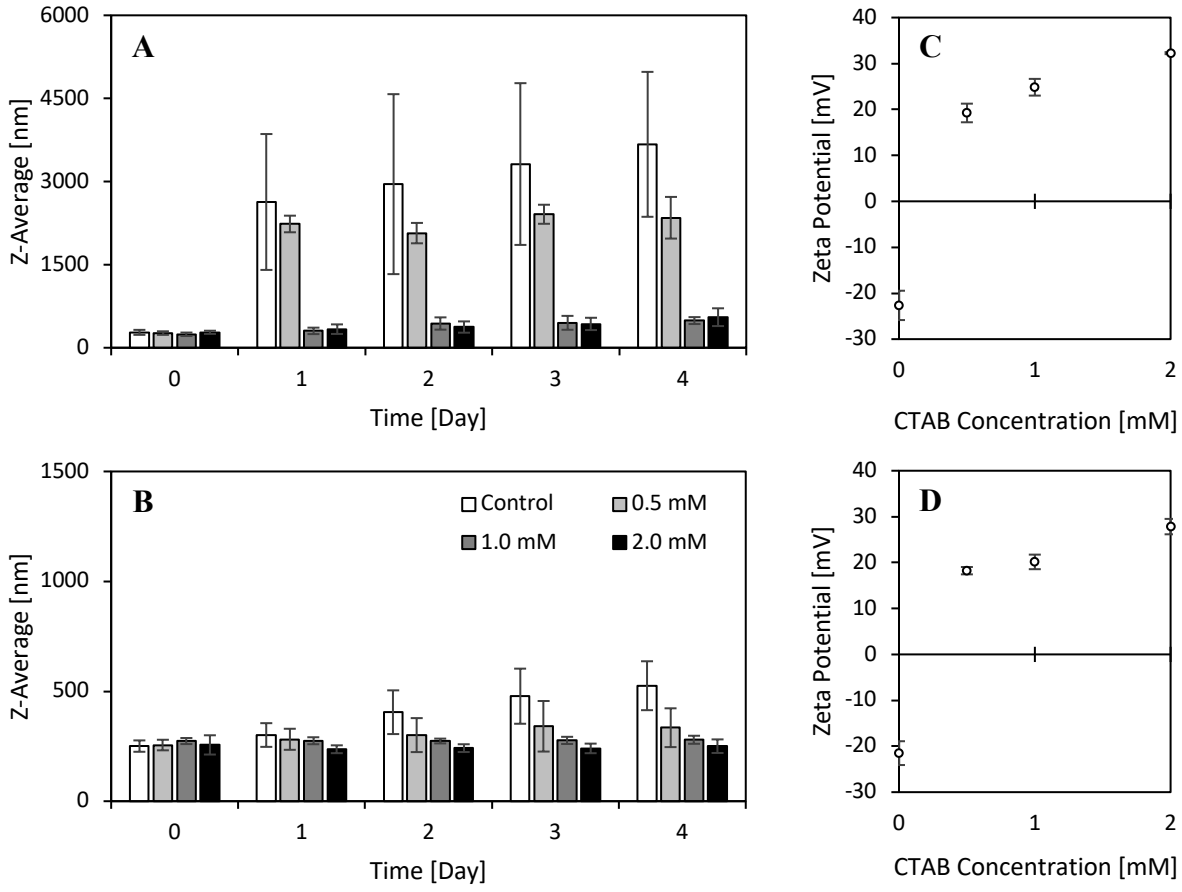

Figure 4.7 – Effect of CTAB on particle size and surface charge. PolyP-based particle size and the zeta potential were measured in varying concentrations of CTAB for **(A)** Ca-polyP and **(B)** Sr-polyP particles. Measurements were performed every day for 4 days to assess size stability. Zeta potential was also measured for sonicated **(C)** Ca-polyP and **(D)** Sr-polyP particles at varying CTAB concentrations. Data are presented as averages ± standard deviation for $n \geq 3$ experiments.

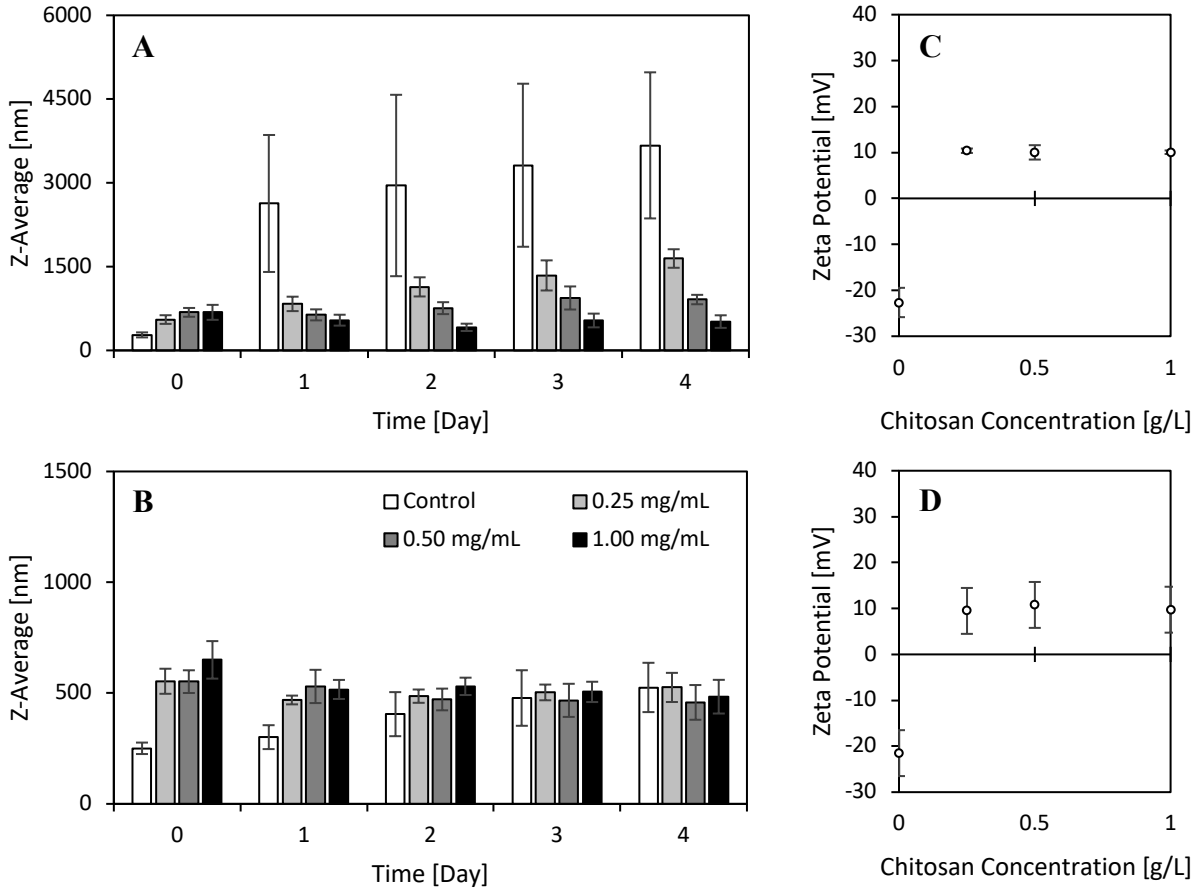

Figure 4.8 – Effect of chitosan on particle size and surface charge. PolyP-based particle size and the zeta potential were measured in varying concentrations of chitosan for **(A)** Ca-polyP and **(B)** Sr-polyP particles. Measurements were performed every day for 4 days to assess size stability. Zeta potential was also measured for sonicated **(C)** Ca-polyP and **(D)** Sr-polyP particles at varying chitosan concentrations. Data are presented as averages ± standard deviation for $n \geq 3$ experiments.

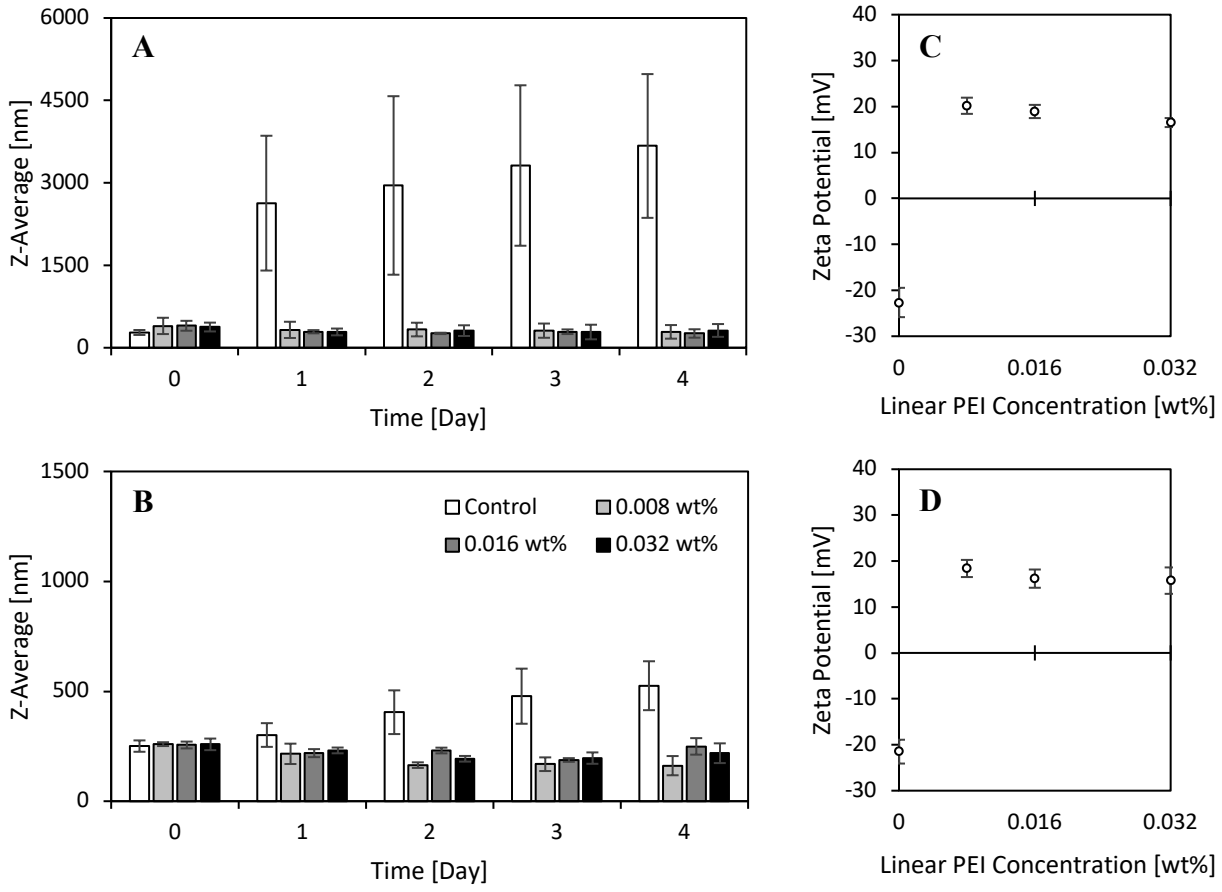

Figure 4.9 – Effect of linear PEI on particle size and surface charge. PolyP-based particle size and the zeta potential were measured in varying concentrations of linear PEI for **(A)** Ca-polyP and **(B)** Sr-polyP particles. Measurements were performed every day for 4 days to assess size stability. Zeta potential was also measured for sonicated **(C)** Ca-polyP and **(D)** Sr-polyP particles at varying linear PEI concentrations. Data are presented as averages ± standard deviation for n ≥ 3 experiments.

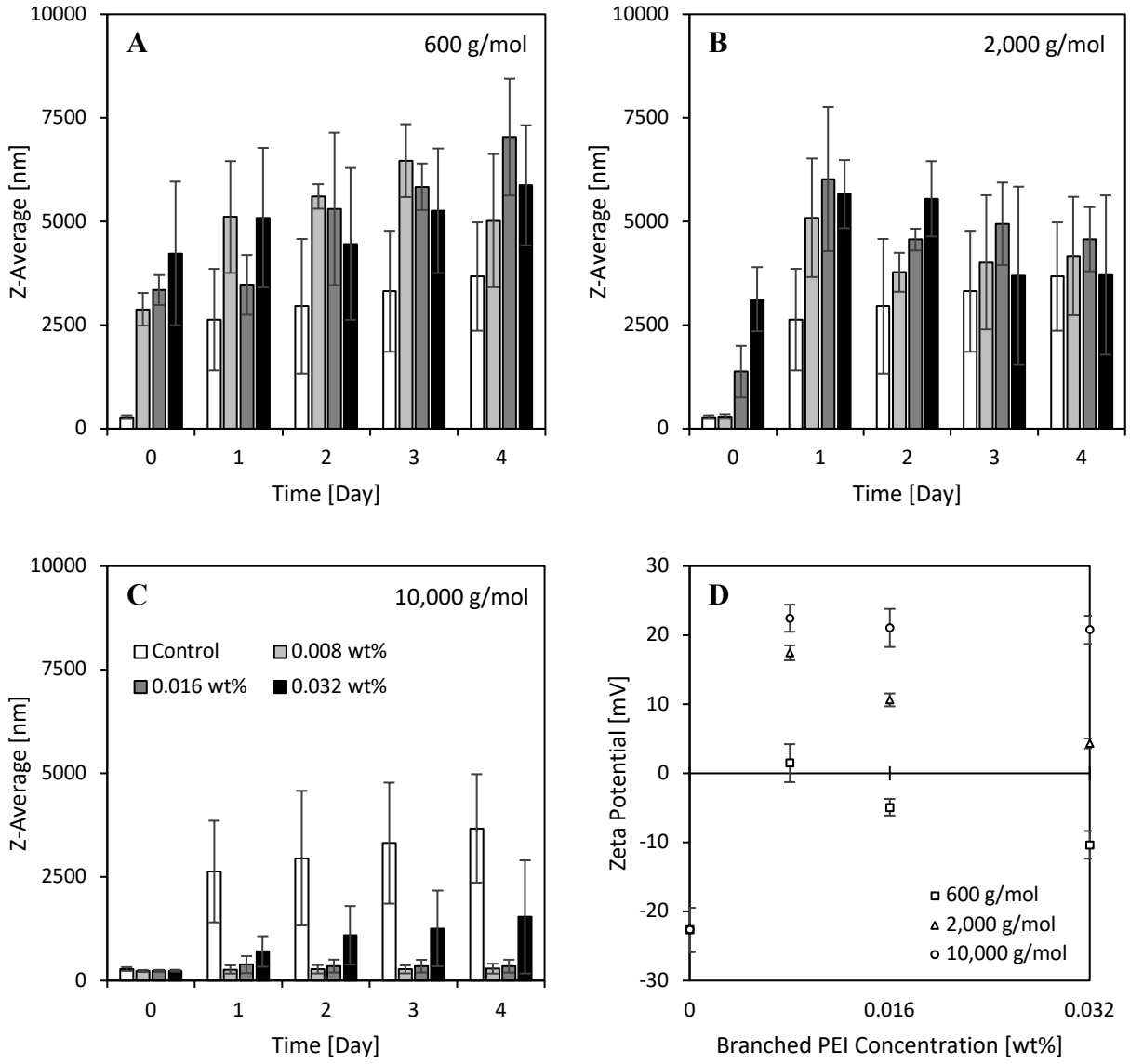

Figure 4.10 – Effect of branched PEI on Ca-polyP particle size and surface charge. Sonicated Ca-polyP particle size was measured by DLS in varying concentrations of branched PEI having an average molecular weight of **(A)** 600, **(B)** 2,000 and **(C)** 10,000 g/mol. Measurements were performed every day for 4 days to assess size stability. **(D)** Zeta potential was also measured at the varying concentrations of branched PEI of different molecular weights. Data are presented as averages ± standard deviation for $n \geq 3$ experiments.

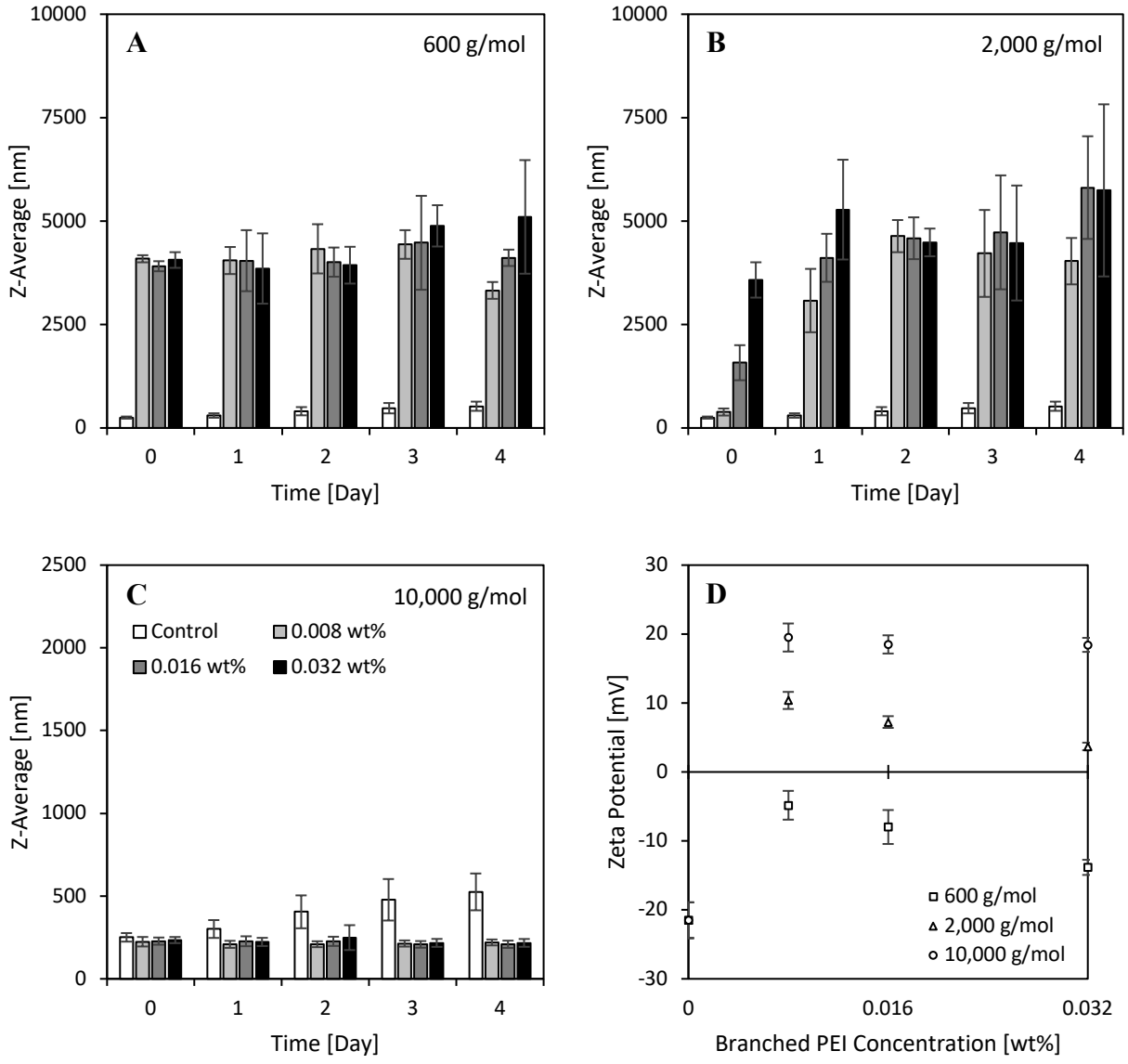

Figure 4.11 – Effect of branched PEI on Sr-polyP particle size and surface charge. Sonicated Sr-polyP particle size was measured by DLS in varying concentrations of branched PEI having an average molecular weight of **(A)** 600, **(B)** 2,000 and **(C)** 10,000 g/mol. Measurements were performed every day for 4 days to assess size stability. **(D)** Zeta potential was also measured at the varying concentrations of branched PEI of different molecular weights. Data are presented as averages ± standard deviation for $n \geq 3$ experiments.

stability of Sr-polyP but it did not increase agglomeration in the long term either. All cationic molecules successfully induced a positive surface charge at all concentrations tested, except for low MW branched PEI, as indicated by the zeta potential measurements.

The poor results observed with low MW branched PEI may possibly be attributed to the zeta potential. As mentioned, a zeta potential greater than +30 mV or lower than -30 mV typically results in a stable colloid due to the electrostatic repulsive forces to prevent agglomeration [137,138]. However, low MW branched PEI led to a more neutral zeta potential, suggesting a loss of electrostatic repulsion. Furthermore, compared to the high MW branched PEI, there may not be sufficient steric effects to prevent particle agglomeration. This can similarly be the cause for medium MW branched PEI failing to prevent agglomeration despite having a relatively positive zeta potential. Meanwhile, the high MW branched PEI has the most positive zeta potential of the three tested and would have improved steric hindrance due to being a bulkier polymer. Therefore, both the low and medium MW branched PEIs were not investigated further.

Despite some success, both CTAB and chitosan were also ruled out as possible candidates as surface coatings. Given that CTAB is a cationic surfactant, it has been demonstrated to be quite cytotoxic due to interfering with the cell membrane and facilitating cell lysis [186–188]. It was also thought that due to only possessing a single positive charge, the ionic binding stability to the polyP-based particles would be weak, potentially resulting in poor CTAB retention following washes. Meanwhile, despite chitosan being a polycationic carbohydrate, the amino groups have a pK_a of approximately 6.5, which requires the pH to be at or below 6.5 to dissolve in aqueous media and have a sufficient positive charge [189]. This makes chitosan very difficult to work with, and potentially incompatible due to being much more acidic than the physiological pH. Furthermore,

polyP is susceptible to hydrolysis under acidic media [190], making chitosan unsuitable for our application.

Therefore, only linear PEI and the high MW branched PEI were subsequently tested as cationic surface coatings. As PEI tends to exhibit some cytotoxicity [191–193], it is desired to wash the particles following coating to remove any excess PEI prior to application to biological systems. Preliminary tests using linear or branched PEI indicated poor retention on the particle surface following washing with diH_2O, as suggested by a near-neutral zeta potential (data not shown). While the less negative zeta potential than uncoated polyP-based particles suggest some retention of the PEIs on their surface, the goal was to obtain a positively charged surface rather than a less negative surface. Furthermore, due to the near-neutral zeta potential, this resulted in a loss of electrostatic repulsion, and probe sonication subsequently failed to properly disperse the particles and instead resulted in immediate agglomeration (data not shown). Incorporation of linear or branched PEI during the synthesis of the nanoparticles was also attempted to test the idea that PEI chains may become partially embedded within the particle, which would improve stability of the surface coating; however, similar results were obtained following washing, with a near-neutral zeta potential and inability to disperse the particles via sonication (data not shown).

Therefore, it is thought that ionic interactions are insufficient for surface coatings of these particles. It may be required to improve the binding stability of these cationic molecules to the surface, such as through covalent modifications. The terminal phosphates of polyP may be coupled with primary amines via a 1-ethyl-3-(3-dimethylaminopropyl)carbodiimide (EDAC)-mediated reaction [194–196]. Choi et al. (2010) successfully utilized this EDAC-mediated chemistry to couple polyP with a variety of molecules, including immobilizing polyP onto PEI-coated surfaces [194], demonstrating the potential to coat these polyP-based particles with PEI or other amine-

containing compounds. This also adds the potential for modulating the surface of the particles by conjugation of bridging molecules to add additional reactive moieties, including peptides [196]. However, as the reaction occurs only on the terminal phosphates, this relies on the assumption that the terminal phosphates will be enriched at the surface of the particle, at sufficient levels to endow a positive surface charge via EDAC-mediated coupling. Nonetheless, this opens many possibilities outside of simply changing the surface charge of the particle, as the biological activities of these particles can be modulated dependent on the chosen surface functionalization.

4.3 Biological Characterization in Chondrocytes and Cartilage Tissue

4.3.1 Cellular Uptake

To confirm the feasibility of applying these polyP-based particles for drug delivery applications, biological characterization was performed of their interactions with primary bovine chondrocytes. Firstly, the ability for chondrocytes to uptake these particles was tested via incubation with DAPI-stained polyP-based particles. Binding of DAPI to polyP shifts the fluorescence emission peak in the yellow-green spectrum, permitting the visualization of polyP from DNA and GAGs [100]. To ensure that only particles that were uptaken by chondrocytes were visualized, extracellular fluorescence was quenched with 0.1% trypan blue. Trypan blue has been demonstrated to quench green fluorescence, and as it is a vital dye, it is unable to pass through the cell membrane of viable cells, allowing for visualization of DAPI-stained particles localized intracellularly only [101,102]. Validation was performed on the DAPI-stained polyP-based particles alone, which confirmed visualization of the particles via fluorescent microscopy and the efficacy of trypan blue to quench the fluorescent signal of the particles entirely (Supplementary Figure 3).

Cellular uptake was confirmed through fluorescent microscopy (Figure 4.12). Images were taken after 1 minute of trypan blue incubation to ensure sufficient time to quench any extracellular fluorescence, and to minimize cell death which would result in intracellular quenching. As can be observed, chondrocytes were able to internalize both the as synthesized and sonicated polyP-based particles. No clear differences in cellular uptake are observed. However, due to the unreliability of fluorescent microscopy imaging for quantitative analysis, a comparison of cellular uptake cannot be made, and the results can only qualitatively demonstrate cellular uptake. To solve for this, protocols have been developed utilizing flow cytometry [197] and microplate-based assays [198] as quantitative methods for the measurement of cellular uptake of fluorescently labelled particles. Additionally, as can be observed from the fluorescence imaging, the nuclei are also labelled by DAPI. Since no DAPI was added to the cells for nuclear staining, this is a result of DAPI dissociating from the polyP-based particles. As this would also affect the quantification of the fluorescent signal, it may be necessary to conjugate the polyP-based particles to a fluorophore by EDAC-mediated end-group labelling [194,195].

Particles may be uptaken by cells through a variety of mechanisms and pathways, including phagocytosis and pinocytosis. Phagocytosis is a process which first relies on opsonization, where opsonins coat the surface of the particle. These opsonins physically bind to specific cell surface receptors, which results in assembly of actin filaments and protrusion of the cell membrane, which then engulfs and internalizes the particle into the phagosome. As a result, phagocytosis is typically done for larger particles above 500 nm in size [199–205]. While this process is primarily performed by professional phagocytes (such as macrophages, monocytes, or neutrophils) in response to pathogens, diseased cells, and foreign material, many cells (termed non-professional phagocytes) have some capacity to perform phagocytosis, including chondrocytes [206]. Pinocytosis may be

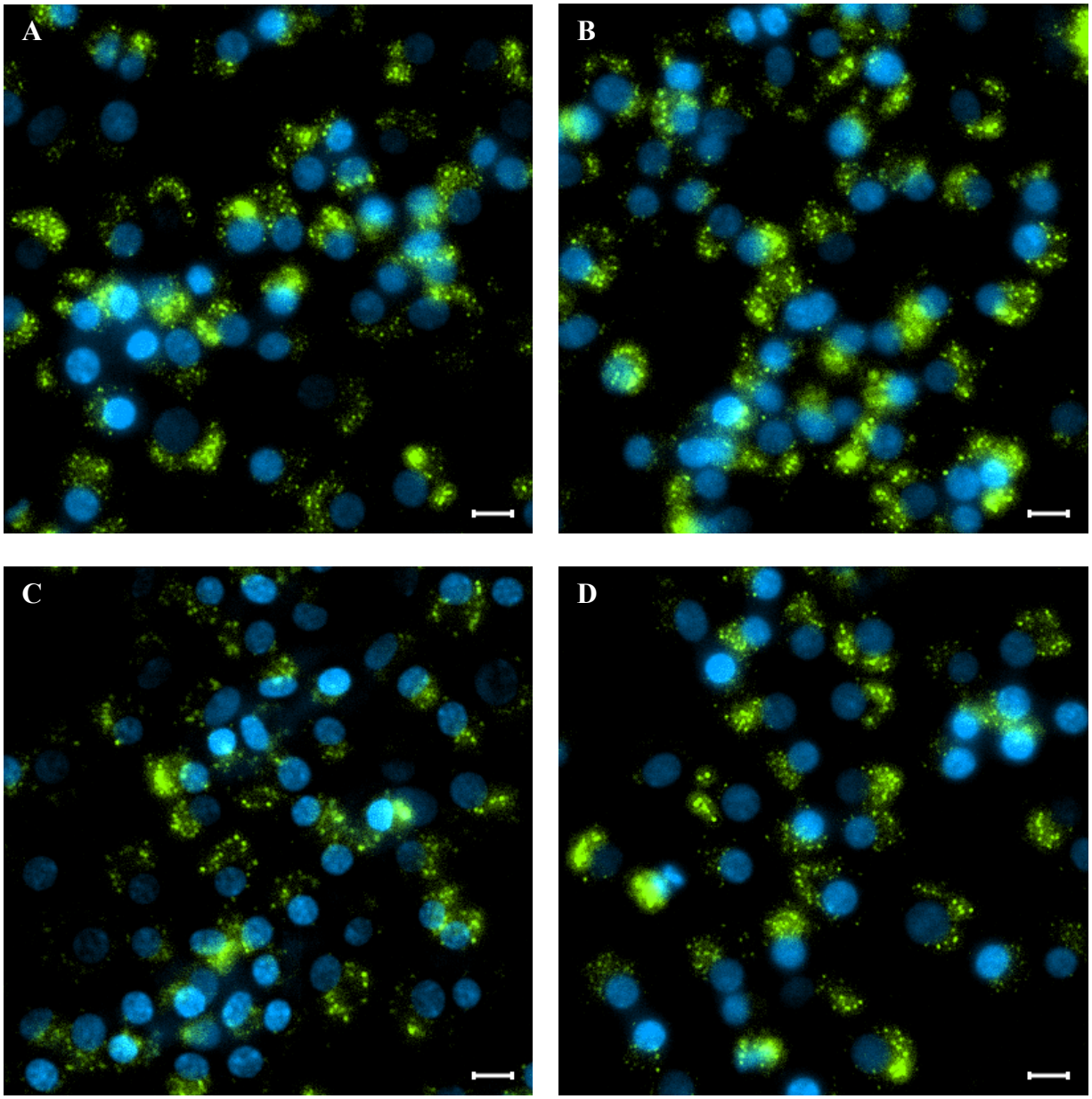

Figure 4.12 – Intracellular uptake of polyP-based particles. Primary bovine chondrocytes were treated with 100 μg/mL of DAPI-stained **(A)** Ca-polyP as synthesized or **(B)** sonicated and **(C)** Sr-polyP as synthesized or **(D)** sonicated for 24 hours. Extracellular fluorescence was quenched with 0.1% trypan blue prior to fluorescent imaging to confirm intracellular localization. Representative images for each condition have both nuclei (blue) and polyP-based particles (green) stained by DAPI. Scale bar = 20 μm.

divided into three main processes: macropinocytosis, clathrin-mediated endocytosis, and caveolin-dependent endocytosis. Macropinocytosis is another endocytic process which enables the uptake of large particles and can be done by almost all cell types. Like phagocytosis, macropinocytosis relies on forming cell membrane extensions from actin filaments. However, it is a non-specific process that is initiated by actin signalling as opposed to binding events on cell surface receptors [199–205]. Meanwhile, clathrin-mediated endocytosis involves the assembly of clathrin-coated pits on the cytosolic side of the cell membrane, which invaginates and pinches off to form clathrin-coated vesicles. Typically, this process involves uptake of smaller nanoparticles up to 100 nm in size. The process is initiated by binding of nanoparticle surface ligands to cell receptors [199–205], such as binding to low density lipoprotein receptor-related protein 1 (LRP1) in chondrocytes [207]. Caveolin-dependent endocytosis relies on flask-shaped, caveolin-coated plasma membrane invaginations known as caveolae. As the openings of caveolae are small, with estimates of 50 nm, this pathway is also limited to smaller nanoparticles [199–205]. Importantly, while caveolae are not present in all cell types, they are present on the cell membrane of chondrocytes [208].

It is likely that the process of phagocytosis is involved in cellular uptake of the larger, as synthesized polyP-based particles. Similarly, macropinocytosis may be important in the uptake of both the as synthesized and sonicated particles. Interestingly, observations have been made that negatively charged nanoparticles are often uptaken by cells via caveolin-dependent endocytosis [199,209–211], which may suggest this as a potential entry route for these polyP-based particles. However, studies are required to elucidate the exact mechanisms by which polyP-based particles are uptaken by chondrocytes. This can be done through inhibiting select cellular uptake pathways and measuring a decrease in particle uptake. However, much care is required in developing these experiments, as many of the typical inhibitors utilized are not specific to one pathway, and there

are no established or appropriate concentrations used with variations of up to 20,000-fold reported between studies [205]. Furthermore, as already discussed, more quantitative methods would be required to quantify particle uptake, which would be essential to confirm small decreases in uptake by inhibition of a single pathway.

Regardless of the uptake mechanism, all pathways ultimately lead to the endocytic system. Vesicles fuse with early endosomes to be trafficked intracellularly to the desired location. Early endosomes then mature to late endosomes, and eventually integrate with lysosomes, degrading the cargo which contains the particles [199–202,204,205]. In some cases, the particles may also escape the endocytic pathway to bypass lysosomal degradation [201–203]. However, in terms of the polyP-based particles, it has been well established that the endosomal environment is acidic, which may facilitate acid hydrolysis of polyP [190]. Therefore, it may be necessary to facilitate endocytic escape to minimize particle degradation during the intracellular trafficking process, and ultimately by lysosomes, for them to have a maximum therapeutic effect for drug delivery. One strategy involves the use of membrane-disrupting modifications to the particles to rupture the endosomes and release their cargo into the cytosol. This can be done by modifying the surface of the particles with PEI, cell-penetrating peptides, and by lipid fusion [204], which may be achieved by EDAC-mediated end-group labelling [194,196].

4.3.2 Cytotoxicity

Cytotoxicity of the polyP-based particles was evaluated through live-dead assays. After staining, the cells were imaged by fluorescent microscopy (Supplementary Figures 4 and 5), and the total number of live and dead cells were counted from five different images per condition (Figure 4.13). Three-way ANOVA demonstrates a significant effect of particle concentration ($p < 0.0001$) and

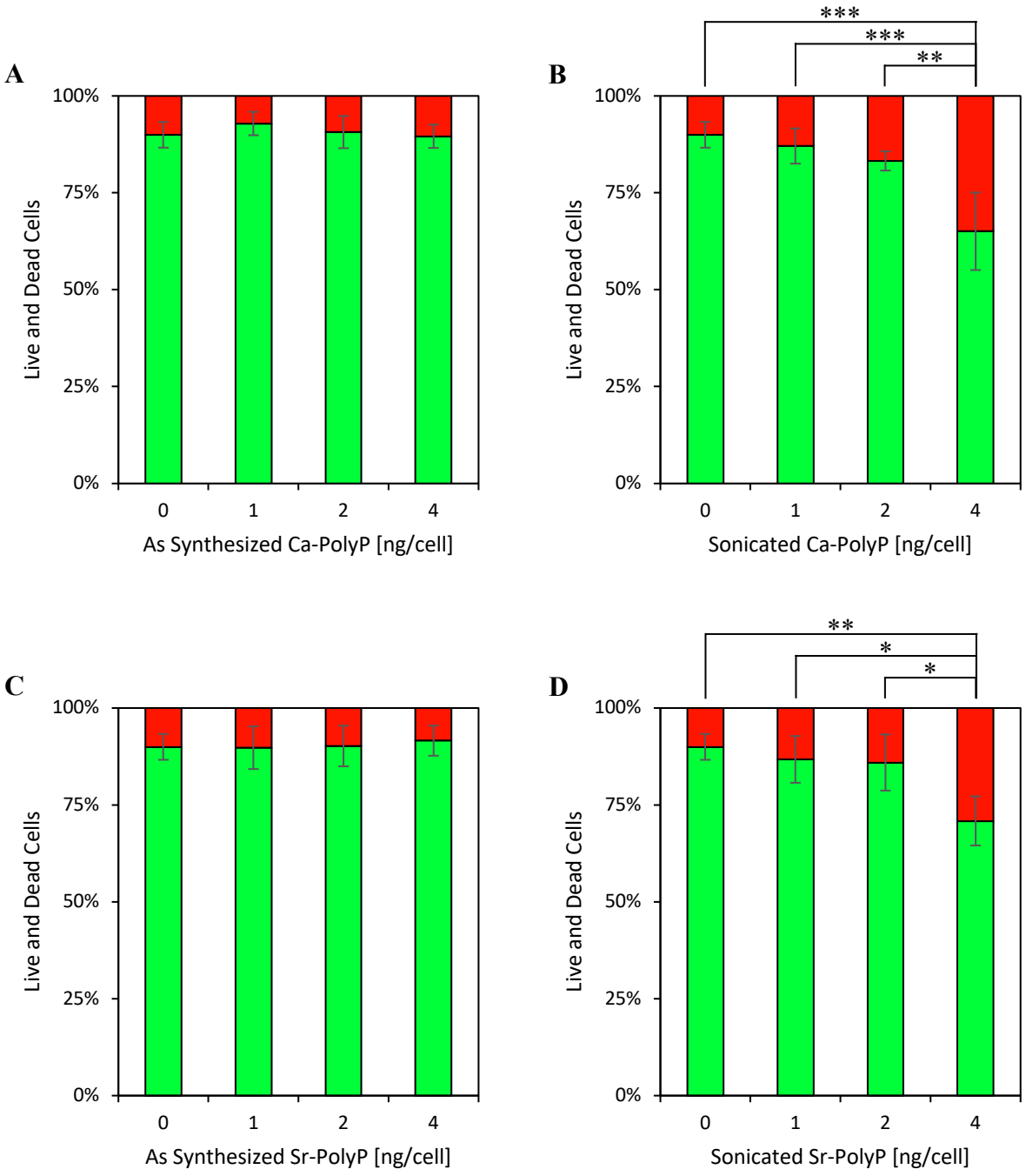

Figure 4.13 – Cytotoxicity of polyP-based particles. Primary bovine chondrocytes were treated with **(A)** Ca-polyP as synthesized or **(B)** sonicated and **(C)** Sr-polyP as synthesized or **(D)** sonicated at varying concentrations for 24 hours. Chondrocytes were incubated with calcein-AM (green) and EthD-1 (red) to stain live and dead cells respectively and imaged under fluorescent microscopy. Data are presented as averages ± standard deviation for n = 4 biological replicates. Significance is defined as $p < 0.05$ (*), $p < 0.01$ (**), and $p < 0.001$ (***).

sonication ($p < 0.0001$) on chondrocyte viability. As can be observed, there appears to be both a concentration-dependent and size-dependent cytotoxicity exhibited by the particles. While there are no significant differences in cell viability for the as synthesized Ca-polyP and Sr-polyP particles, the sonicated particles appear to have appreciable cytotoxic effects. Interestingly, no significant cell death is observed at 1 or 2 ng/cell compared to the control for both sonicated Ca-polyP and Sr-polyP. However, as the concentration increased to 4 ng/cell, significant differences are observed between the 4 ng/cell condition compared with all other conditions. The control group had an average cell viability of 90.0 ± 3.3%, while chondrocytes treated with either sonicated Ca-polyP and Sr-polyP at 4 ng/cell exhibited a cell viability of 65.1 ± 10.0% and 70.9 ± 6.3% respectively. This level of cytotoxicity is not unexpected, given that the mass of a mammalian cell is estimated to be 3 – 4 ng [212], which is roughly equivalent to the mass of particles applied per cell.

As no cytotoxic effects are observed at all concentrations for the as synthesized particles and knowing that cellular uptake occurs for all conditions (Figure 4.12), it is unlikely that the composition of the particle is at play. However, as particle uptake has not been quantified between conditions, it is possible that the smaller, sonicated particles are internalized more readily, resulting in potential cytotoxic effects due to an increased dosage. Therefore, it is possible that cytotoxicity is related to increased release of either polyP or the counterions. As discussed previously, the fate of nanoparticles following endocytic uptake ultimately ends with lysosomal degradation. This may cause a surge of free polyP or free cations in the cell. As the environment of the endosome and lysosome is acidic, this would also facilitate degradation of polyP into inorganic phosphates, which may influence cytotoxicity [213–215]. Similarly, altering calcium homeostasis by addition of Ca-polyP could potentially affect cell viability [216]. However, if this were the case, as no significant

differences are observed between the cytotoxicity of Ca-polyP and Sr-polyP, this makes polyP or inorganic phosphate the likelier candidates.

It has been well established that smaller nanoparticles typically exhibit greater cytotoxic effects [217–219], with multiple studies reporting a decrease in cell viability for smaller particles and at higher particle concentrations [176,220–225]. However, many studies have also reported size-dependent trends that differ from this. Pan et al. (2007) observed size-dependent cytotoxicity in gold nanoparticles, however there appeared to be an intermediate size (1.4 nm) that resulted in the greatest cytotoxicity, with smaller and larger particles being less cytotoxic [226]. Meanwhile, Bayal et al. (2019) highlights an increase in cytotoxicity at increasing sizes of ZnS nanoparticles [227]. Some studies have also indicated inconclusive results regarding size-dependence [228,229], as well as significantly different responses between different cell types [230]. Overall, this supports the idea that size-dependence of nanoparticle cytotoxicity can be highly variable, depending on the particle composition, material, and the cell type studied. Regardless, there is strong rationale which explains the cytotoxicity of smaller nanoparticles. Decreasing the particle size results in a greater surface area, which presents a larger contribution of the surface atoms as compared to the bulk material. As interactions with cellular components and nanoparticles occur at the surface, the potential for unwanted interactions will increase [231]. This can be of great concern, given that nanoparticles may be of similar scale to biomacromolecules, such as proteins (~2 – 10 nm), DNA (~2 nm) and cell membranes (~10 nm), which facilitates these undesired interactions [232]. Furthermore, smaller nanoparticles will also more accessibility to areas within the cell. For example, Huo et al. (2014) identified that gold nanoparticles smaller than 10 nm may enter the nucleus of cells [233], providing opportunities for off-target effects. In fact, as mentioned in the study performed by Pan et al. (2007), gold nanoparticles having a size of 1.4 nm exhibited the

greatest cytotoxicity compared to all other sizes [226], and this has been attributed to interactions with the major groove of DNA resulting in inhibition of transcriptional processes [234].

4.3.3 Cell Proliferation

The EdU cell proliferation assay was similarly performed on primary bovine chondrocytes treated with varying concentrations of as synthesized or sonicated Ca-polyP or Sr-polyP particles, and cells were counted from five images per condition (Supplementary Figures 6 and 7). Due to the variability of proliferating cells between biological replicates, the percentage of proliferating cells was normalized to the control samples (Figure 4.14, A – B). Three-way ANOVA indicates a significant effect of particle concentration ($p < 0.001$) and sonication ($p < 0.0001$) on chondrocyte proliferation. As can be seen, while the as synthesized particles have little effect on cellular proliferation, the sonicated particles resulted in a significant decrease in cell proliferation at 50 μg/mL and 100 μg/mL for Ca-polyP and at all concentrations of Sr-polyP compared to the control. Furthermore, there appears to be a slight concentration-dependent effect, with a greater reduction in cell proliferation as the particle concentration is increased. However, this is only significant between 25 μg/mL and 100 μg/mL of sonicated Sr-polyP ($p < 0.05$). Additional work to confirm that a reduction in cell proliferation ultimately leads to reduced cell numbers would be required over a longer culture period.

St-Pierre et al. (2012) demonstrated that treatment of chondrocytes with 1 mM of polyP resulted in significant decrease in DNA content of the in vitro grown tissues at 2 and 4 weeks of culture. While the DNA content of non-treated tissues increased by over 125%, polyP-treated tissues exhibited a more modest increase of 75% [74]. Meanwhile, Gawri et al. (2022) observed minor decreases in the DNA content of tissues grown with 1 mM of polyP with or without 1.5 mM

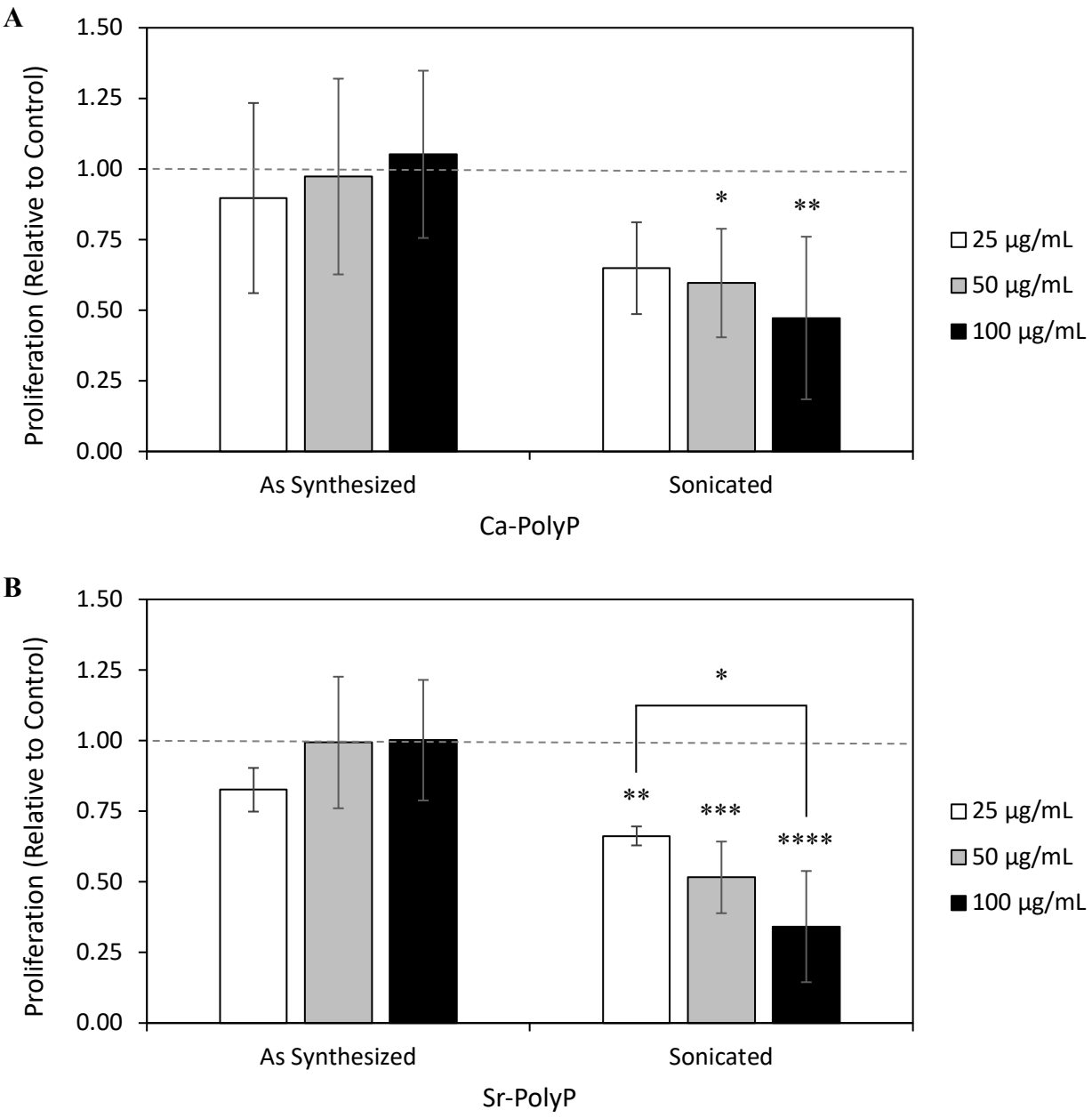

Figure 4.14 – Cell proliferation in response to incubation with polyP-based particles. Primary bovine chondrocytes were treated with **(A)** Ca-polyP and **(B)** Sr-polyP as synthesized or sonicated at varying concentrations for 24 hours. Cell proliferation was assessed by the EdU cell proliferation assay. Proliferating cells were labelled with an Alexa Fluor 488 azide and the total number of cells was characterized by nuclear staining with Hoechst 33342, imaged under fluorescent microscopy. Values were normalized to the control samples cultured in the absence of particles, represented by the dotted lines. Data are presented as averages ± standard deviation for n = 4 biological replicates. Significance is defined as $p < 0.05$ (*), $p < 0.01$ (**), $p < 0.001$ (***), and $p < 0.0001$ (****).

$CaCl_2$ supplementation after 2 weeks of culture [75]. Conversely, polyP increased proliferation in human and mouse fibroblast cells through the FGF signaling pathway [235], as well as in human breast cancer cell lines through mTOR signaling pathway [236]. Müller et al. (2015, 2018) performed an XTT assay on mouse calvaria cells and human mesenchymal stem cells treated with Ca-polyP particles and noted significant increases at a concentration of 30 μg/mL after 72 hours, suggesting an increase in cell viability and proliferation [78,83]. Similar findings in human mesenchymal stem cells were observed with Sr-polyP after 3 days of incubation [81]. However, differences in the response to polyP and polyP-based particles may be attributed to the cell type utilized, suggesting that polyP has cell-specific effects [74]. Overall, these results appear to be consistent from previous studies in chondrocytes; however, the mechanism at which polyP inhibits proliferation has not been identified.

4.3.4 Metabolic Activity

MTT assays were performed on primary bovine chondrocytes following incubation with varying concentrations of the as synthesized or sonicated Ca-polyP or Sr-polyP particles (Figure 4.15). Three-way ANOVA indicates significant effects of the cation type ($p < 0.05$), sonication ($p < 0.0001$), and particle concentration ($p < 0.0001$) on the metabolic activity. As can be observed, statistically significant decreases in metabolic activity were observed in almost all conditions compared to the control, suggesting that these polyP-based particles may have a biological effect on chondrocytes. However, the MTT assay has many critiques and limitations, which makes the interpretation of the results difficult [105]. In particular, the MTT assay is often used as a cell viability assay due to metabolic activity (or formazan production) correlating with cell numbers. While the results of the MTT assays are supported by the EdU assays, given that a decrease in cell

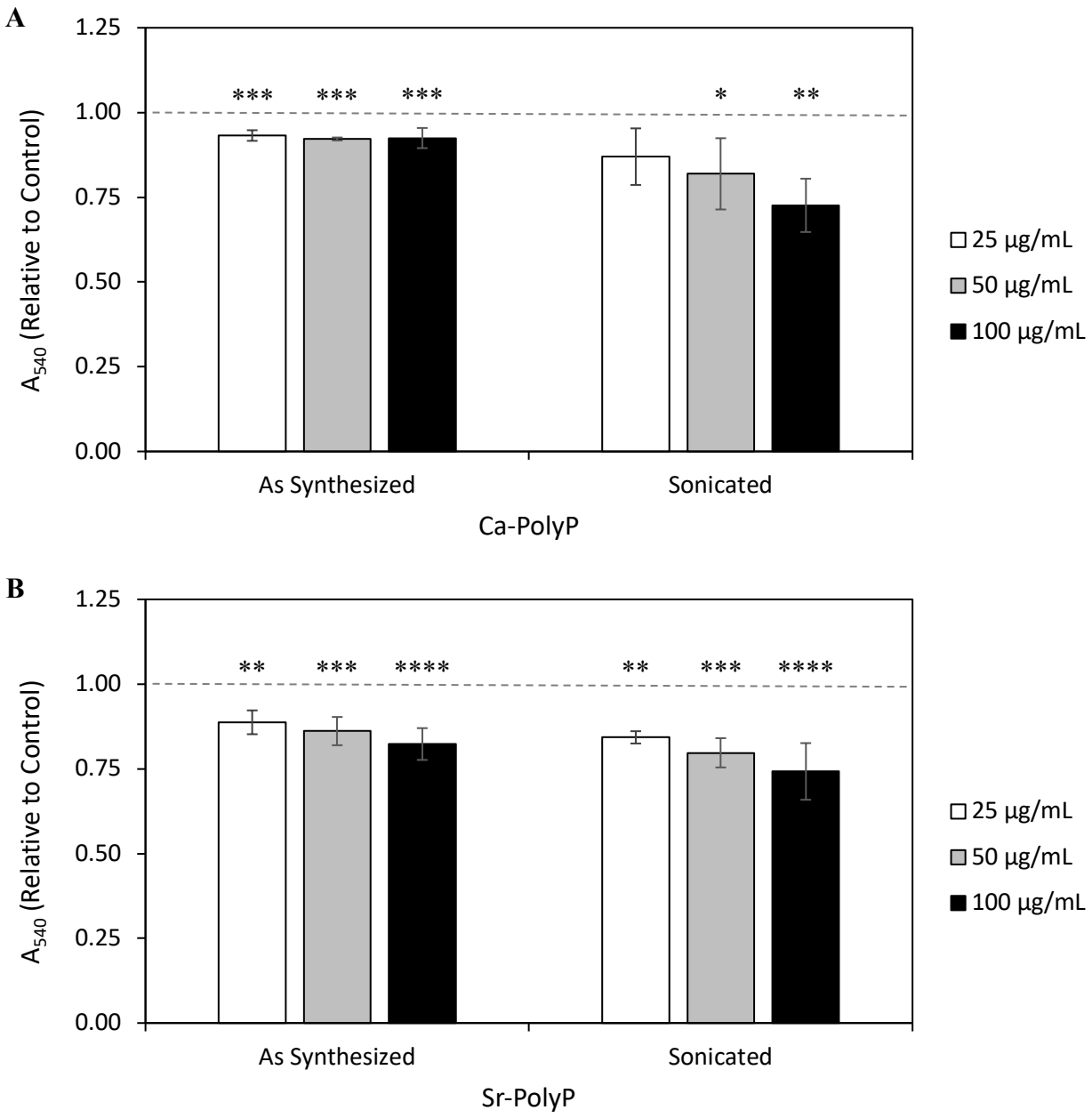

Figure 4.15 – Metabolic activity in response to incubation with polyP-based particles. Primary bovine chondrocytes were treated with **(A)** Ca-polyP and **(B)** Sr-polyP as synthesized or sonicated at varying concentrations for 24 hours. Metabolic activity was assessed with the MTT assay, and values were normalized to the control samples cultured in the absence of particles. Data are presented as averages ± standard deviation for n = 4 biological replicates. Significance is defined as $p < 0.05$ (*), $p < 0.01$ (**), $p < 0.001$ (***), and $p < 0.0001$ (****).

proliferation would also suggest a decrease in metabolic activity due to the energy demands of biosynthetic pathways for biomacromolecules required for cell growth [237], this can also lead to a decrease in cell numbers which may result in the decrease in formazan production. To discern whether this is attributed to a decrease in cell numbers, a decrease in the metabolic activity per cell, or a combination of these factors, additional experiments were performed in parallel.

DNA quantification was performed following identical culture conditions to that of the MTT assay as an estimate of cell numbers (Supplementary Figure 8). However, the results were found to be unreliable due to a high variability that was not seen in the MTT data. Furthermore, the estimated cell numbers from the DNA assay were consistently much lower than the expected 80,000 cells that were initially seeded, suggesting that there may have been potential issues with the procedure, most likely related to the DNA recovery process. To circumvent these issues, two other methods of validation were performed. Firstly, live-dead assays were similarly performed under identical culture conditions to the MTT assay (Supplementary Figures 9 – 11) to verify whether a decrease in formazan signal was due to a decrease in cell viability. This can be of concern due to the cytotoxic effects of high concentrations of polyP-based particles as observed previously (Figure 4.13). However, no significant differences in cell viability were observed for Ca-polyP and Sr-polyP, and at all particle concentrations under the conditions used for the evaluation of metabolic activity. The average cell viability of the control was 96.6 ± 2.1%, while the average cell viability of all the treated conditions combined (0.125 – 0.5 ng/cell) was 95.4 ± 0.3%. This also demonstrates that the particle mass per cell is more important than the particle concentration in solution, as the same particle concentrations (25 – 100 μg/mL) were used.

As an additional validation, the total cell numbers were counted from nuclear staining with Hoechst 33342 and normalized to the control (Supplementary Figures 12 and 13). On average, the

control wells contained 72,707 ± 8680 cells, while the average cell count of all treated conditions contained 71,204 ± 5821 cells, confirming negligible differences in cell numbers due to treatment with the polyP-based particles. Furthermore, while there may be some aspects that make these total cell counts unreliable, such as the loss of cells by accidental contact with the surface of the well (during media change, cell fixation, washing, and/or staining steps), the total cell counts all fall very closely with the 80,000 cells initially seeded unlike the DNA assays, suggesting these errors have minimal effects on the results, and can even be attributed to the inherent uncertainty of cell counting with a hemocytometer used for cell seeding. It should be noted that the culture conditions selected for these experiments cause limited chondrocyte proliferation, such that a cell number slightly below the seeding number at the timepoint investigated was expected. Overall, this supports the possibility of the MTT assay results suggesting a decrease in metabolic activity per cell.

PolyP has been implicated in having a major biological role on metabolic processes. Firstly, polyP is a polymer of phosphate residues linked by high-energy phosphoanhydride bonds, similar to those found in ATP [238], suggesting the potential for polyP as a means for energy storage. It is present in the cytosol, nucleus, lysosomes, and mitochondria of eukaryotic cells [239], and localization of polyP to the mitochondria implicates a functional role in metabolic processes. PolyP levels have been linked to mitochondrial activity, with decreased levels as a result of mitochondrial inhibition, and increased levels from supplementation of glutamine and pyruvate, both substrates of complex I, as well as supplementation of succinate, a substrate of complex II [240]. F_0F_1 ATP synthase and ATPase activity has also been proposed to be involved in the synthesis and hydrolysis of polyP respectively [241]. Additionally, altered levels of polyP have also been demonstrated to directly affect metabolic activity and processes. Depletion of mitochondrial polyP in HEK293 cells

via expression of exopolyphosphatase resulted in a metabolic switch, with a reduction in oxidative phosphorylation and elevated glycolysis activity, indicating that polyP may have a regulatory role in metabolic pathways [242]. Similarly, depletion of mitochondrial polyP in neuroblastoma cells resulted in dysregulation of mitochondrial physiology and bioenergetics [243]. Conversely, Müller et al. (2015) found that treating osteoblast-like cells with Ca-polyP particles resulted in an increase in the number of mitochondria, as well as an increase in intracellular and extracellular ATP levels [79]. While the exact mechanism for this observed decrease in metabolic activity because of Ca-polyP and Sr-polyP treatment can only be speculated, it is clear that polyP modulates metabolic activity in mammalian cells. This decrease in metabolic activity may be a compensatory response in chondrocytes by reducing endogenous polyP synthesis, especially given that the production of polyP has been linked to mitochondrial activity.

To better elucidate the bioactivity of these particles on the bioenergetics of chondrocytes, ATP assays were also performed following treatment of 100 μg/mL of polyP-based particles, given that this concentration had the highest effect on both cell proliferation and metabolic activity (Supplementary Figure 14). However, it was determined that the particles themselves have some level of interference with the assay, resulting in a decrease in luminescence (data not shown). While these results cannot be used quantitatively due to these technical issues, intracellular ATP levels were similarly reduced in chondrocytes treated with 0.5 mM and 1 mM of soluble polyP under the same culture conditions (data not shown), which has also been corroborated by others in murine preosteoblast cells [244]. It is possible that the reduction in luminescence may not solely be due to assay interference and can partially be attributed to an actual reduction in ATP levels. However, further work is required to validate this.

4.3.5 Cartilage Tissue Uptake

To determine the potential for these polyP-based particles to be utilized as a drug delivery carrier, preliminary experiments were performed to establish whether the particles may penetrate through AC. This was done by incubating bovine cartilage explants in a bath containing DAPI-stained particles and evaluating the change in fluorescence in both the cartilage tissue explants and solution, based on previously published studies for particle uptake in cartilage tissues [245–248]. After 3 days of incubation, cross-sections of the cartilage explants were imaged under fluorescent microscopy (Figure 4.16, A – E), and fluorescent profiles were measured across the depth of each cartilage tissue and compared to the control which was incubated in the absence of DAPI-stained particles (Figure 4.16, F – I). As can be seen, the fluorescent green signal is higher at all depths of cartilage for both the as synthesized and sonicated particles, and for both Ca-polyP and Sr-polyP, suggesting successful uptake of the particles into the cartilage.

To further validate these results, the fluorescent signal of the incubating bath was compared to an identical solution incubated in the absence of cartilage tissue to calculate the percentage of particles uptaken by the cartilage tissue explants from the original solution (Figure 4.17, A). An average percent uptake of 54.7 ± 3.1% and 53.0 ± 4.6% for the as synthesized Ca-polyP and Sr-polyP respectively, and 49.0 ± 6.3% and 49.5 ± 7.7% for sonicated Ca-polyP and Sr-polyP respectively, with no significant differences observed between conditions. Particle retention was also evaluated by incubating the cartilage explants in a fresh wash solution for 3 days. The fluorescent signal of the wash solution was then compared to the initial particle solution incubated in the absence of cartilage tissue to calculate the percentage of particle retention by the cartilage tissue explants based on the initial amount uptaken (Figure 4.17, B). Consistent with the results observed in particle penetration, no significant differences were observed between the conditions,

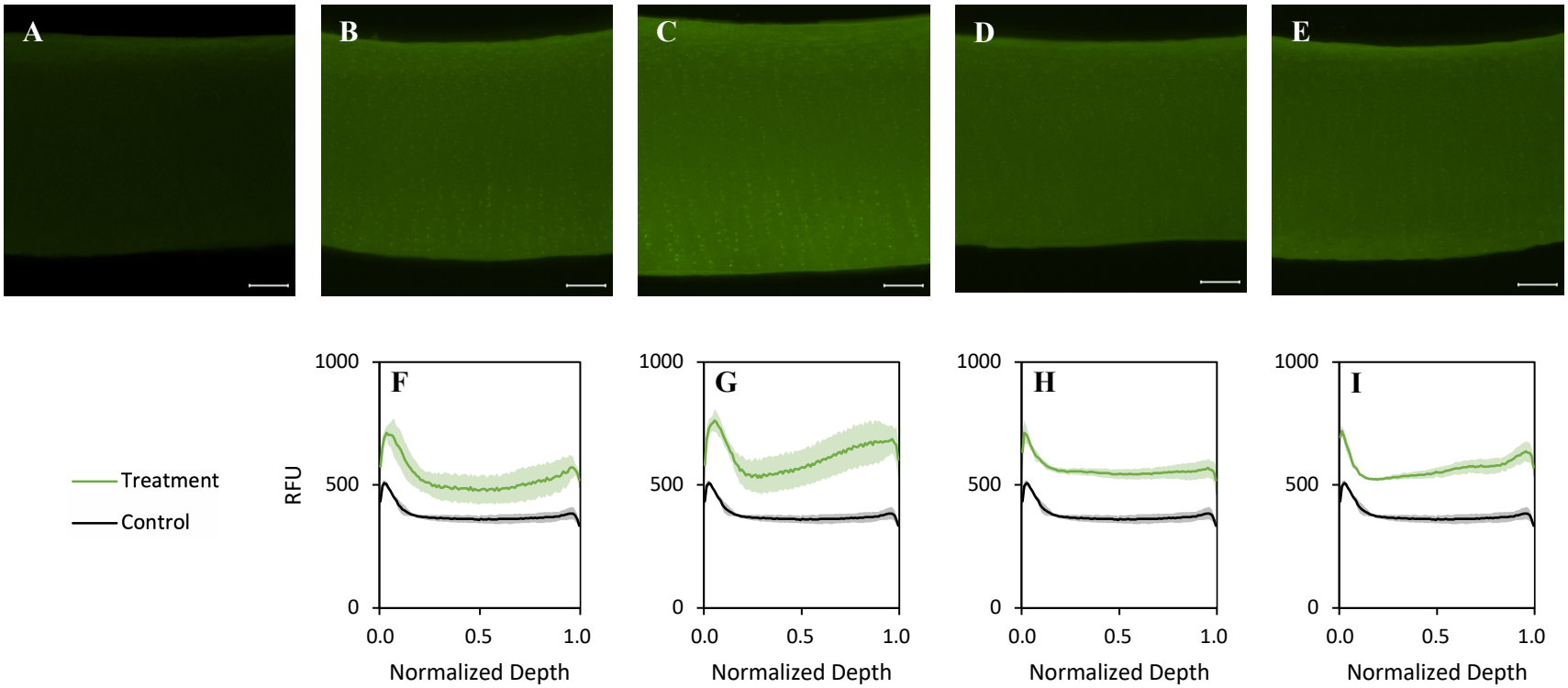

Figure 4.16 – Fluorescent microscopy of cartilage tissue explants incubated with polyP-based particles. Bovine cartilage explants punched into 6 mm diameter discs were incubated with 100 μg/mL of DAPI-stained particles (green) for 3 days on an orbital rocker at 37°C. Thin cross-sections of the cartilage incubated with **(A)** no particles as the control tissue, **(B, F)** Ca-polyP as synthesized or **(C, G)** sonicated, and **(D, H)** Sr-polyP as synthesized or **(E, I)** sonicated were imaged under fluorescent microscopy. Representative fluorescent profiles across the depth of cartilage were measured from three different regions of each cross-section and compared to the control tissue (the control profiles are reproduced in F – I). The normalized depth of "0" represents the superficial zone while the normalized value of "1" represents the deep zone. Data are presented as averages ± standard deviation of the three different regions. Scale bar = 100 μm.

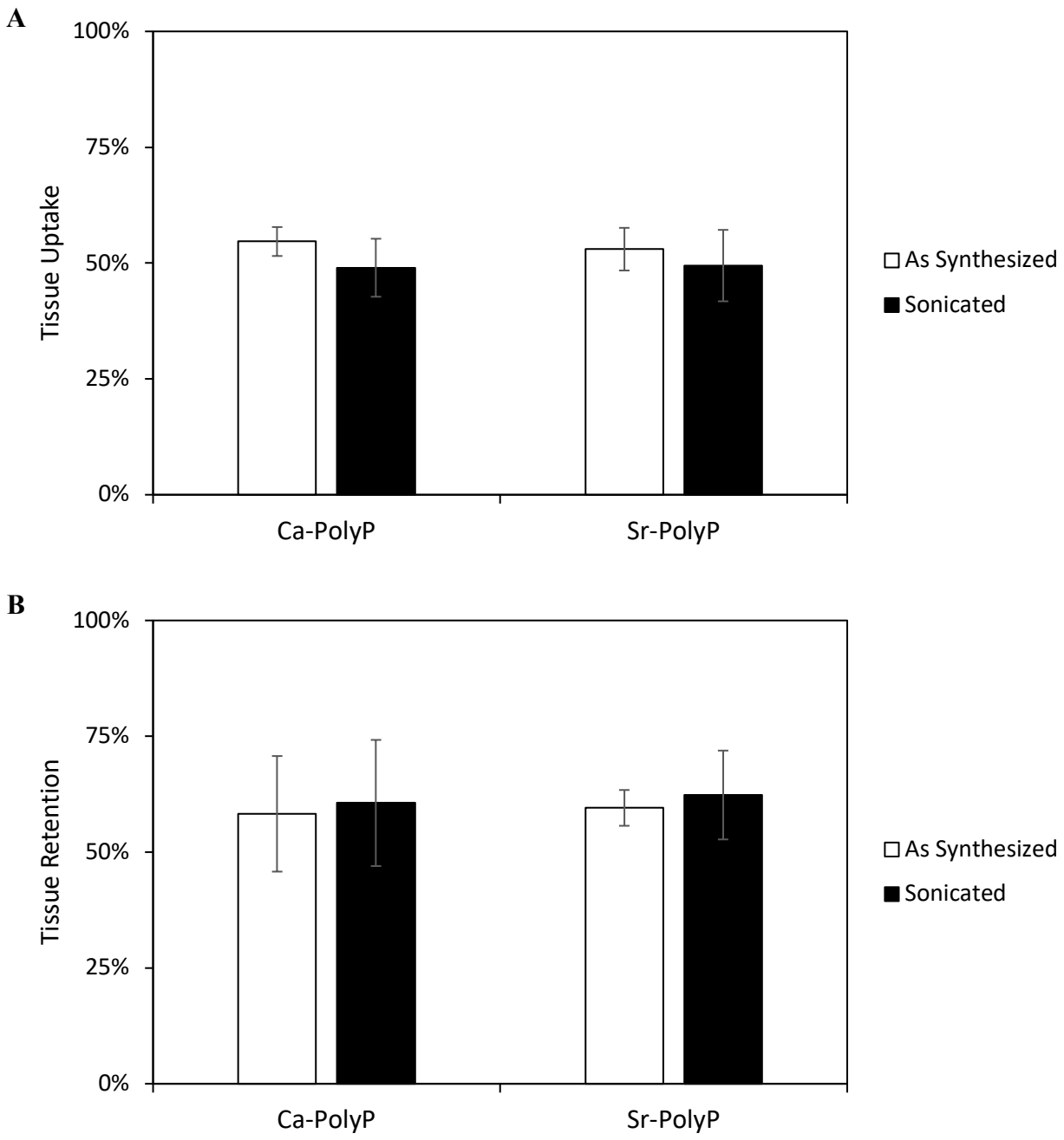

Figure 4.17 – Quantification of particle penetration and retention in cartilage tissue explants. Bovine cartilage explants punched into 6 mm diameter discs were incubated with 100 μg/mL of DAPI-stained particles for 3 days on an orbital rocker at 37°C. **(A)** Quantification of fluorescence decrease in solution, corresponding to particle uptake into the cartilage tissue, compared to the initial solution. **(B)** Cartilage explants were then subsequently incubated in the absence of particles and fluorescence in solution was quantified after an additional 3 days, corresponding to particle release, and compared to the amount of uptake prior to washing to determine particle retention. Data are presented as averages ± standard deviation for $n \geq 3$ biological replicates.

with an average percent retention of 58.3 ± 12.5% and 59.5 ± 3.9% for the as synthesized Ca-polyP and Sr-polyP respectively, and 60.6 ± 13.6% and 62.3 ± 9.6% for sonicated Ca-polyP and Sr-polyP respectively.

Both particle uptake and retention were much higher than expected. The wet weights of the explants were measured for each experiment, with an average mass of 21.2 ± 3.8 mg (Supplementary Table 2). Meanwhile, the thickness of the cartilage explants was measured to be 0.70 ± 0.09 mm from one experiment. Therefore, for a 6 mm diameter cylinder, the average volume of each cartilage explant may be estimated to be about ~20 μL. This matches very closely with the measured wet weights, as the density of AC may be assumed to be close to that of water (~1 mg/μL), as up to 80% of the wet weight of cartilage is attributed to water [1]. If particle uptake into the tissue was solely due to diffusion, incubating cartilage explants with an estimated volume of ~20 μL in 400 μL of solution would result in less than 5% of the particles entering the tissue. Therefore, this may suggest some preferential uptake into the tissue, despite the electrostatic repulsive forces between the negative surface charge of the polyP-based particles and the highly fixed negative charge of AC.

It is important to note that particle uptake is most likely overestimated of what can actually be expected in an in vivo context due to the limitations of the experiment. Firstly, as can be observed in the fluorescent images of the cartilage explants, there is no obvious sign of surface binding of the particles. However, these tissues were briefly rinsed in PBS, which may remove weakly bound particles prior to imaging. Meanwhile, the solution along with the cartilage explant was well mixed prior to measuring the fluorescence of the bath to remove surface-bound particles from the cartilage tissue. However, there is a very high chance that mixing is insufficient given the cartilage explant remained in the same solution, and re-adsorption would most likely occur rapidly.

Therefore, the decrease in fluorescence may be partially attributed to loss of particles from surface-binding as opposed to actual penetration into the tissue.

Secondly, an indirect method of quantification was used to quantify particle uptake, based on the loss of fluorescence measured, rather than directly measuring the loss of the particles in solution, which would be difficult to achieve. Dissociation of DAPI from the DAPI-polyP complex and into the cartilage tissue will also result in a decrease in fluorescent signal in the bath. This can be cause for concern given that DAPI binds to DNA and GAGs [100], both of which are abundantly present in cartilage tissue. This was observed in the cellular uptake experiment, in which DAPI from the particles stained the nuclei (Figure 4.12). To prevent this potential issue, EDAC-mediated end-labelling may be utilized to covalently link the polyP-based particles with a fluorophore [194,195].

Thirdly, as the entire cartilage explant is exposed in the solution, this does not represent the application of particles in vivo. While only the superficial surface of the cartilage would be exposed given that the deep zone of cartilage is interfaced with the subchondral bone, here both sides, as well as the edges, are exposed to solution. As a result, more particles would be entering the tissue due to an increased surface area of contact. Furthermore, as cartilage is anisotropic, the kinetics of particle uptake would be different entering through the deep zone, due to the differences in tissue structure and composition compared to the superficial zone. Therefore, further work to improve the method, in which only the superficial zone would be exposed, would be beneficial to validate that entry can occur through the superficial zone. However, this would be technically challenging to accomplish quantitatively. Qualitative assessment of particle penetration through the superficial zone can be performed with ex vivo studies on cartilage including underlying bone, or quantitatively using in vivo studies through intra-articular injection of the particles.

Lastly, it is important to note the potential for tissue damage and degradation over time. To obtain the cartilage explants, the cartilage tissue was excised using a scalpel blade, which may cause physical damage to the tissue, particularly at the deep zone where the cut is made. Similarly, damage made to the tissue at the circumferential edge of the explants from the biopsy punch may also occur. Any damage to the tissue could facilitate particle entry into the cartilage. Degradation of the cartilage tissue would also occur over the course of the incubation, especially given that the cartilage was maintained in PBS supplemented with 10% heat-inactivated FBS for 3 days when assessing particle uptake, and an additional 3 days for assessing particle retention. This does not contain the required nutrients to maintain the cartilage tissue over a long period of time, resulting in potential degradation of the ECM due to chondrocyte death [249]. An initial attempt was made using phenol-free DMEM instead of PBS, however due to the high background signal in the green fluorescence range, both fluorescent microscopy and microplate readings failed to discriminate the signal of DAPI-stained particles from the background signal of DMEM (data not shown). To circumvent this, proprietary medium designed specifically for fluorescent imaging has been demonstrated to have comparable background to that of PBS in the green fluorescence range [250], which can be used to maintain the tissues over the long incubation period.

On the contrary, the experiment may also underestimate particle uptake in a clinical context due to using healthy cartilage explants. As the proposed application of these particles is for the treatment of OA, it is expected that the target tissue would have some level of ECM degeneration or tissue defect which would facilitate particle entry. Conversely, this would also overestimate particle retention, given increased loss of particles will also occur. Similar studies have attempted to mimic OA-afflicted cartilage to better reflect this. For example, Brown et al. (2018, 2019) incubated cartilage explants with 0.2% collagenase for 30 minutes to partially digest collagen to

recapitulate the biomechanical properties of OA cartilage [246,247]. Meanwhile, Bajpayee et al. (2014) used either 0.1 U/mL of chondroitinase-ABC or 1 mg/mL of trypsin for 24 hours for GAG depletion [248]. Further work can be done using similar treatments to model the effect of OA on tissue penetration and retention.

4.3.6 In Vitro Tissue Culture

To evaluate the potential for these polyP-based particles to be used for cartilage tissue engineering applications and eventually in vivo, chondrocytes were cultured on inserts over 4 weeks in various cell culture media. After harvesting, the wet and dry weight, as well as the sGAG, collagen, and DNA content of the in vitro tissues were quantified (Tables 4.2 – 4.5). While the different media tested had a notable effect on ECM accumulation and chondrocyte proliferation of the tissues, the application of sonicated Ca-polyP and Sr-polyP had negligible effects for both. As such, these results conflict with previous studies done with soluble polyP which demonstrated a significant increase in sGAG content (normalized to DNA) at 2 and 4 weeks of culture, as well as a significant increase in collagen content (normalized to DNA) by 4 weeks of culture [74]. Further, these results also somewhat disagree with our results in 2D cultures, as cell proliferation was also expected to decrease as observed with the EdU assay (Figure 4.14).

There are many potential factors resulting in the negligible effects observed. In comparing to previous studies, the frequency of polyP delivery may have been too low to observe anabolic effects. St-Pierre et al. (2012) suggested that anabolic effects require continuous administration of polyP, as no significant differences were found at 4 weeks of culture when supplementing 1 mM of polyP for only the first 1 or 2 weeks of culture [74]. For our experiment, polyP-based particles were applied continuously, but only on a once per week basis (on days 0, 7, 14, and 21), where

Table 4.2 – 3D tissue cultures grown in high glucose DMEM supplemented with 10% FBS over 4 weeks. Data are presented as averages ± standard deviation of 3 individual tissue cultures for n = 1 biological experiments.

	Control	Ca-PolyP	Sr-PolyP
Wet Weight [mg]	56.8 ± 6.4	57.6 ± 8.3	51.3 ± 6.8
Dry Weight [mg]	3.3 ± 0.2	3.4 ± 0.3	3.3 ± 0.3
Water Content [%]	94.2 ± 0.3	94.1 ± 0.3	93.6 ± 0.4
sGAG [µg]	622 ± 107	617 ± 71	589 ± 82
Collagen [µg]	464 ± 90	472 ± 66	387 ± 69
DNA [µg]	33.7 ± 4.8	32.6 ± 4.2	33.6 ± 4.0
sGAG/DNA [µg/µg]	18.5 ± 2.2	19.2 ± 3.5	17.5 ± 0.4
Collagen/DNA [µg/µg]	13.8 ± 1.6	14.5 ± 0.5	11.6 ± 2.0
Collagen/sGAG [µg/µg]	0.745 ± 0.024	0.771 ± 0.144	0.662 ± 0.115

Table 4.3 – 3D tissue cultures grown in high glucose DMEM supplemented with 10% heat-inactivated FBS over 4 weeks. Data are presented as averages ± standard deviation of 3 – 4 individual tissue cultures for n = 1 biological experiments.

	Control	Ca-PolyP	Sr-PolyP
Wet Weight [mg]	57.0 ± 5.4	59.4 ± 4.1	54.2 ± 4.5
Dry Weight [mg]	5.4 ± 0.4	5.4 ± 0.2	5.1 ± 0.2
Water Content [%]	90.6 ± 0.6	90.9 ± 0.6	90.7 ± 0.3
sGAG [µg]	1326 ± 20	1370 ± 92	1293 ± 40
Collagen [µg]	1089 ± 123	1022 ± 42	1093 ± 81
DNA [µg]	39.0 ± 1.6	35.1 ± 0.6	33.7 ± 3.6
sGAG/DNA [µg/µg]	34.0 ± 1.0	39.0 ± 2.9	38.7 ± 4.7
Collagen/DNA [µg/µg]	27.9 ± 2.4	29.1 ± 1.4	32.5 ± 1.7
Collagen/sGAG [µg/µg]	0.821 ± 0.090	0.749 ± 0.054	0.846 ± 0.066

Table 4.4 – 3D tissue cultures grown in high glucose DMEM without pyruvate or L-glutamine and supplemented with 10% heat-inactivated FBS over 4 weeks. Data are presented as averages ± standard deviation of 2 – 3 individual tissue cultures for n = 1 biological experiments.

	Control	Ca-PolyP	Sr-PolyP
Wet Weight [mg]	22.2 ± 0.7	20.7 ± 2.7	23.6 ± 0.8
Dry Weight [mg]	1.9 ± 0.2	1.8 ± 0.1	2.0 ± 0.1
Water Content [%]	91.3 ± 1.0	91.4 ± 0.9	91.5 ± 0.3
sGAG [µg]	130 ± 31	123 ± 6	149 ± 4
Collagen [µg]	162 ± 33	156 ± 20	185 ± 5
DNA [µg]	27.2 ± 4.7	27.8 ± 0.8	31.2 ± 0.1
sGAG/DNA [µg/µg]	4.74 ± 0.56	4.43 ± 0.14	4.77 ± 0.11
Collagen/DNA [µg/µg]	5.95 ± 0.82	5.60 ± 0.60	5.93 ± 0.16
Collagen/sGAG [µg/µg]	1.26 ± 0.07	1.26 ± 0.10	1.24 ± 0.01

Table 4.5 – 3D tissue cultures grown in Ham's F-12 supplemented with 1.5 mM $CaCl_2$ and 10% heat-inactivated FBS over 4 weeks. Data are presented as averages ± standard deviation of 2 – 3 individual tissue cultures for n = 1 biological experiments.

	Control	Ca-PolyP	Sr-PolyP
Wet Weight [mg]	51.4 ± 2.9	54.4 ± 6.5	54.3 ± 3.6
Dry Weight [mg]	3.0 ± 0.3	3.0 ± 0.2	3.1 ± 0.2
Water Content [%]	94.2 ± 0.2	94.5 ± 0.5	94.3 ± 0.2
sGAG [µg]	301 ± 34	325 ± 30	339 ± 11
Collagen [µg]	349 ± 9	351 ± 35	370 ± 10
DNA [µg]	35.5 ± 5.2	34.8 ± 5.4	37.2 ± 1.1
sGAG/DNA [µg/µg]	8.48 ± 0.28	9.42 ± 0.96	9.11 ± 0.16
Collagen/DNA [µg/µg]	9.92 ± 1.20	10.22 ± 1.54	9.95 ± 0.54
Collagen/sGAG [µg/µg]	1.17 ± 0.10	1.08 ± 0.05	1.09 ± 0.07

previous experiments with soluble polyP involved administration every 2 – 3 days. Therefore, more frequent applications, such as during every media change (corresponding to three times a week), may lead to more promising results.

In comparing to our 2D culture experiments, the mass of particles per cell is much lower in the 3D tissue cultures. This was due to limitations with sonication; at concentrations above 1 mg/mL, the polyP-based particles would fail to disperse (data not shown). As a result, the amount of particles added within the insert was 200 μg, which corresponds to 0.2 ng/cell based on the initial 1 million cells seeded onto the membrane. While the amount utilized in the MTT and EdU assays corresponds to 0.125 – 0.5 ng/cell, suggesting a similar dosage, the MTT and EdU assays were cultured for a total of 2 days (1 day for seeding, and 1 day of particle treatment), where minimal cell growth would occur. For the in vitro tissues, the average DNA content after 4 weeks of culture for all media conditions was 33.5 ± 3.4 μg, which is estimated to be approximately ~4.3 million cells, assuming 7.7 pg of DNA per chondrocyte [251]. As a result of this over 4-fold increase in cell numbers, the particle mass per cell falls below 0.05 ng/cell. Meanwhile, the MTT and EdU assays exhibited the most prominent effects at the highest tested ratio of 0.5 ng/cell. In order to increase the amount of particles applied to the insert, the particles need to be concentrated following sonication without affecting their dispersion.

Another possibility is the inability for these particles to reach the chondrocytes once the cells begin depositing their ECM. While preliminary results suggest that these particles may enter cartilage tissue explants (Figure 4.16 and Figure 4.17, A), the bioactivity of these particles may rely on cellular uptake, which has not been confirmed for our engineered tissues or native cartilage, given that the ECM may act as a barrier towards particle uptake. As a result, it may be beneficial to repeat these experiments under a shorter culture period to observe the effects of the polyP-based

particles on the initial ECM deposition, where minimal ECM is present which may disrupt particle uptake. Additionally, this could be beneficial as it is possible that the effect of polyP is lost over longer culture periods. Furthermore, at shorter culture periods, the particle mass to cell ratio will be at its maximum, which may not require efforts to increase the dosage to observe substantial effects.

Another potential explanation may be the bioavailability of polyphosphate. While studies with 2D cultures indicate that the particles have a biological effect, there is a possibility that these effects are not directly a result of polyP. As discussed previously, following endocytic processes leading to particle internalization, ultimately the cargo will be degraded by lysosomes. Therefore, it is possible that the dosage of polyP is much lower than intended as currently, functionalization has not been performed on these particles to facilitate endocytic escape. Additionally, it is also possible that the polyP within the particles is not in a biologically active form. It has been suggested that polyP is only physiologically active as a coacervate, while the particles are biologically inert and used as a means of storage [82,85,86,252]. Overall, additional studies are required to evaluate the potential use of these polyP-based particles for cartilage tissue engineering applications. Ultimately, this will require further developmental studies to achieve and maintain improved colloid stability at high concentrations in culture media and other physiological fluids.

4.3.7 Biological Characterization Summary

Cellular uptake of these polyP-based particles was confirmed in chondrocytes, which also exhibit a size and concentration-dependent cytotoxicity based on live-dead assays. Importantly, these particles were identified to be bioactive in chondrocytes, decreasing both cell proliferation and metabolic activity as determined by EdU and MTT assays respectively. However, additional work

is required to validate the feasibility of these polyP-based particles for drug delivery applications into the joint and for the regeneration of cartilage tissue.

CHAPTER 5: CONCLUSIONS AND FUTURE WORK

5.1 Conclusions

Through the body of this work, we have successfully synthesized and characterized Ca-polyP and Sr-polyP particles. Sonication successfully broke up particle agglomerates, and both particles have a negative zeta potential. SEM imaging indicated that the particles have a spherical morphology and suggests that the particles are nanoscale in size. Sr-polyP exhibited much greater size stability than Ca-polyP, however the mechanism for this is not yet understood. The particles were tested under a variety of environmental conditions and have been determined to exhibit size stability for in vitro cell culture studies when incubated in culture medium supplemented with serum. Cellular uptake was validated in chondrocytes, and biological characterization demonstrated both a size- and concentration-dependent cytotoxicity at high particle loading, a reduction in metabolic activity for as synthesized and sonicated particles, and a decrease in cell proliferation for sonicated particles. Altogether, this study demonstrates that these polyP-based particles elicit a biological response in chondrocytes. Preliminary studies also indicate that polyP-based particles may penetrate and be retained in cartilage tissue explants.

5.2 Ongoing and Future Work

Further characterization of these polyP-based particles is required in synovial fluid in order to better recapitulate a physiological environment. This will be done as validation for the feasibility of the particles as a drug delivery strategy via intra-articular injection into the joint and position the study to eventually transition towards biological characterization of the particles towards an in vivo context. As previously discussed, our initial results appear to suggest that the particles may

exhibit instability in synovial fluid, due to the observation of agglomeration of sonicated particles and potential degradation of the as synthesized particles. However, more work is required as these results are inconclusive.

While particle uptake by chondrocytes has been validated, the exact mechanism of cellular uptake remains unknown. Future experimental plans will involve inhibition of select endocytic mechanisms, allowing for the evaluation of the contribution each mechanism may have on the uptake of polyP-based particles in chondrocytes. EDAC-mediated end-group labelling will be utilized to covalently link a fluorophore to the particles, to ensure that the fluorescent signal remains stable and can therefore be reliably quantified. Secondly, cellular uptake will be quantified through methods such as flow cytometry or microplate-based assays to reliably identify decreases in the fluorescent signal following the inhibition of endocytic pathways compared to the control.

The MTT assay results, while inconclusive, do suggest that these polyP-based particles modulate the metabolic activity of chondrocytes. Similarly, the evaluation of ATP levels was also inconclusion due to assay interference by the particles themselves. Other metrics, such as lactate levels following Ca-polyP and Sr-polyP treatment in chondrocytes can be done. Similarly, the EdU assays demonstrate a reduction in cellular proliferation for the sonicated polyP-based particles. However, additional work is required to demonstrate that this effect translates to a reduction in cell numbers over longer culture periods. This may be evaluated through DNA assays if the protocol can be improved and validated, or through total cell counts via nuclear staining and fluorescent microscopy. However, under the culture conditions utilized in the EdU assays, cell growth is expected to be very slow.

The methodology in assessing cartilage tissue penetration and retention of the polyP-based particles is desired to be improved. As discussed, there are many shortcomings with the experiment

to strengthen the conclusions that can be derived from the data. Similar to the quantification of cellular uptake, the particles can be fluorescently labelled via EDAC-mediated end-group labelling to ensure that the fluorescent signal can be reliably correlated to the particle concentration. Secondly, it is highly desired to validate that tissue uptake occurs in the superficial zone of cartilage. While this can be done using in vivo animal studies, developing a methodology for ex vivo studies would be ideal.

Our initial interest in utilizing these polyP-based particles stems largely from the anabolic effects of polyP previously observed in chondrocytes, suggesting that polyP may be a molecule of interest for cartilage tissue engineering applications. Despite this, treating chondrocytes with these polyP-based particles resulted in no beneficial effects on ECM accumulation in 3D tissue cultures. Therefore, future work is required to better determine optimal culture conditions and particle concentrations which demonstrate a therapeutic or regenerative effect of polyP for cartilage tissue. In particular, improving our ability to prepare stable colloidal solutions of particles at high concentrations will be important for these efforts.

Lastly, it is desired to develop strategies to tailor the chemistry of particle surfaces. For example, we would like to endow a positively charged surface which remains stably bound to the particle. Again, this can potentially be accomplished by EDAC-mediated end-group labelling with cationic molecules. If successful, studies may be done to compare the efficacy of cartilage tissue uptake and retention between the unfunctionalized, negatively charged particles and the functionalized, positively charged particles. Of course, select experiments would also be repeated utilizing these positively charged particles to confirm that the size stability and biological activity remains unchanged due to these modifications. Importantly, assessing their behaviour in synovial fluid would be necessary to verify the feasibility of these particles for intra-articular injection, as

the ionic interactions between the particle and environment will be much different as compared to the naked particles. Furthermore, surface functionalization opens up opportunities to tune the size and degradation rate of the particles, as well as the co-delivery of other bioactive molecules, which may be used to impart additional effects and potentially broaden the application of these particles.

CHAPTER 6: ADDITIONAL CONTRIBUTIONS

6.1 National Research Council of Canada (NRC)

In collaboration with Dr. Ying Betty Li and Dr. Anna Jezierski in the Human Health Therapeutics Research Centre of the NRC, I have contributed towards a multidisciplinary project related to 3D bioprinting of alginate-collagen bioinks for the development of complex vascular networks. In this study, I was responsible for the design and performance of experiments related to the mechanical characterization of acellular alginate and alginate-collagen hydrogels by indentation testing and degradation assays to assess the feasibility and stability of these hydrogels for neurovascular tissue engineering. Furthermore, the mechanical properties of alginate-collagen constructs encapsulating adult rat brain endothelial cells were measured by indentation testing to assess structural changes in the construct due to extracellular matrix deposition and remodeling over long-term cultures. This work, performed jointly with Hannah Prazak and under the supervision of Dr. Jean-Philippe St-Pierre, has been included as part of a journal article in *Bioprinting* [253].

6.2 Western University

In collaboration with Jue Gong and Dr. Elizabeth R. Gillies at Western University, I assisted in the evaluation of cartilage tissue uptake of novel polycationic polymers as well as the evaluation of the cytotoxicity of this polymer library, which were based on techniques developed specifically for the experiments presented within this thesis. This work, performed alongside Jue Gong and Dr. Jean-Philippe St-Pierre, will be included in a manuscript currently in preparation to be submitted.

REFERENCES

[1] A.J. Sophia Fox, A. Bedi, S.A. Rodeo, The Basic Science of Articular Cartilage: Structure, Composition, and Function, Sports Health: A Multidisciplinary Approach. 1 (2009) 461–468. https://doi.org/10.1177/1941738109350438.

[2] A.M. Bhosale, J.B. Richardson, Articular cartilage: structure, injuries and review of management, Br Med Bull. 87 (2008) 77–95. https://doi.org/10.1093/bmb/ldn025.

[3] C.W. Archer, P. Francis-West, The chondrocyte, Int J Biochem Cell Biol. 35 (2003) 401–404. https://doi.org/10.1016/S1357-2725(02)00301-1.

[4] D.R. Eyre, The collagens of articular cartilage, Semin Arthritis Rheum. 21 (1991) 2–11. https://doi.org/10.1016/0049-0172(91)90035-X.

[5] D. Eyre, Articular cartilage and changes in Arthritis: Collagen of articular cartilage, Arthritis Res. 4 (2002) 30. https://doi.org/10.1186/ar380.

[6] Y. Luo, D. Sinkeviciute, Y. He, M. Karsdal, Y. Henrotin, A. Mobasheri, P. Önnerfjord, A. Bay-Jensen, The minor collagens in articular cartilage, Protein Cell. 8 (2017) 560–572. https://doi.org/10.1007/s13238-017-0377-7.

[7] D. Eyre, M. Weis, J.-J. Wu, Articular cartilage collagen: an irreplaceable framework?, Eur Cell Mater. 12 (2006) 57–63. https://doi.org/10.22203/eCM.v012a07.

[8] L. Alcaide-Ruggiero, V. Molina-Hernández, M.M. Granados, J.M. Domínguez, Main and Minor Types of Collagens in the Articular Cartilage: The Role of Collagens in Repair Tissue Evaluation in Chondral Defects, Int J Mol Sci. 22 (2021) 13329. https://doi.org/10.3390/ijms222413329.

[9] J. Eschweiler, N. Horn, B. Rath, M. Betsch, A. Baroncini, M. Tingart, F. Migliorini, The Biomechanics of Cartilage—An Overview, Life. 11 (2021) 302. https://doi.org/10.3390/life11040302.

[10] P.J. Roughley, J.S. Mort, The role of aggrecan in normal and osteoarthritic cartilage, J Exp Orthop. 1 (2014) 8. https://doi.org/10.1186/s40634-014-0008-7.

[11] C. Kiani, L. Chen, Y.J. Wu, A.J. Yee, B.B. Yang, Structure and function of aggrecan, Cell Res. 12 (2002) 19–32. https://doi.org/10.1038/sj.cr.7290106.

[12] A. Maroudas, Balance between swelling pressure and collagen tension in normal and degenerate cartilage, Nature. 260 (1976) 808–809. https://doi.org/10.1038/260808a0.

[13] M.S. Bergholt, J.-P. St-Pierre, G.S. Offeddu, P.A. Parmar, M.B. Albro, J.L. Puetzer, M.L. Oyen, M.M. Stevens, Raman Spectroscopy Reveals New Insights into the Zonal Organization of Native and Tissue-Engineered Articular Cartilage, ACS Cent Sci. 2 (2016) 885–895. https://doi.org/10.1021/acscentsci.6b00222.

[14] I.-S. Park, W.H. Choi, D.Y. Park, S.R. Park, S.-H. Park, B.-H. Min, Effect of joint mimicking loading system on zonal organization into tissue-engineered cartilage, PLoS One. 13 (2018) e0202834. https://doi.org/10.1371/journal.pone.0202834.

[15] E.E. Coates, J.P. Fisher, Phenotypic Variations in Chondrocyte Subpopulations and Their Response to In Vitro Culture and External Stimuli, Ann Biomed Eng. 38 (2010) 3371–3388. https://doi.org/10.1007/s10439-010-0096-1.

[16] A. Khalafi, T.M. Schmid, C. Neu, A.H. Reddi, Increased accumulation of superficial zone protein (SZP) in articular cartilage in response to bone morphogenetic protein-7 and growth factors, Journal of Orthopaedic Research. 25 (2007) 293–303. https://doi.org/10.1002/jor.20329.

[17] H. Akkiraju, A. Nohe, Role of Chondrocytes in Cartilage Formation, Progression of Osteoarthritis and Cartilage Regeneration, J Dev Biol. 3 (2015) 177–192. https://doi.org/10.3390/jdb3040177.

[18] A.R. Poole, M. Kobayashi, T. Yasuda, S. Laverty, F. Mwale, T. Kojima, T. Sakai, C. Wahl, S. El-Maadawy, G. Webb, E. Tchetina, W. Wu, Type II collagen degradation and its regulation in articular cartilage in osteoarthritis, Ann Rheum Dis. 61 (2002) 78ii–7881. https://doi.org/10.1136/ard.61.suppl_2.ii78.

[19] A. Maroudas, Glycosaminoglycan turn-over in articular cartilage, Philosophical Transactions of the Royal Society of London. B, Biological Sciences. 271 (1975) 293–313. https://doi.org/10.1098/rstb.1975.0054.

[20] A. Mobasheri, M.P. Rayman, O. Gualillo, J. Sellam, P. van der Kraan, U. Fearon, The role of metabolism in the pathogenesis of osteoarthritis, Nat Rev Rheumatol. 13 (2017) 302–311. https://doi.org/10.1038/nrrheum.2017.50.

[21] D.J. Hunter, S. Bierma-Zeinstra, Osteoarthritis, The Lancet. 393 (2019) 1745–1759. https://doi.org/10.1016/S0140-6736(19)30417-9.

[22] D. Heinegård, T. Saxne, The role of the cartilage matrix in osteoarthritis, Nat Rev Rheumatol. 7 (2011) 50–56. https://doi.org/10.1038/nrrheum.2010.198.

[23] M. Maldonado, J. Nam, The Role of Changes in Extracellular Matrix of Cartilage in the Presence of Inflammation on the Pathology of Osteoarthritis, Biomed Res Int. 2013 (2013) 1–10. https://doi.org/10.1155/2013/284873.

[24] Z. Peng, H. Sun, V. Bunpetch, Y. Koh, Y. Wen, D. Wu, H. Ouyang, The regulation of cartilage extracellular matrix homeostasis in joint cartilage degeneration and regeneration, Biomaterials. 268 (2021) 120555. https://doi.org/10.1016/j.biomaterials.2020.120555.

[25] A.R. Poole, M. Kobayashi, T. Yasuda, S. Laverty, F. Mwale, T. Kojima, T. Sakai, C. Wahl, S. El-Maadawy, G. Webb, E. Tchetina, W. Wu, Type II collagen degradation and its regulation in articular cartilage in osteoarthritis, Ann Rheum Dis. 61 (2002) 78ii–7881. https://doi.org/10.1136/ard.61.suppl_2.ii78.

[26] N. Miosge, M. Hartmann, C. Maelicke, R. Herken, Expression of collagen type I and type II in consecutive stages of human osteoarthritis, Histochem Cell Biol. 122 (2004) 229–236. https://doi.org/10.1007/s00418-004-0697-6.

[27] M. Kapoor, J. Martel-Pelletier, D. Lajeunesse, J.-P. Pelletier, H. Fahmi, Role of proinflammatory cytokines in the pathophysiology of osteoarthritis, Nat Rev Rheumatol. 7 (2011) 33–42. https://doi.org/10.1038/nrrheum.2010.196.

[28] D. Primorac, V. Molnar, E. Rod, Ž. Jeleč, F. Čukelj, V. Matišić, T. Vrdoljak, D. Hudetz, H. Hajsok, I. Borić, Knee Osteoarthritis: A Review of Pathogenesis and State-Of-The-Art Non-Operative Therapeutic Considerations, Genes (Basel). 11 (2020) 854. https://doi.org/10.3390/genes11080854.

[29] Q. Ji, X. Xu, Q. Zhang, L. Kang, Y. Xu, K. Zhang, L. Li, Y. Liang, T. Hong, Q. Ye, Y. Wang, The IL-1β/AP-1/miR-30a/ADAMTS-5 axis regulates cartilage matrix degradation in human osteoarthritis, J Mol Med. 94 (2016) 771–785. https://doi.org/10.1007/s00109-016-1418-z.

[30] E.B. Hunziker, K. Lippuner, M.J.B. Keel, N. Shintani, An educational review of cartilage repair: precepts & practice – myths & misconceptions – progress & prospects, Osteoarthritis Cartilage. 23 (2015) 334–350. https://doi.org/10.1016/j.joca.2014.12.011.

[31] E.A. Makris, A.H. Gomoll, K.N. Malizos, J.C. Hu, K.A. Athanasiou, Repair and tissue engineering techniques for articular cartilage, Nat Rev Rheumatol. 11 (2015) 21–34. https://doi.org/10.1038/nrrheum.2014.157.

[32] H. Kwon, W.E. Brown, C.A. Lee, D. Wang, N. Paschos, J.C. Hu, K.A. Athanasiou, Surgical and tissue engineering strategies for articular cartilage and meniscus repair, Nat Rev Rheumatol. 15 (2019) 550–570. https://doi.org/10.1038/s41584-019-0255-1.

[33] D. Goyal, S. Keyhani, E.H. Lee, J.H.P. Hui, Evidence-Based Status of Microfracture Technique: A Systematic Review of Level I and II Studies, Arthroscopy: The Journal of Arthroscopic & Related Surgery. 29 (2013) 1579–1588. https://doi.org/10.1016/j.arthro.2013.05.027.

[34] B. Arzi, G.D. DuRaine, C.A. Lee, D.J. Huey, D.L. Borjesson, B.G. Murphy, J.C.Y. Hu, N. Baumgarth, K.A. Athanasiou, Cartilage immunoprivilege depends on donor source and lesion location, Acta Biomater. 23 (2015) 72–81. https://doi.org/10.1016/j.actbio.2015.05.025.

[35] A. Pareek, P.J. Reardon, T.G. Maak, B.A. Levy, M.J. Stuart, A.J. Krych, Long-term Outcomes After Osteochondral Autograft Transfer: A Systematic Review at Mean Follow-up of 10.2 Years, Arthroscopy: The Journal of Arthroscopic & Related Surgery. 32 (2016) 1174–1184. https://doi.org/10.1016/j.arthro.2015.11.037.

[36] F. Familiari, M.E. Cinque, J. Chahla, J.A. Godin, M.L. Olesen, G. Moatshe, R.F. LaPrade, Clinical Outcomes and Failure Rates of Osteochondral Allograft Transplantation in the Knee: A Systematic Review, Am J Sports Med. 46 (2018) 3541–3549. https://doi.org/10.1177/0363546517732531.

[37] D. Primorac, V. Molnar, V. Matišić, D. Hudetz, Ž. Jeleč, E. Rod, F. Čukelj, D. Vidović, T. Vrdoljak, B. Dobričić, D. Antičević, M. Smolić, M. Miškulin, D. Ćaćić, I. Borić, Comprehensive Review of Knee Osteoarthritis Pharmacological Treatment and the Latest Professional Societies' Guidelines, Pharmaceuticals. 14 (2021) 205. https://doi.org/10.3390/ph14030205.

[38] A. Latourte, M. Kloppenburg, P. Richette, Emerging pharmaceutical therapies for osteoarthritis, Nat Rev Rheumatol. 16 (2020) 673–688. https://doi.org/10.1038/s41584-020-00518-6.

[39] C.H. Evans, V.B. Kraus, L.A. Setton, Progress in intra-articular therapy, Nat Rev Rheumatol. 10 (2014) 11–22. https://doi.org/10.1038/nrrheum.2013.159.

[40] I.A. Jones, R. Togashi, M.L. Wilson, N. Heckmann, C.T. Vangsness, Intra-articular treatment options for knee osteoarthritis, Nat Rev Rheumatol. 15 (2019) 77–90. https://doi.org/10.1038/s41584-018-0123-4.

[41] E. Ayhan, Intraarticular injections (corticosteroid, hyaluronic acid, platelet rich plasma) for the knee osteoarthritis, World J Orthop. 5 (2014) 351. https://doi.org/10.5312/wjo.v5.i3.351.

[42] G. Testa, S.M.C. Giardina, A. Culmone, A. Vescio, M. Turchetta, S. Cannavò, V. Pavone, Intra-Articular Injections in Knee Osteoarthritis: A Review of Literature, J Funct Morphol Kinesiol. 6 (2021) 15. https://doi.org/10.3390/jfmk6010015.

[43] C. Larsen, J. Østergaard, S.W. Larsen, H. Jensen, S. Jacobsen, C. Lindegaard, P.H. Andersen, Intra-articular depot formulation principles: Role in the management of postoperative pain and arthritic disorders, J Pharm Sci. 97 (2008) 4622–4654. https://doi.org/10.1002/jps.21346.

[44] L. Han, A.J. Grodzinsky, C. Ortiz, Nanomechanics of the Cartilage Extracellular Matrix, Annu Rev Mater Res. 41 (2011) 133–168. https://doi.org/10.1146/annurev-matsci-062910-100431.

[45] A.G. Bajpayee, A.J. Grodzinsky, Cartilage-targeting drug delivery: can electrostatic interactions help?, Nat Rev Rheumatol. 13 (2017) 183–193. https://doi.org/10.1038/nrrheum.2016.210.

[46] J. Mahendran, J.-P. St-Pierre, Nanomaterials Applications in Cartilage Tissue Engineering, in: Nanoengineering Materials for Biomedical Uses, Springer International Publishing, Cham, 2019: pp. 81–105. https://doi.org/10.1007/978-3-030-31261-9_5.

[47] A. Vedadghavami, C. Zhang, A.G. Bajpayee, Overcoming negatively charged tissue barriers: Drug delivery using cationic peptides and proteins, Nano Today. 34 (2020) 100898. https://doi.org/10.1016/j.nantod.2020.100898.

[48] C.D. DiDomenico, M. Lintz, L.J. Bonassar, Molecular transport in articular cartilage — what have we learned from the past 50 years?, Nat Rev Rheumatol. 14 (2018) 393–403. https://doi.org/10.1038/s41584-018-0033-5.

[49] M.L. Cook Sangar, E.J. Girard, G. Hopping, C. Yin, F. Pakiam, M.-Y. Brusniak, E. Nguyen, R. Ruff, M.M. Gewe, K. Byrnes-Blake, N.W. Nairn, D.M. Miller, C. Mehlin, A.D. Strand, A.J. Mhyre, C.E. Correnti, R.K. Strong, J.A. Simon, J.M. Olson, A potent peptide-steroid conjugate accumulates in cartilage and reverses arthritis without evidence of systemic corticosteroid exposure, Sci Transl Med. 12 (2020). https://doi.org/10.1126/scitranslmed.aay1041.

[50] A. Vedadghavami, B. Hakim, T. He, A.G. Bajpayee, Cationic peptide carriers enable long-term delivery of insulin-like growth factor-1 to suppress osteoarthritis-induced

matrix degradation, Arthritis Res Ther. 24 (2022) 172. https://doi.org/10.1186/s13075-022-02855-1.

[51] A.G. Bajpayee, M.A. Quadir, P.T. Hammond, A.J. Grodzinsky, Charge based intra-cartilage delivery of single dose dexamethasone using Avidin nano-carriers suppresses cytokine-induced catabolism long term, Osteoarthritis Cartilage. 24 (2016) 71–81. https://doi.org/10.1016/j.joca.2015.07.010.

[52] T. He, C. Zhang, A. Vedadghavami, S. Mehta, H.A. Clark, R.M. Porter, A.G. Bajpayee, Multi-arm Avidin nano-construct for intra-cartilage delivery of small molecule drugs, Journal of Controlled Release. 318 (2020) 109–123. https://doi.org/10.1016/j.jconrel.2019.12.020.

[53] Y. Krishnan, H.A. Rees, C.P. Rossitto, S.-E. Kim, H.-H.K. Hung, E.H. Frank, B.D. Olsen, D.R. Liu, P.T. Hammond, A.J. Grodzinsky, Green fluorescent proteins engineered for cartilage-targeted drug delivery: Insights for transport into highly charged avascular tissues, Biomaterials. 183 (2018) 218–233. https://doi.org/10.1016/j.biomaterials.2018.08.050.

[54] S. Perni, P. Prokopovich, Poly-beta-amino-esters nano-vehicles based drug delivery system for cartilage, Nanomedicine. 13 (2017) 539–548. https://doi.org/10.1016/j.nano.2016.10.001.

[55] S. Perni, P. Prokopovich, Optimisation and feature selection of poly-beta-amino-ester as a drug delivery system for cartilage, J Mater Chem B. 8 (2020) 5096–5108. https://doi.org/10.1039/C9TB02778E.

[56] B.C. Geiger, S. Wang, R.F. Padera, A.J. Grodzinsky, P.T. Hammond, Cartilage-penetrating nanocarriers improve delivery and efficacy of growth factor treatment of osteoarthritis, Sci Transl Med. 10 (2018). https://doi.org/10.1126/scitranslmed.aat8800.

[57] F.A. Formica, G. Barreto, M. Zenobi-Wong, Cartilage-targeting dexamethasone prodrugs increase the efficacy of dexamethasone, Journal of Controlled Release. 295 (2019) 118–129. https://doi.org/10.1016/j.jconrel.2018.12.025.

[58] D.A. Rothenfluh, H. Bermudez, C.P. O'Neil, J.A. Hubbell, Biofunctional polymer nanoparticles for intra-articular targeting and retention in cartilage, Nat Mater. 7 (2008) 248–254. https://doi.org/10.1038/nmat2116.

[59] J.T. Hulme, W.N. D'Souza, H.J. McBride, B.-R.P. Yoon, A.M. Willee, A. Duguay, M. Thomas, B. Fan, M.R. Dayao, J.B. Rottman, K. Merriam, J. Xie, R. Smith, B.M. Alba, R.B. Case, K. Dang, A. Montalvan, N. Grinberg, H. Sun, R.A. Black, C.A. Gabel, J.E. Sims, K. Moore, A. Bakker, P. Li, Novel protein therapeutic joint retention strategy based on collagen-binding Avimers, Journal of Orthopaedic Research. (2017). https://doi.org/10.1002/jor.23756.

[60] T. Zhao, Z. Wei, W. Zhu, X. Weng, Recent Developments and Current Applications of Hydrogels in Osteoarthritis, Bioengineering. 9 (2022) 132. https://doi.org/10.3390/bioengineering9040132.

[61] O. Jeznach, D. Kołbuk, P. Sajkiewicz, Injectable hydrogels and nanocomposite hydrogels for cartilage regeneration, J Biomed Mater Res A. 106 (2018) 2762–2776. https://doi.org/10.1002/jbm.a.36449.

[62] T. Tanaka, T. Matsushita, K. Nishida, K. Takayama, K. Nagai, D. Araki, T. Matsumoto, Y. Tabata, R. Kuroda, Attenuation of osteoarthritis progression in mice following intra-

articular administration of simvastatin-conjugated gelatin hydrogel, J Tissue Eng Regen Med. 13 (2019) 423–432. https://doi.org/10.1002/term.2804.

[63] L. García-Fernández, M. Olmeda-Lozano, L. Benito-Garzón, A. Pérez-Caballer, J. San Román, B. Vázquez-Lasa, Injectable hydrogel-based drug delivery system for cartilage regeneration, Materials Science and Engineering: C. 110 (2020) 110702. https://doi.org/10.1016/j.msec.2020.110702.

[64] W. Ha, Z. Wang, X. Zhao, Y. Shi, Reinforced Supramolecular Hydrogels from Attapulgite and Cyclodextrin Pseudopolyrotaxane for Sustained Intra-Articular Drug Delivery, Macromol Biosci. 21 (2021) 2000299. https://doi.org/10.1002/mabi.202000299.

[65] A. Petit, M. Sandker, B. Müller, R. Meyboom, P. van Midwoud, P. Bruin, E.M. Redout, M. Versluijs-Helder, C.H.A. van der Lest, S.J. Buwalda, L.G.J. de Leede, T. Vermonden, R.J. Kok, H. Weinans, W.E. Hennink, Release behavior and intra-articular biocompatibility of celecoxib-loaded acetyl-capped PCLA-PEG-PCLA thermogels, Biomaterials. 35 (2014) 7919–7928. https://doi.org/10.1016/j.biomaterials.2014.05.064.

[66] S.-J. Wang, J.-Z. Qin, T.-E. Zhang, C. Xia, Intra-articular Injection of Kartogenin-Incorporated Thermogel Enhancing Osteoarthritis Treatment, Front Chem. 7 (2019). https://doi.org/10.3389/fchem.2019.00677.

[67] A. Singh, R. Agarwal, C.A. Diaz-Ruiz, N.J. Willett, P. Wang, L.A. Lee, Q. Wang, R.E. Guldberg, A.J. García, Nanoengineered Particles for Enhanced Intra-Articular Retention and Delivery of Proteins, Adv Healthc Mater. 3 (2014) 1562–1567. https://doi.org/10.1002/adhm.201400051.

[68] S. Zhu, P. Lu, H. Liu, P. Chen, Y. Wu, Y. Wang, H. Sun, X. Zhang, Q. Xia, B.C. Heng, Y. Zhou, H.W. Ouyang, Inhibition of Rac1 activity by controlled release of NSC23766 from

chitosan microspheres effectively ameliorates osteoarthritis development in vivo, Ann Rheum Dis. 74 (2015) 285–293. https://doi.org/10.1136/annrheumdis-2013-203901.

[69] I. Rudnik-Jansen, S. Colen, J. Berard, S. Plomp, I. Que, M. van Rijen, N. Woike, A. Egas, G. van Osch, E. van Maarseveen, K. Messier, A. Chan, J. Thies, L. Creemers, Prolonged inhibition of inflammation in osteoarthritis by triamcinolone acetonide released from a polyester amide microsphere platform, Journal of Controlled Release. 253 (2017) 64–72. https://doi.org/10.1016/j.jconrel.2017.03.014.

[70] K.M. Dhanabalan, V.K. Gupta, R. Agarwal, Rapamycin–PLGA microparticles prevent senescence, sustain cartilage matrix production under stress and exhibit prolonged retention in mouse joints, Biomater Sci. 8 (2020) 4308–4321. https://doi.org/10.1039/D0BM00596G.

[71] M. Deloney, K. Smart, B.A. Christiansen, A. Panitch, Thermoresponsive, hollow, degradable core-shell nanoparticles for intra-articular delivery of anti-inflammatory peptide, Journal of Controlled Release. 323 (2020) 47–58. https://doi.org/10.1016/j.jconrel.2020.04.007.

[72] Y. Wei, L. Yan, L. Luo, T. Gui, B. Jang, A. Amirshaghaghi, T. You, A. Tsourkas, L. Qin, Z. Cheng, Phospholipase A $_2$ inhibitor–loaded micellar nanoparticles attenuate inflammation and mitigate osteoarthritis progression, Sci Adv. 7 (2021). https://doi.org/10.1126/sciadv.abe6374.

[73] Y. Wei, L. Luo, T. Gui, F. Yu, L. Yan, L. Yao, L. Zhong, W. Yu, B. Han, J.M. Patel, J.F. Liu, F. Beier, L.S. Levin, C. Nelson, Z. Shao, L. Han, R.L. Mauck, A. Tsourkas, J. Ahn, Z. Cheng, L. Qin, Targeting cartilage EGFR pathway for osteoarthritis treatment, Sci Transl Med. 13 (2021). https://doi.org/10.1126/scitranslmed.abb3946.

[74] J.-P. St-Pierre, Q. Wang, S.Q. Li, R.M. Pilliar, R.A. Kandel, Inorganic Polyphosphate Stimulates Cartilage Tissue Formation, Tissue Eng Part A. 18 (2012) 1282–1292. https://doi.org/10.1089/ten.tea.2011.0356.

[75] R. Gawri, R. Bielecki, E.W. Salter, A. Zelinka, T. Shiba, G. Collingridge, A. Nagy, R.A. Kandel, The anabolic effect of inorganic polyphosphate on chondrocytes is mediated by calcium signalling, Journal of Orthopaedic Research. 40 (2022) 310–322. https://doi.org/10.1002/jor.25032.

[76] X. Wang, M. Ackermann, E. Tolba, M. Neufurth, F. Wurm, Q. Feng, S. Wang, H. Schröder, W. Müller, Artificial cartilage bio-matrix formed of hyaluronic acid and Mg2+-polyphosphate, Eur Cell Mater. 32 (2016) 271–283. https://doi.org/10.22203/eCM.v032a18.

[77] W.E.G. Müller, E. Tolba, H.C. Schröder, S. Wang, G. Glaßer, R. Muñoz-Espí, T. Link, X. Wang, A new polyphosphate calcium material with morphogenetic activity, Mater Lett. 148 (2015) 163–166. https://doi.org/10.1016/j.matlet.2015.02.070.

[78] W.E.G. Müller, E. Tolba, H.C. Schröder, B. Diehl-Seifert, X. Wang, Retinol encapsulated into amorphous Ca2+ polyphosphate nanospheres acts synergistically in MC3T3-E1 cells, European Journal of Pharmaceutics and Biopharmaceutics. 93 (2015) 214–223. https://doi.org/10.1016/j.ejpb.2015.04.005.

[79] W.E.G. Müller, E. Tolba, Q. Feng, H.C. Schröder, J.S. Markl, M. Kokkinopoulou, X. Wang, Amorphous Ca2+ polyphosphate nanoparticles regulate the ATP level in bone-like SaOS-2 cells, J Cell Sci. 128 (2015) 2202–2207. https://doi.org/10.1242/jcs.170605.

[80] W.E.G. Müller, S. Wang, M. Wiens, M. Neufurth, M. Ackermann, D. Relkovic, M. Kokkinopoulou, Q. Feng, H.C. Schröder, X. Wang, Uptake of polyphosphate

microparticles in vitro (SaOS-2 and HUVEC cells) followed by an increase of the intracellular ATP pool size, PLoS One. 12 (2017) e0188977. https://doi.org/10.1371/journal.pone.0188977.

[81] W.E.G. Müller, E. Tolba, M. Ackermann, M. Neufurth, S. Wang, Q. Feng, H.C. Schröder, X. Wang, Fabrication of amorphous strontium polyphosphate microparticles that induce mineralization of bone cells in vitro and in vivo, Acta Biomater. 50 (2017) 89–101. https://doi.org/10.1016/j.actbio.2016.12.045.

[82] W.E.G. Müller, S. Wang, E. Tolba, M. Neufurth, M. Ackermann, R. Muñoz-Espí, I. Lieberwirth, G. Glasser, H.C. Schröder, X. Wang, Transformation of Amorphous Polyphosphate Nanoparticles into Coacervate Complexes: An Approach for the Encapsulation of Mesenchymal Stem Cells, Small. 14 (2018) 1801170. https://doi.org/10.1002/smll.201801170.

[83] W. Müller, M. Neufurth, S. Wang, M. Ackermann, R. Muñoz-Espí, Q. Feng, Q. Lu, H. Schröder, X. Wang, Amorphous, Smart, and Bioinspired Polyphosphate Nano/Microparticles: A Biomaterial for Regeneration and Repair of Osteo-Articular Impairments In-Situ, Int J Mol Sci. 19 (2018) 427. https://doi.org/10.3390/ijms19020427.

[84] W.E.G. Müller, H. Schepler, E. Tolba, S. Wang, M. Ackermann, R. Muñoz-Espí, S. Xiao, R. Tan, Z. She, M. Neufurth, H.C. Schröder, X. Wang, A physiologically active interpenetrating collagen network that supports growth and migration of epidermal keratinocytes: zinc-polyP nanoparticles integrated into compressed collagen, J Mater Chem B. 8 (2020) 5892–5902. https://doi.org/10.1039/D0TB01240H.

[85] W.E.G. Müller, E. Tolba, S. Wang, M. Neufurth, I. Lieberwirth, M. Ackermann, H.C. Schröder, X. Wang, Nanoparticle-directed and ionically forced polyphosphate

coacervation: a versatile and reversible core–shell system for drug delivery, Sci Rep. 10 (2020) 17147. https://doi.org/10.1038/s41598-020-73100-5.

[86] W.E.G. Müller, M. Neufurth, I. Lieberwirth, S. Wang, H.C. Schröder, X. Wang, Functional importance of coacervation to convert calcium polyphosphate nanoparticles into the physiologically active state, Mater Today Bio. 16 (2022) 100404. https://doi.org/10.1016/j.mtbio.2022.100404.

[87] L.M. Mancipe Castro, A.J. García, R.E. Guldberg, Biomaterial strategies for improved intra-articular drug delivery, J Biomed Mater Res A. 109 (2021) 426–436. https://doi.org/10.1002/jbm.a.37074.

[88] R.E. Whitmire, D. Scott Wilson, A. Singh, M.E. Levenston, N. Murthy, A.J. García, Self-assembling nanoparticles for intra-articular delivery of anti-inflammatory proteins, Biomaterials. 33 (2012) 7665–7675. https://doi.org/10.1016/j.biomaterials.2012.06.101.

[89] K.A. Elsaid, L. Ferreira, T. Truong, A. Liang, J. Machan, G.G. D'Souza, Pharmaceutical nanocarrier association with chondrocytes and cartilage explants: influence of surface modification and extracellular matrix depletion, Osteoarthritis Cartilage. 21 (2013) 377–384. https://doi.org/10.1016/j.joca.2012.11.011.

[90] M. Morgen, D. Tung, B. Boras, W. Miller, A.-M. Malfait, M. Tortorella, Nanoparticles for Improved Local Retention after Intra-Articular Injection into the Knee Joint, Pharm Res. 30 (2013) 257–268. https://doi.org/10.1007/s11095-012-0870-x.

[91] H. Cho, J.M. Stuart, R. Magid, D.C. Danila, T. Hunsaker, E. Pinkhassik, K.A. Hasty, Theranostic immunoliposomes for osteoarthritis, Nanomedicine. 10 (2014) 619–627. https://doi.org/10.1016/j.nano.2013.09.004.

[92] M.J. Kang, S.R. Kim, M.J. Ho, E. Lee, J.W. Lee, Y.W. Choi, Cationic PLGA/Eudragit RL nanoparticles for increasing retention time in synovial cavity after intra-articular injection in knee joint, Int J Nanomedicine. (2015) 5263. https://doi.org/10.2147/IJN.S88363.

[93] H. Yan, X. Duan, H. Pan, N. Holguin, M.F. Rai, A. Akk, L.E. Springer, S.A. Wickline, L.J. Sandell, C.T.N. Pham, Suppression of NF-κB activity via nanoparticle-based siRNA delivery alters early cartilage responses to injury, Proceedings of the National Academy of Sciences. 113 (2016). https://doi.org/10.1073/pnas.1608245113.

[94] A. Petit, M. Sandker, B. Müller, R. Meyboom, P. van Midwoud, P. Bruin, E.M. Redout, M. Versluijs-Helder, C.H.A. van der Lest, S.J. Buwalda, L.G.J. de Leede, T. Vermonden, R.J. Kok, H. Weinans, W.E. Hennink, Release behavior and intra-articular biocompatibility of celecoxib-loaded acetyl-capped PCLA-PEG-PCLA thermogels, Biomaterials. 35 (2014) 7919–7928. https://doi.org/10.1016/j.biomaterials.2014.05.064.

[95] Z. Naghizadeh, A. Karkhaneh, A. Khojasteh, Simultaneous release of melatonin and methylprednisolone from an injectable *in situ* self-crosslinked hydrogel/microparticle system for cartilage tissue engineering, J Biomed Mater Res A. 106 (2018) 1932–1940. https://doi.org/10.1002/jbm.a.36401.

[96] S. Fattahpour, M. Shamanian, N. Tavakoli, M. Fathi, H. Sadeghi-aliabadi, S.R. Sheykhi, M. Fesharaki, S. Fattahpour, An injectable carboxymethyl chitosan-methylcellulose-pluronic hydrogel for the encapsulation of meloxicam loaded nanoparticles, Int J Biol Macromol. 151 (2020) 220–229. https://doi.org/10.1016/j.ijbiomac.2020.02.002.

[97] J. Yang, Y. Zhu, F. Wang, L. Deng, X. Xu, W. Cui, Microfluidic liposomes-anchored microgels as extended delivery platform for treatment of osteoarthritis, Chemical Engineering Journal. 400 (2020) 126004. https://doi.org/10.1016/j.cej.2020.126004.

[98] M. Tsubosaka, S. Kihara, S. Hayashi, J. Nagata, T. Kuwahara, M. Fujita, K. Kikuchi, Y. Takashima, T. Kamenaga, Y. Kuroda, K. Takeuchi, K. Fukuda, K. Takayama, S. Hashimoto, T. Matsumoto, T. Niikura, Y. Tabata, R. Kuroda, Gelatin hydrogels with eicosapentaenoic acid can prevent osteoarthritis progression in vivo in a mouse model, Journal of Orthopaedic Research. 38 (2020) 2157–2169. https://doi.org/10.1002/jor.24688.

[99] I.M. Oliveira, M.R. Carvalho, D.C. Fernandes, C.M. Abreu, F.R. Maia, H. Pereira, D. Caballero, S.C. Kundu, R.L. Reis, J.M. Oliveira, Modulation of inflammation by anti-TNF α mAb-dendrimer nanoparticles loaded in tyramine-modified gellan gum hydrogels in a cartilage-on-a-chip model, J Mater Chem B. 9 (2021) 4211–4218. https://doi.org/10.1039/D1TB00802A.

[100] R.A. Allan, J.J. Miller, Influence of *S* -adenosylmethionine on DAPI-induced fluorescence of polyphosphate in the yeast vacuole, Can J Microbiol. 26 (1980) 912–920. https://doi.org/10.1139/m80-158.

[101] S. Sahlin, J. Hed, I. Runfquist, Differentiation between attached and ingested immune complexes by a fluorescence quenching cytofluorometric assay, J Immunol Methods. 60 (1983) 115–124. https://doi.org/10.1016/0022-1759(83)90340-X.

[102] S. Vranic, N. Boggetto, V. Contremoulins, S. Mornet, N. Reinhardt, F. Marano, A. Baeza-Squiban, S. Boland, Deciphering the mechanisms of cellular uptake of engineered nanoparticles by accurate evaluation of internalization using imaging flow cytometry, Part Fibre Toxicol. 10 (2013) 2. https://doi.org/10.1186/1743-8977-10-2.

[103] A. Kummrow, M. Frankowski, N. Bock, C. Werner, T. Dziekan, J. Neukammer, Quantitative assessment of cell viability based on flow cytometry and microscopy, Cytometry Part A. 83A (2013) 197–204. https://doi.org/10.1002/cyto.a.22213.

[104] F.A. Flomerfelt, R.E. Gress, Analysis of Cell Proliferation and Homeostasis Using EdU Labeling, in: Methods in Molecular Biology, Humana Press, New York, 2016: pp. 211–220. https://doi.org/10.1007/978-1-4939-2809-5_18.

[105] M. Ghasemi, T. Turnbull, S. Sebastian, I. Kempson, The MTT Assay: Utility, Limitations, Pitfalls, and Interpretation in Bulk and Single-Cell Analysis, Int J Mol Sci. 22 (2021) 12827. https://doi.org/10.3390/ijms222312827.

[106] H.J. Shulman, A. Opler, The stimulatory effect of calcium on the synthesis of cartilage proteoglycan, Biochem Biophys Res Commun. 59 (1974) 914–919. https://doi.org/10.1016/S0006-291X(74)80066-5.

[107] Y. Henrotin, A. Labasse, S.X. Zheng, Ph. Galais, Y. Tsouderos, J.M. Crielaard, J.Y. Reginster, Strontium Ranelate Increases Cartilage Matrix Formation, Journal of Bone and Mineral Research. 16 (2001) 299–308. https://doi.org/10.1359/jbmr.2001.16.2.299.

[108] J. Wang, X. Zhu, L. Liu, X. Shi, L. Yin, Y. Zhang, X. Li, Z. Wang, G. Liu, Effects of Strontium on Collagen Content and Expression of Related Genes in Rat Chondrocytes Cultured In Vitro, Biol Trace Elem Res. 153 (2013) 212–219. https://doi.org/10.1007/s12011-013-9640-9.

[109] C. Deng, H. Zhu, J. Li, C. Feng, Q. Yao, L. Wang, J. Chang, C. Wu, Bioactive Scaffolds for Regeneration of Cartilage and Subchondral Bone Interface, Theranostics. 8 (2018) 1940–1955. https://doi.org/10.7150/thno.23674.

[110] N. Okita, Y. Honda, N. Kishimoto, W. Liao, E. Azumi, Y. Hashimoto, N. Matsumoto, Supplementation of Strontium to a Chondrogenic Medium Promotes Chondrogenic Differentiation of Human Dedifferentiated Fat Cells, Tissue Eng Part A. 21 (2015) 1695–1704. https://doi.org/10.1089/ten.tea.2014.0282.

[111] H. Yu, Y. Liu, X. Yang, J. He, F. Zhang, Q. Zhong, X. Guo, Strontium ranelate promotes chondrogenesis through inhibition of the Wnt/β-catenin pathway, Stem Cell Res Ther. 12 (2021) 296. https://doi.org/10.1186/s13287-021-02372-z.

[112] P. Hu, J. Du, S. Zhang, T. Wang, J. Li, G. Chen, G. Zhou, Oral Administration of Strontium Gluconate Effectively Reduces Articular Cartilage Degeneration Through Enhanced Anabolic Activity of Chondrocytes and Chondrogenetic Differentiation of Mesenchymal Stromal Cells, Biol Trace Elem Res. 193 (2020) 422–433. https://doi.org/10.1007/s12011-019-01711-9.

[113] J.-P. Pelletier, M. Kapoor, H. Fahmi, D. Lajeunesse, A. Blesius, J. Maillet, J. Martel-Pelletier, Strontium ranelate reduces the progression of experimental dog osteoarthritis by inhibiting the expression of key proteases in cartilage and of IL-1β in the synovium, Ann Rheum Dis. 72 (2013) 250–257. https://doi.org/10.1136/annrheumdis-2012-201710.

[114] J.-P. Pelletier, C. Roubille, J.-P. Raynauld, F. Abram, M. Dorais, P. Delorme, J. Martel-Pelletier, Disease-modifying effect of strontium ranelate in a subset of patients from the Phase III knee osteoarthritis study SEKOIA using quantitative MRI: reduction in bone marrow lesions protects against cartilage loss, Ann Rheum Dis. 74 (2015) 422–429. https://doi.org/10.1136/annrheumdis-2013-203989.

[115] P. Alexandersen, M.A. Karsdal, I. Byrjalsen, C. Christiansen, Strontium ranelate effect in postmenopausal women with different clinical levels of osteoarthritis, Climacteric. 14 (2011) 236–243. https://doi.org/10.3109/13697137.2010.507887.

[116] O. Bruyere, D. Delferriere, C. Roux, J.D. Wark, T. Spector, J.-P. Devogelaer, K. Brixen, S. Adami, J. Fechtenbaum, S. Kolta, J.-Y. Reginster, Effects of strontium ranelate on spinal osteoarthritis progression, Ann Rheum Dis. 67 (2007) 335–339. https://doi.org/10.1136/ard.2007.075572.

[117] T. Jiang, H.-M. Kan, K. Rajpura, E.J. Carbone, Y. Li, K.W.-H. Lo, Development of Targeted Nanoscale Drug Delivery System for Osteoarthritic Cartilage Tissue, J Nanosci Nanotechnol. 18 (2018) 2310–2317. https://doi.org/10.1166/jnn.2018.14311.

[118] H. Huang, Z. Lou, S. Zheng, J. Wu, Q. Yao, R. Chen, L. Kou, D. Chen, Intra-articular drug delivery systems for osteoarthritis therapy: shifting from sustained release to enhancing penetration into cartilage, Drug Deliv. 29 (2022) 767–791. https://doi.org/10.1080/10717544.2022.2048130.

[119] Y. Takechi-Haraya, T. Ohgita, Y. Demizu, H. Saito, K. Izutsu, K. Sakai-Kato, Current Status and Challenges of Analytical Methods for Evaluation of Size and Surface Modification of Nanoparticle-Based Drug Formulations, AAPS PharmSciTech. 23 (2022) 150. https://doi.org/10.1208/s12249-022-02303-y.

[120] S. Mahmood, U.K. Mandal, B. Chatterjee, M. Taher, Advanced characterizations of nanoparticles for drug delivery: investigating their properties through the techniques used in their evaluations, Nanotechnol Rev. 6 (2017) 355–372. https://doi.org/10.1515/ntrev-2016-0050.

[121] N. Jurga, D. Przybylska, P. Kamiński, T. Grzyb, Improvement of ligand-free modification strategy to obtain water-stable up-converting nanoparticles with bright emission and high reaction yield, Sci Rep. 11 (2021) 18846. https://doi.org/10.1038/s41598-021-98240-0.

[122] M.-D. Yan, Y.-J. Ou, Y.-J. Lin, R.-M. Liu, Y. Fang, W.-L. Wu, L. Zhou, X. Yao, J. Chen, Does the incorporation of strontium into calcium phosphate improve bone repair? A meta-analysis, BMC Oral Health. 22 (2022) 62. https://doi.org/10.1186/s12903-022-02092-7.

[123] K. Qiu, X.J. Zhao, C.X. Wan, C.S. Zhao, Y.W. Chen, Effect of strontium ions on the growth of ROS17/2.8 cells on porous calcium polyphosphate scaffolds, Biomaterials. 27 (2006) 1277–1286. https://doi.org/10.1016/j.biomaterials.2005.08.006.

[124] M. Tian, F. Chen, W. Song, Y. Song, Y. Chen, C. Wan, X. Yu, X. Zhang, In vivo study of porous strontium-doped calcium polyphosphate scaffolds for bone substitute applications, J Mater Sci Mater Med. 20 (2009) 1505–1512. https://doi.org/10.1007/s10856-009-3713-5.

[125] F. Liu, X. Zhang, X. Yu, Y. Xu, T. Feng, D. Ren, In vitro study in stimulating the secretion of angiogenic growth factors of strontium-doped calcium polyphosphate for bone tissue engineering, J Mater Sci Mater Med. 22 (2011) 683–692. https://doi.org/10.1007/s10856-011-4247-1.

[126] Z. Gu, X. Zhang, L. Li, Q. Wang, X. Yu, T. Feng, Acceleration of segmental bone regeneration in a rabbit model by strontium-doped calcium polyphosphate scaffold through stimulating VEGF and bFGF secretion from osteoblasts, Materials Science and Engineering: C. 33 (2013) 274–281. https://doi.org/10.1016/j.msec.2012.08.040.

[127] H.T. Phan, A.J. Haes, What Does Nanoparticle Stability Mean?, The Journal of Physical Chemistry C. 123 (2019) 16495–16507. https://doi.org/10.1021/acs.jpcc.9b00913.

[128] X. Zhao, S. Ng, B.C. Heng, J. Guo, L. Ma, T.T.Y. Tan, K.W. Ng, S.C.J. Loo, Cytotoxicity of hydroxyapatite nanoparticles is shape and cell dependent, Arch Toxicol. 87 (2013) 1037–1052. https://doi.org/10.1007/s00204-012-0827-1.

[129] P.A. Hassan, S. Rana, G. Verma, Making Sense of Brownian Motion: Colloid Characterization by Dynamic Light Scattering, Langmuir. 31 (2015) 3–12. https://doi.org/10.1021/la501789z.

[130] A. Kim, W.B. Ng, W. Bernt, N.-J. Cho, Validation of Size Estimation of Nanoparticle Tracking Analysis on Polydisperse Macromolecule Assembly, Sci Rep. 9 (2019) 2639. https://doi.org/10.1038/s41598-019-38915-x.

[131] P. Eaton, P. Quaresma, C. Soares, C. Neves, M.P. de Almeida, E. Pereira, P. West, A direct comparison of experimental methods to measure dimensions of synthetic nanoparticles, Ultramicroscopy. 182 (2017) 179–190. https://doi.org/10.1016/j.ultramic.2017.07.001.

[132] J.-P. St-Pierre, L. Gan, J. Wang, R.M. Pilliar, M.D. Grynpas, R.A. Kandel, The incorporation of a zone of calcified cartilage improves the interfacial shear strength between in vitro-formed cartilage and the underlying substrate, Acta Biomater. 8 (2012) 1603–1615. https://doi.org/10.1016/j.actbio.2011.12.022.

[133] M.L. Renier, D.H. Kohn, Development and characterization of a biodegradable polyphosphate., J Biomed Mater Res. 34 (1997) 95–104. https://doi.org/10.1002/(sici)1097-4636(199701)34:1<95::aid-jbm13>3.0.co;2-o.

[134] Z. He, C.W. Honeycutt, B. Xing, R.W. McDowell, P.J. Pellechia, T. Zhang, SOLID-STATE FOURIER TRANSFORM INFRARED AND 31P NUCLEAR MAGNETIC

RESONANCE SPECTRAL FEATURES OF PHOSPHATE COMPOUNDS, Soil Sci. 172 (2007) 501–515. https://doi.org/10.1097/SS.0b013e318053dba0.

[135] A. Khoshmanesh, P.L.M. Cook, B.R. Wood, Quantitative determination of polyphosphate in sediments using Attenuated Total Reflectance-Fourier Transform Infrared (ATR-FTIR) spectroscopy and partial least squares regression, Analyst. 137 (2012) 3704. https://doi.org/10.1039/c2an35289c.

[136] J.J. Christ, S. Willbold, L.M. Blank, Methods for the Analysis of Polyphosphate in the Life Sciences, Anal Chem. 92 (2020) 4167–4176. https://doi.org/10.1021/acs.analchem.9b05144.

[137] J.D. Clogston, A.K. Patri, Zeta Potential Measurement, in: Characterization of Nanoparticles Intended for Drug Delivery, Humana Press, 2011: pp. 63–70. https://doi.org/10.1007/978-1-60327-198-1_6.

[138] A. Sikora, D. Bartczak, D. Geißler, V. Kestens, G. Roebben, Y. Ramaye, Z. Varga, M. Palmai, A.G. Shard, H. Goenaga-Infante, C. Minelli, A systematic comparison of different techniques to determine the zeta potential of silica nanoparticles in biological medium, Analytical Methods. 7 (2015) 9835–9843. https://doi.org/10.1039/C5AY02014J.

[139] E.S. Baluyot, C. G. Hartford, Comparison of polyphosphate analysis by ion chromatography and by modified end-group titration, J Chromatogr A. 739 (1996) 217–222. https://doi.org/10.1016/0021-9673(96)00027-1.

[140] U. Pilatus, A. Mayer, A. Hildebrandt, Nuclear polyphosphate as a possible source of energy during the sporulation of Physarum polycephalum, Arch Biochem Biophys. 275 (1989) 215–223. https://doi.org/10.1016/0003-9861(89)90366-4.

[141] B.L. Turner, N. Mahieu, L.M. Condron, Phosphorus-31 Nuclear Magnetic Resonance Spectral Assignments of Phosphorus Compounds in Soil NaOH–EDTA Extracts, Soil Science Society of America Journal. 67 (2003) 497. https://doi.org/10.2136/sssaj2003.0497.

[142] L.B. Casabianca, Solid-state nuclear magnetic resonance studies of nanoparticles, Solid State Nucl Magn Reson. 107 (2020) 101664. https://doi.org/10.1016/j.ssnmr.2020.101664.

[143] B. Reif, S.E. Ashbrook, L. Emsley, M. Hong, Solid-state NMR spectroscopy, Nature Reviews Methods Primers. 1 (2021) 2. https://doi.org/10.1038/s43586-020-00002-1.

[144] N.A. Cummings, G.L. Nordby, Measurement of synovial fluid pH in normal and arthritic knees, Arthritis Rheum. 9 (1966) 47–56. https://doi.org/10.1002/art.1780090106.

[145] E.H. Jebens, M.E. Monk-Jones, ON THE VISCOSITY AND pH OF SYNOVIAL FLUID AND THE pH OF BLOOD, J Bone Joint Surg Br. 41-B (1959) 388–400. https://doi.org/10.1302/0301-620X.41B2.388.

[146] I. Milošev, V. Levašič, J. Vidmar, S. Kovač, R. Trebše, pH and metal concentration of synovial fluid of osteoarthritic joints and joints with metal replacements, J Biomed Mater Res B Appl Biomater. 105 (2017) 2507–2515. https://doi.org/10.1002/jbm.b.33793.

[147] A. Hall, E. Horwitz, R. Wilkins, The cellular physiology of articular cartilage, Exp Physiol. 81 (1996) 535–545. https://doi.org/10.1113/expphysiol.1996.sp003956.

[148] Y.T. Konttinen, J. Mandelin, T.-F. Li, J. Salo, J. Lassus, M. Liljeström, M. Hukkanen, M. Takagi, I. Virtanen, S. Santavirta, Acidic cysteine endoproteinase cathepsin K in the degeneration of the superficial articular hyaline cartilage in osteoarthritis, Arthritis Rheum. 46 (2002) 953–960. https://doi.org/10.1002/art.10185.

[149] R.A. French, A.R. Jacobson, B. Kim, S.L. Isley, R.L. Penn, P.C. Baveye, Influence of Ionic Strength, pH, and Cation Valence on Aggregation Kinetics of Titanium Dioxide Nanoparticles, Environ Sci Technol. 43 (2009) 1354–1359. https://doi.org/10.1021/es802628n.

[150] I.P.D. Picola, K.A.N. Busson, A.H. Casé, F.D. Nasário, V.A. de O. Tiera, S.R. Taboga, J.R. Neto, M.J. Tiera, Effect of ionic strength solution on the stability of chitosan–DNA nanoparticles, J Exp Nanosci. 8 (2013) 703–716. https://doi.org/10.1080/17458080.2011.602120.

[151] L. Wang, X. Yang, Q. Wang, Y. Zeng, L. Ding, W. Jiang, Effects of ionic strength and temperature on the aggregation and deposition of multi-walled carbon nanotubes, Journal of Environmental Sciences. 51 (2017) 248–255. https://doi.org/10.1016/j.jes.2016.07.003.

[152] B. Derjaguin, L. Landau, Theory of the stability of strongly charged lyophobic sols and of the adhesion of strongly charged particles in solutions of electrolytes, Acta Physicochimica U. R. S. S. 14 (1941) 633–662.

[153] E.J.W. Verwey, J.Th.G. Overbeek, Theory of the Stability of Lyophobic Colloids, Elsevier, Amsterdam, 1948.

[154] W. Choi, U. Mahajan, S.-M. Lee, J. Abiade, R.K. Singh, Effect of Slurry Ionic Salts at Dielectric Silica CMP, J Electrochem Soc. 151 (2004) G185. https://doi.org/10.1149/1.1644609.

[155] H. Falahati, L. Wong, L. Davarpanah, A. Garg, P. Schmitz, D.P.J. Barz, The zeta potential of PMMA in contact with electrolytes of various conditions: Theoretical and experimental investigation, Electrophoresis. 35 (2014) 870–882. https://doi.org/10.1002/elps.201300436.

[156] S. Dong, Z. Zeng, W. Cai, Z. Zhou, C. Dou, H. Liu, J. Xia, The zeta potentials of g-C3N4 nanoparticles: Effect of electrolyte, ionic strength, pH, and humic acid, Journal of Nanoparticle Research. 21 (2019) 233. https://doi.org/10.1007/s11051-019-4686-z.

[157] D. Bastos, F.J. de las Nieves, Effect of electrolyte type on the electrokinetic behavior of sulfonated polystyrene model colloids, Colloid Polym Sci. 271 (1993) 860–867. https://doi.org/10.1007/BF00652768.

[158] M. Elimelech, C.R. O'Melia, Effect of electrolyte type on the electrophoretic mobility of polystyrene latex colloids, Colloids and Surfaces. 44 (1990) 165–178. https://doi.org/10.1016/0166-6622(90)80194-9.

[159] R. Folkersma, A.J.G. van Diemen, H.N. Stein, Electrophoretic Properties of Polystyrene Spheres, Langmuir. 14 (1998) 5973–5976. https://doi.org/10.1021/la980225b.

[160] P. Leroy, C. Tournassat, O. Bernard, N. Devau, M. Azaroual, The electrophoretic mobility of montmorillonite. Zeta potential and surface conductivity effects, J Colloid Interface Sci. 451 (2015) 21–39. https://doi.org/10.1016/j.jcis.2015.03.047.

[161] F. Yang, W. Wu, S. Chen, W. Gan, The ionic strength dependent zeta potential at the surface of hexadecane droplets in water and the corresponding interfacial adsorption of surfactants, Soft Matter. 13 (2017) 638–646. https://doi.org/10.1039/C6SM02174C.

[162] R. Rampado, S. Crotti, P. Caliceti, S. Pucciarelli, M. Agostini, Recent Advances in Understanding the Protein Corona of Nanoparticles and in the Formulation of "Stealthy" Nanomaterials, Front Bioeng Biotechnol. 8 (2020). https://doi.org/10.3389/fbioe.2020.00166.

[163] N. Singh, C. Marets, J. Boudon, N. Millot, L. Saviot, L. Maurizi, *In vivo* protein corona on nanoparticles: does the control of all material parameters orient the biological behavior?, Nanoscale Adv. 3 (2021) 1209–1229. https://doi.org/10.1039/D0NA00863J.

[164] A. Tomak, S. Cesmeli, B.D. Hanoglu, D. Winkler, C. Oksel Karakus, Nanoparticle-protein corona complex: understanding multiple interactions between environmental factors, corona formation, and biological activity, Nanotoxicology. 15 (2021) 1331–1357. https://doi.org/10.1080/17435390.2022.2025467.

[165] P. Bihari, M. Vippola, S. Schultes, M. Praetner, A.G. Khandoga, C.A. Reichel, C. Coester, T. Tuomi, M. Rehberg, F. Krombach, Optimized dispersion of nanoparticles for biological in vitro and in vivo studies, Part Fibre Toxicol. 5 (2008) 14. https://doi.org/10.1186/1743-8977-5-14.

[166] R.C. Murdock, L. Braydich-Stolle, A.M. Schrand, J.J. Schlager, S.M. Hussain, Characterization of Nanomaterial Dispersion in Solution Prior to In Vitro Exposure Using Dynamic Light Scattering Technique, Toxicological Sciences. 101 (2008) 239–253. https://doi.org/10.1093/toxsci/kfm240.

[167] D. Mahl, C. Greulich, W. Meyer-Zaika, M. Köller, M. Epple, Gold nanoparticles: dispersibility in biological media and cell-biological effect, J Mater Chem. 20 (2010) 6176. https://doi.org/10.1039/c0jm01071e.

[168] Z. Ji, X. Jin, S. George, T. Xia, H. Meng, X. Wang, E. Suarez, H. Zhang, E.M.V. Hoek, H. Godwin, A.E. Nel, J.I. Zink, Dispersion and Stability Optimization of TiO_2 Nanoparticles in Cell Culture Media, Environ Sci Technol. 44 (2010) 7309–7314. https://doi.org/10.1021/es100417s.

[169] S. Kittler, C. Greulich, J.S. Gebauer, J. Diendorf, L. Treuel, L. Ruiz, J.M. Gonzalez-Calbet, M. Vallet-Regi, R. Zellner, M. Köller, M. Epple, The influence of proteins on the dispersability and cell-biological activity of silver nanoparticles, J Mater Chem. 20 (2010) 512–518. https://doi.org/10.1039/B914875B.

[170] H.T.R. Wiogo, M. Lim, V. Bulmus, L. Gutiérrez, R.C. Woodward, R. Amal, Insight into Serum Protein Interactions with Functionalized Magnetic Nanoparticles in Biological Media, Langmuir. 28 (2012) 4346–4356. https://doi.org/10.1021/la204740t.

[171] C. Graf, Q. Gao, I. Schütz, C.N. Noufele, W. Ruan, U. Posselt, E. Korotianskiy, D. Nordmeyer, F. Rancan, S. Hadam, A. Vogt, J. Lademann, V. Haucke, E. Rühl, Surface Functionalization of Silica Nanoparticles Supports Colloidal Stability in Physiological Media and Facilitates Internalization in Cells, Langmuir. 28 (2012) 7598–7613. https://doi.org/10.1021/la204913t.

[172] J. Cohen, G. DeLoid, G. Pyrgiotakis, P. Demokritou, Interactions of engineered nanomaterials in physiological media and implications for *in vitro* dosimetry, Nanotoxicology. 7 (2013) 417–431. https://doi.org/10.3109/17435390.2012.666576.

[173] C.S. Chern, C.K. Lee, C.C. Ho, Electrostatic interaction between chitosan-modified latex particles and bovine serum albumin, Colloid Polym Sci. 277 (1999) 979–985. https://doi.org/10.1007/s003960050478.

[174] T.L. Moore, L. Rodriguez-Lorenzo, V. Hirsch, S. Balog, D. Urban, C. Jud, B. Rothen-Rutishauser, M. Lattuada, A. Petri-Fink, Nanoparticle colloidal stability in cell culture media and impact on cellular interactions, Chem Soc Rev. 44 (2015) 6287–6305. https://doi.org/10.1039/C4CS00487F.

[175] A.C. Sabuncu, J. Grubbs, S. Qian, T.M. Abdel-Fattah, M.W. Stacey, A. Beskok, Probing nanoparticle interactions in cell culture media, Colloids Surf B Biointerfaces. 95 (2012) 96–102. https://doi.org/10.1016/j.colsurfb.2012.02.022.

[176] Y. Ma, Y. Guo, S. Wu, Z. Lv, Q. Zhang, Y. Ke, Titanium dioxide nanoparticles induce size-dependent cytotoxicity and genomic DNA hypomethylation in human respiratory cells, RSC Adv. 7 (2017) 23560–23572. https://doi.org/10.1039/C6RA28272E.

[177] I. Szilagyi, A. Sadeghpour, M. Borkovec, Destabilization of Colloidal Suspensions by Multivalent Ions and Polyelectrolytes: From Screening to Overcharging, Langmuir. 28 (2012) 6211–6215. https://doi.org/10.1021/la300542y.

[178] M.P. Monopoli, D. Walczyk, A. Campbell, G. Elia, I. Lynch, F. Baldelli Bombelli, K.A. Dawson, Physical−Chemical Aspects of Protein Corona: Relevance to *in Vitro* and *in Vivo* Biological Impacts of Nanoparticles, J Am Chem Soc. 133 (2011) 2525–2534. https://doi.org/10.1021/ja107583h.

[179] M. Schäffler, M. Semmler-Behnke, H. Sarioglu, S. Takenaka, A. Wenk, C. Schleh, S.M. Hauck, B.D. Johnston, W.G. Kreyling, Serum protein identification and quantification of the corona of 5, 15 and 80 nm gold nanoparticles, Nanotechnology. 24 (2013) 265103. https://doi.org/10.1088/0957-4484/24/26/265103.

[180] K. Partikel, R. Korte, D. Mulac, H.-U. Humpf, K. Langer, Serum type and concentration both affect the protein-corona composition of PLGA nanoparticles, Beilstein Journal of Nanotechnology. 10 (2019) 1002–1015. https://doi.org/10.3762/bjnano.10.101.

[181] A.Y. Hui, W.J. McCarty, K. Masuda, G.S. Firestein, R.L. Sah, A systems biology approach to synovial joint lubrication in health, injury, and disease, WIREs Systems Biology and Medicine. 4 (2012) 15–37. https://doi.org/10.1002/wsbm.157.

[182] S. Shanreld, P. Campbell, M. Baumgarten, R. Bloebaum, A. Sarmiento, Synovial Fluid Osmolality in Osteoarthritis and Rheumatoid Arthritis, Clin Orthop Relat Res. 235 (1988) 289–295. https://doi.org/10.1097/00003086-198810000-00029.

[183] M. Baumgarten, R.D. Bloebaum, S.D. Ross, P. Campbell, A. Sarmiento, Normal Human Synovial Fluid: Osmolality and Exercise-Induced Changes, J Bone Joint Surg. 67 (1985) 1336–1339. https://doi.org/10.2106/00004623-198567090-00005.

[184] H. Brouwers, J.H. von Hegedus, E. van der Linden, R. Mahdad, M. Kloppenburg, R. Toes, M. Giera, A. Ioan-Facsinay, Hyaluronidase treatment of synovial fluid is required for accurate detection of inflammatory cells and soluble mediators, Arthritis Res Ther. 24 (2022) 18. https://doi.org/10.1186/s13075-021-02696-4.

[185] T.M. Tamer, Hyaluronan and synovial joint: function, distribution and healing, Interdiscip Toxicol. 6 (2013) 111–125. https://doi.org/10.2478/intox-2013-0019.

[186] A.M. Alkilany, P.K. Nagaria, C.R. Hexel, T.J. Shaw, C.J. Murphy, M.D. Wyatt, Cellular Uptake and Cytotoxicity of Gold Nanorods: Molecular Origin of Cytotoxicity and Surface Effects, Small. 5 (2009) 701–708. https://doi.org/10.1002/smll.200801546.

[187] Y. Zhang, B. Newton, E. Lewis, P.P. Fu, R. Kafoury, P.C. Ray, H. Yu, Cytotoxicity of organic surface coating agents used for nanoparticles synthesis and stability, Toxicology in Vitro. 29 (2015) 762–768. https://doi.org/10.1016/j.tiv.2015.01.017.

[188] Y.P. Jia, K. Shi, J.F. Liao, J.R. Peng, Y. Hao, Y. Qu, L.J. Chen, L. Liu, X. Yuan, Z.Y. Qian, X.W. Wei, Effects of Cetyltrimethylammonium Bromide on the Toxicity of Gold Nanorods Both In Vitro and In Vivo: Molecular Origin of Cytotoxicity and Inflammation, Small Methods. 4 (2020) 1900799. https://doi.org/10.1002/smtd.201900799.

[189] I. Aranaz, A.R. Alcántara, M.C. Civera, C. Arias, B. Elorza, A. Heras Caballero, N. Acosta, Chitosan: An Overview of Its Properties and Applications, Polymers (Basel). 13 (2021) 3256. https://doi.org/10.3390/polym13193256.

[190] H.-J. de Jager, A.M. Heyns, Study of the Hydrolysis of Sodium Polyphosphate in Water Using Raman Spectroscopy, Appl Spectrosc. 52 (1998) 808–814. https://doi.org/10.1366/0003702981944535.

[191] S.M. Moghimi, P. Symonds, J.C. Murray, A.C. Hunter, G. Debska, A. Szewczyk, A two-stage poly(ethylenimine)-mediated cytotoxicity: implications for gene transfer/therapy, Molecular Therapy. 11 (2005) 990–995. https://doi.org/10.1016/j.ymthe.2005.02.010.

[192] V. Kafil, Y. Omidi, Cytotoxic impacts of linear and branched polyethylenimine nanostructures in a431 cells., BioImpacts. 1 (2011) 23–30. https://doi.org/10.5681/bi.2011.004.

[193] Z. Xu, G. Shen, X. Xia, X. Zhao, P. Zhang, H. Wu, Q. Guo, Z. Qian, Y. Wei, S. Liang, Comparisons of three polyethyleneimine-derived nanoparticles as a gene therapy delivery system for renal cell carcinoma, J Transl Med. 9 (2011) 46. https://doi.org/10.1186/1479-5876-9-46.

[194] S.H. Choi, J.N.R. Collins, S.A. Smith, R.L. Davis-Harrison, C.M. Rienstra, J.H. Morrissey, Phosphoramidate End Labeling of Inorganic Polyphosphates: Facile Manipulation of Polyphosphate for Investigating and Modulating Its Biological Activities, Biochemistry. 49 (2010) 9935–9941. https://doi.org/10.1021/bi1014437.

[195] G.M. Fernandes-Cunha, C.J. McKinlay, J.R. Vargas, H.J. Jessen, R.M. Waymouth, P.A. Wender, Delivery of Inorganic Polyphosphate into Cells Using Amphipathic

Oligocarbonate Transporters, ACS Cent Sci. 4 (2018) 1394–1402. https://doi.org/10.1021/acscentsci.8b00470.

[196] C.J. Baker, S.A. Smith, J.H. Morrissey, Diversification of polyphosphate end-labeling via bridging molecules, PLoS One. 15 (2020) e0237849. https://doi.org/10.1371/journal.pone.0237849.

[197] H.J. Shin, M. Kwak, S. Joo, J.Y. Lee, Quantifying fluorescent nanoparticle uptake in mammalian cells using a plate reader, Sci Rep. 12 (2022) 20146. https://doi.org/10.1038/s41598-022-24480-3.

[198] H. Shin, M. Kwak, T.G. Lee, J.Y. Lee, Quantifying the level of nanoparticle uptake in mammalian cells using flow cytometry, Nanoscale. 12 (2020) 15743–15751. https://doi.org/10.1039/D0NR01627F.

[199] G. Sahay, D.Y. Alakhova, A. V. Kabanov, Endocytosis of nanomedicines, Journal of Controlled Release. 145 (2010) 182–195. https://doi.org/10.1016/j.jconrel.2010.01.036.

[200] B. Yameen, W. il Choi, C. Vilos, A. Swami, J. Shi, O.C. Farokhzad, Insight into nanoparticle cellular uptake and intracellular targeting, Journal of Controlled Release. 190 (2014) 485–499. https://doi.org/10.1016/j.jconrel.2014.06.038.

[201] S. Behzadi, V. Serpooshan, W. Tao, M.A. Hamaly, M.Y. Alkawareek, E.C. Dreaden, D. Brown, A.M. Alkilany, O.C. Farokhzad, M. Mahmoudi, Cellular uptake of nanoparticles: journey inside the cell, Chem Soc Rev. 46 (2017) 4218–4244. https://doi.org/10.1039/C6CS00636A.

[202] P. Foroozandeh, A.A. Aziz, Insight into Cellular Uptake and Intracellular Trafficking of Nanoparticles, Nanoscale Res Lett. 13 (2018) 339. https://doi.org/10.1186/s11671-018-2728-6.

[203] J. Zhao, M.H. Stenzel, Entry of nanoparticles into cells: the importance of nanoparticle properties, Polym Chem. 9 (2018) 259–272. https://doi.org/10.1039/C7PY01603D.

[204] N.D. Donahue, H. Acar, S. Wilhelm, Concepts of nanoparticle cellular uptake, intracellular trafficking, and kinetics in nanomedicine, Adv Drug Deliv Rev. 143 (2019) 68–96. https://doi.org/10.1016/j.addr.2019.04.008.

[205] G. Griffiths, J. Gruenberg, M. Marsh, J. Wohlmann, A.T. Jones, R.G. Parton, Nanoparticle entry into cells; the cell biology weak link, Adv Drug Deliv Rev. 188 (2022) 114403. https://doi.org/10.1016/j.addr.2022.114403.

[206] E.C.G. Castillo, J.B. Kourí, A new role for chondrocytes as non-professional phagocytes. An in vitro study, Microsc Res Tech. 64 (2004) 269–278. https://doi.org/10.1002/jemt.20080.

[207] K. Kawata, S. Kubota, T. Eguchi, E. Aoyama, N.H. Moritani, S. Kondo, T. Nishida, M. Takigawa, Role of low-density lipoprotein receptor related protein 1 (LRP1) in CCN2/connective tissue growth factor (CTGF) protein transport in chondrocytes, J Cell Sci. (2012). https://doi.org/10.1242/jcs.101956.

[208] N.J. Wilsman, C.E. Farnum, D.K. Reed-Aksamit, Caveolar system of the articular chondrocyte, J Ultrastruct Res. 74 (1981) 1–10. https://doi.org/10.1016/S0022-5320(81)80105-0.

[209] J. Voigt, J. Christensen, V.P. Shastri, Differential uptake of nanoparticles by endothelial cells through polyelectrolytes with affinity for caveolae, Proceedings of the National Academy of Sciences. 111 (2014) 2942–2947. https://doi.org/10.1073/pnas.1322356111.

[210] A.M. Bannunah, D. Vllasaliu, J. Lord, S. Stolnik, Mechanisms of Nanoparticle Internalization and Transport Across an Intestinal Epithelial Cell Model: Effect of Size

and Surface Charge, Mol Pharm. 11 (2014) 4363–4373. https://doi.org/10.1021/mp500439c.

[211] B. Halamoda-Kenzaoui, M. Ceridono, P. Urbán, A. Bogni, J. Ponti, S. Gioria, A. Kinsner-Ovaskainen, The agglomeration state of nanoparticles can influence the mechanism of their cellular internalisation, J Nanobiotechnology. 15 (2017) 48. https://doi.org/10.1186/s12951-017-0281-6.

[212] C.E. Sims, N.L. Allbritton, Analysis of single mammalian cells on-chip, Lab Chip. 7 (2007) 423. https://doi.org/10.1039/b615235j.

[213] P. He, O. Mann-Collura, J. Fling, N. Edara, R. Hetz, M.S. Razzaque, High phosphate actively induces cytotoxicity by rewiring pro-survival and pro-apoptotic signaling networks in HEK293 and HeLa cells, The FASEB Journal. 35 (2021). https://doi.org/10.1096/fj.202000799RR.

[214] R. Alexander, N. Debiec, M.S. Razzaque, P. He, Inorganic phosphate-induced cytotoxicity, IUBMB Life. 74 (2022) 117–124. https://doi.org/10.1002/iub.2561.

[215] R. Hetz, E. Beeler, A. Janoczkin, S. Kiers, L. Li, B.B. Willard, M.S. Razzaque, P. He, Excessive Inorganic Phosphate Burden Perturbed Intracellular Signaling: Quantitative Proteomics and Phosphoproteomics Analyses, Front Nutr. 8 (2022). https://doi.org/10.3389/fnut.2021.765391.

[216] G.E. Kass, S. Orrenius, Calcium signaling and cytotoxicity., Environ Health Perspect. 107 (1999) 25–35. https://doi.org/10.1289/ehp.99107s125.

[217] M. Akter, Md.T. Sikder, Md.M. Rahman, A.K.M.A. Ullah, K.F.B. Hossain, S. Banik, T. Hosokawa, T. Saito, M. Kurasaki, A systematic review on silver nanoparticles-induced

cytotoxicity: Physicochemical properties and perspectives, J Adv Res. 9 (2018) 1–16. https://doi.org/10.1016/j.jare.2017.10.008.

[218] X. Dong, Z. Wu, X. Li, L. Xiao, M. Yang, Y. Li, J. Duan, Z. Sun, The Size-dependent Cytotoxicity of Amorphous Silica Nanoparticles: A Systematic Review of in vitro Studies, Int J Nanomedicine. 15 (2020) 9089–9113. https://doi.org/10.2147/IJN.S276105.

[219] H.I. Chiu, N.A. Samad, L. Fang, V. Lim, Cytotoxicity of targeted PLGA nanoparticles: a systematic review, RSC Adv. 11 (2021) 9433–9449. https://doi.org/10.1039/D1RA00074H.

[220] M.V.D.Z. Park, A.M. Neigh, J.P. Vermeulen, L.J.J. de la Fonteyne, H.W. Verharen, J.J. Briedé, H. van Loveren, W.H. de Jong, The effect of particle size on the cytotoxicity, inflammation, developmental toxicity and genotoxicity of silver nanoparticles, Biomaterials. 32 (2011) 9810–9817. https://doi.org/10.1016/j.biomaterials.2011.08.085.

[221] A.R. Gliga, S. Skoglund, I. Odnevall Wallinder, B. Fadeel, H.L. Karlsson, Size-dependent cytotoxicity of silver nanoparticles in human lung cells: the role of cellular uptake, agglomeration and Ag release, Part Fibre Toxicol. 11 (2014) 11. https://doi.org/10.1186/1743-8977-11-11.

[222] A. Ivask, I. Kurvet, K. Kasemets, I. Blinova, V. Aruoja, S. Suppi, H. Vija, A. Käkinen, T. Titma, M. Heinlaan, M. Visnapuu, D. Koller, V. Kisand, A. Kahru, Size-Dependent Toxicity of Silver Nanoparticles to Bacteria, Yeast, Algae, Crustaceans and Mammalian Cells In Vitro, PLoS One. 9 (2014) e102108. https://doi.org/10.1371/journal.pone.0102108.

[223] D. Sahu, G.M. Kannan, M. Tailang, R. Vijayaraghavan, *In Vitro* Cytotoxicity of Nanoparticles: A Comparison between Particle Size and Cell Type, Journal of Nanoscience. 2016 (2016) 1–9. https://doi.org/10.1155/2016/4023852.

[224] Q. Feng, Y. Liu, J. Huang, K. Chen, J. Huang, K. Xiao, Uptake, distribution, clearance, and toxicity of iron oxide nanoparticles with different sizes and coatings, Sci Rep. 8 (2018) 2082. https://doi.org/10.1038/s41598-018-19628-z.

[225] Q. Xia, J. Huang, Q. Feng, X. Chen, X. Liu, X. Li, T. Zhang, S. Xiao, H. Li, Z. Zhong, K. Xiao, Size- and cell type-dependent cellular uptake, cytotoxicity and in vivo distribution of gold nanoparticles, Int J Nanomedicine. 14 (2019) 6957–6970. https://doi.org/10.2147/IJN.S214008.

[226] Y. Pan, S. Neuss, A. Leifert, M. Fischler, F. Wen, U. Simon, G. Schmid, W. Brandau, W. Jahnen-Dechent, Size-Dependent Cytotoxicity of Gold Nanoparticles, Small. 3 (2007) 1941–1949. https://doi.org/10.1002/smll.200700378.

[227] M. Bayal, P. Janardhanan, E. Tom, N. Chandran, S. Devadathan, D. Ranjeet, U. Unniyampurath, R. Pilankatta, S.S. Nair, Cytotoxicity of nanoparticles - Are the size and shape only matters? or the media parameters too?: a study on band engineered ZnS nanoparticles and calculations based on equivolume stress model, Nanotoxicology. 13 (2019) 1005–1020. https://doi.org/10.1080/17435390.2019.1602678.

[228] N. Arrieta-Sandoval, P. Estrada Rojas, I. Olivas-Armendáriz, L.E. Valencia Gómez, J.F. Hernández Paz, B.E. Monarrez Cordero, C.A. Rodríguez González, Effect of Ag2S-BSA nanoparticle size on 3T3 fibroblast cell line cytotoxicity, Journal of Nanoparticle Research. 22 (2020) 106. https://doi.org/10.1007/s11051-020-04834-6.

[229] I. Na, D.C. Kennedy, Size-Specific Copper Nanoparticle Cytotoxicity Varies between Human Cell Lines, Int J Mol Sci. 22 (2021) 1548. https://doi.org/10.3390/ijms22041548.

[230] S.K. Sohaebuddin, P.T. Thevenot, D. Baker, J.W. Eaton, L. Tang, Nanomaterial cytotoxicity is composition, size, and cell type dependent, Part Fibre Toxicol. 7 (2010) 22. https://doi.org/10.1186/1743-8977-7-22.

[231] S. Sharifi, S. Behzadi, S. Laurent, M. Laird Forrest, P. Stroeve, M. Mahmoudi, Toxicity of nanomaterials, Chem. Soc. Rev. 41 (2012) 2323–2343. https://doi.org/10.1039/C1CS15188F.

[232] A. Sukhanova, S. Bozrova, P. Sokolov, M. Berestovoy, A. Karaulov, I. Nabiev, Dependence of Nanoparticle Toxicity on Their Physical and Chemical Properties, Nanoscale Res Lett. 13 (2018) 44. https://doi.org/10.1186/s11671-018-2457-x.

[233] S. Huo, S. Jin, X. Ma, X. Xue, K. Yang, A. Kumar, P.C. Wang, J. Zhang, Z. Hu, X.-J. Liang, Ultrasmall Gold Nanoparticles as Carriers for Nucleus-Based Gene Therapy Due to Size-Dependent Nuclear Entry, ACS Nano. 8 (2014) 5852–5862. https://doi.org/10.1021/nn5008572.

[234] G. Schmid, The relevance of shape and size of Au55 clusters, Chem Soc Rev. 37 (2008) 1909. https://doi.org/10.1039/b713631p.

[235] L. Wang, C.D. Fraley, J. Faridi, A. Kornberg, R.A. Roth, Inorganic polyphosphate stimulates mammalian TOR, a kinase involved in the proliferation of mammary cancer cells, Proceedings of the National Academy of Sciences. 100 (2003) 11249–11254. https://doi.org/10.1073/pnas.1534805100.

[236] T. Shiba, D. Nishimura, Y. Kawazoe, Y. Onodera, K. Tsutsumi, R. Nakamura, M. Ohshiro, Modulation of Mitogenic Activity of Fibroblast Growth Factors by Inorganic

Polyphosphate, Journal of Biological Chemistry. 278 (2003) 26788–26792. https://doi.org/10.1074/jbc.M303468200.

[237] J. Zhu, C.B. Thompson, Metabolic regulation of cell growth and proliferation, Nat Rev Mol Cell Biol. 20 (2019) 436–450. https://doi.org/10.1038/s41580-019-0123-5.

[238] W.E.G. Müller, H.C. Schröder, X. Wang, Inorganic Polyphosphates As Storage for and Generator of Metabolic Energy in the Extracellular Matrix, Chem Rev. 119 (2019) 12337–12374. https://doi.org/10.1021/acs.chemrev.9b00460.

[239] S.N.J. Moreno, R. Docampo, Polyphosphate and Its Diverse Functions in Host Cells and Pathogens, PLoS Pathog. 9 (2013) e1003230. https://doi.org/10.1371/journal.ppat.1003230.

[240] E. Pavlov, R. Aschar-Sobbi, M. Campanella, R.J. Turner, M.R. Gómez-García, A.Y. Abramov, Inorganic Polyphosphate and Energy Metabolism in Mammalian Cells, Journal of Biological Chemistry. 285 (2010) 9420–9428. https://doi.org/10.1074/jbc.M109.013011.

[241] A.Y. Baev, P.R. Angelova, A.Y. Abramov, Inorganic polyphosphate is produced and hydrolyzed in F0F1-ATP synthase of mammalian mitochondria, Biochemical Journal. 477 (2020) 1515–1524. https://doi.org/10.1042/BCJ20200042.

[242] M.E. Solesio, L. Xie, B. McIntyre, M. Ellenberger, E. Mitaishvili, S. Bhadra-Lobo, L.F. Bettcher, J.N. Bazil, D. Raftery, U. Jakob, E. v. Pavlov, Depletion of mitochondrial inorganic polyphosphate (polyP) in mammalian cells causes metabolic shift from oxidative phosphorylation to glycolysis, Biochemical Journal. 478 (2021) 1631–1646. https://doi.org/10.1042/BCJ20200975.

[243] M. Guitart-Mampel, P. Urquiza, F. Carnevale Neto, J.R. Anderson, V. Hambardikar, E.R. Scoma, G.E. Merrihew, L. Wang, M.J. MacCoss, D. Raftery, M.J. Peffers, M.E. Solesio, Mitochondrial Inorganic Polyphosphate (polyP) Is a Potent Regulator of Mammalian Bioenergetics in SH-SY5Y Cells: A Proteomics and Metabolomics Study, Front Cell Dev Biol. 10 (2022). https://doi.org/10.3389/fcell.2022.833127.

[244] K. Tsutsumi, T. Sasase, Cellular calcification induced by inorganic polyphosphate involves ATP depletion and opening of the mitochondrial permeability transition pore (mPTP), FEBS Open Bio. 9 (2019) 1617–1622. https://doi.org/10.1002/2211-5463.12703.

[245] U. von Mentzer, T. Selldén, L. Råberg, G. Erensoy, A.-K. Hultgård Ekwall, A. Stubelius, Synovial fluid profile dictates nanoparticle uptake into cartilage - implications of the protein corona for novel arthritis treatments, Osteoarthritis Cartilage. 30 (2022) 1356–1364. https://doi.org/10.1016/j.joca.2022.07.002.

[246] S. Brown, J. Pistiner, I.M. Adjei, B. Sharma, Nanoparticle Properties for Delivery to Cartilage: The Implications of Disease State, Synovial Fluid, and Off-Target Uptake, Mol Pharm. 16 (2019) 469–479. https://doi.org/10.1021/acs.molpharmaceut.7b00484.

[247] S.B. Brown, L. Wang, R.R. Jungels, B. Sharma, Effects of cartilage-targeting moieties on nanoparticle biodistribution in healthy and osteoarthritic joints, Acta Biomater. 101 (2020) 469–483. https://doi.org/10.1016/j.actbio.2019.10.003.

[248] A.G. Bajpayee, C.R. Wong, M.G. Bawendi, E.H. Frank, A.J. Grodzinsky, Avidin as a model for charge driven transport into cartilage and drug delivery for treating early stage post-traumatic osteoarthritis, Biomaterials. 35 (2014) 538–549. https://doi.org/10.1016/j.biomaterials.2013.09.091.

[249] S. Salucci, E. Falcieri, M. Battistelli, Chondrocyte death involvement in osteoarthritis, Cell Tissue Res. 389 (2022) 159–170. https://doi.org/10.1007/s00441-022-03639-4.

[250] S.D. Klimaj, Y. Licon Munoz, K. del Toro, W.C. Hines, A high-throughput imaging and quantification pipeline for the EVOS imaging platform, PLoS One. 15 (2020) e0236397. https://doi.org/10.1371/journal.pone.0236397.

[251] Y.-J. Kim, R.L.Y. Sah, J.-Y.H. Doong, A.J. Grodzinsky, Fluorometric assay of DNA in cartilage explants using Hoechst 33258, Anal Biochem. 174 (1988) 168–176. https://doi.org/10.1016/0003-2697(88)90532-5.

[252] H.C. Schröder, M. Neufurth, H. Zhou, S. Wang, X. Wang, W.E.G. Müller, Inorganic Polyphosphate: Coacervate Formation and Functional Significance in Nanomedical Applications, Int J Nanomedicine. 17 (2022) 5825–5850. https://doi.org/10.2147/IJN.S389819.

[253] Y.B. Li, C. Sodja, M. Rukhlova, J. Nhan, J.J.A. Poole, H. Allen, S. Yimer, E. Baumann, E. Bedford, H. Prazak, W.J. Costain, S. Murugkar, J.-P. St-Pierre, L. Mostaço-Guidolin, A. Jezierski, Angiogenesis driven extracellular matrix remodeling of 3D bioprinted vascular networks, Bioprinting. 30 (2023) e00258. https://doi.org/10.1016/j.bprint.2023.e00258.

[254] A. Anwar, Q. Kanwal, S. Akbar, A. Munawar, A. Durrani, M. Hassan Farooq, Synthesis and characterization of pure and nanosized hydroxyapatite bioceramics, Nanotechnol Rev. 6 (2017) 149–157. https://doi.org/10.1515/ntrev-2016-0020.

APPENDICES

A.1 Supplementary Figures and Tables

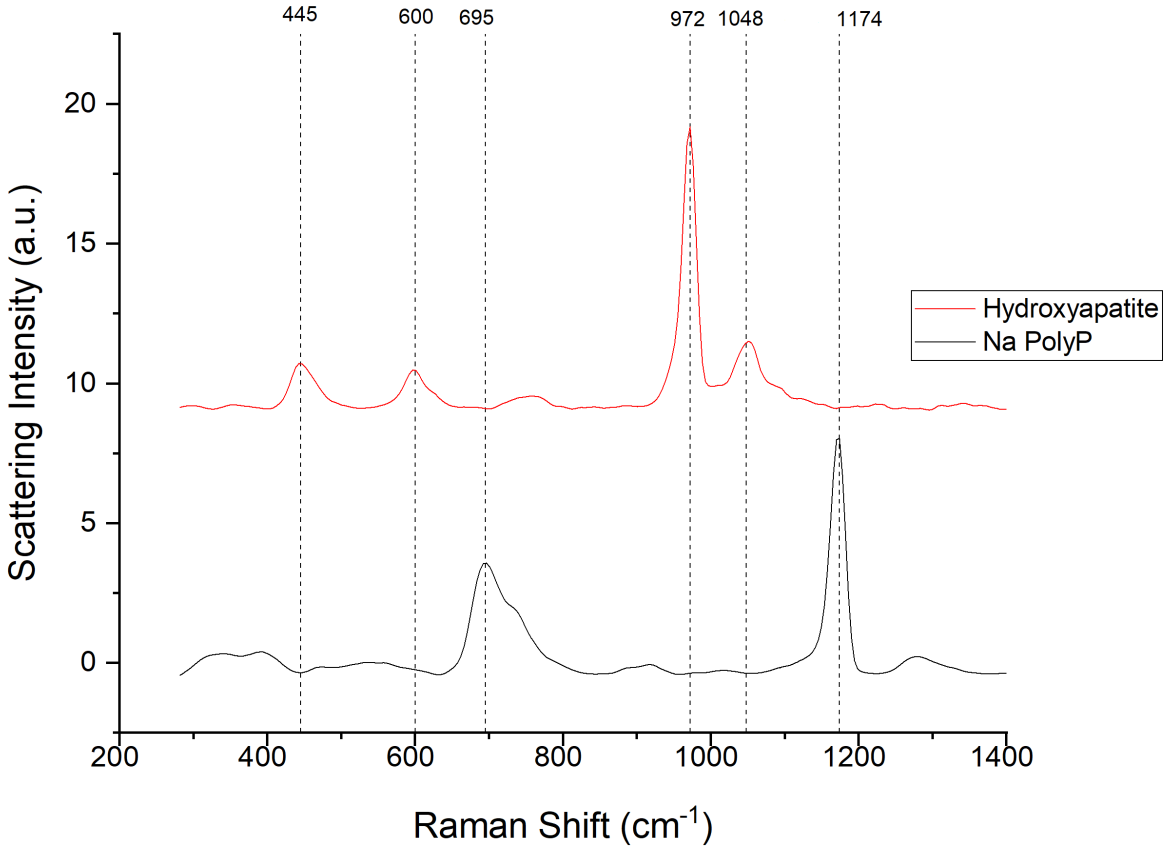

Supplementary Figure 1 – Raman spectra of Na-polyP and hydroxyapatite. Characteristic peaks of Na-polyP are present at 695 cm^{-1} (P–O–P stretching of the phosphate ester linkage) and 1174 cm^{-1} (symmetric stretching of PO_2^-). Meanwhile, characteristic peaks of hydroxyapatite at 445 $cm^{-1}$and 600 cm^{-1} (O–P–O bending), 972 cm^{-1} (symmetric stretching of P–O), and 1048 cm^{-1} (asymmetric stretching of P–O) are absent in polyP. Peaks were assigned from [136,254].

Supplementary Table 1 – Degree of ionization of phosphate groups of polyphosphate. Degree of ionization is defined as $[A^-]/[HA]$ and was estimated from the Henderson-Hasselbalch equation assuming each group behaves as a weak acid.

P-Subunit	pH = 7.0	pH = 8.5	pH = 10.0	pH = 11.5
$pK_a = 0.0$	1.00	1.00	1.00	1.00
$pK_a = 1.5$	1.00	1.00	1.00	1.00
$pK_a = 3.0$	1.00	1.00	1.00	1.00
End-Group	pH = 7.0	pH = 8.5	pH = 10.0	pH = 11.5
$pK_a = 7.0$	0.50	0.97	1.00	1.00
$pK_a = 8.0$	0.09	0.76	0.99	1.00
$pK_a = 9.0$	0.01	0.24	0.91	1.00

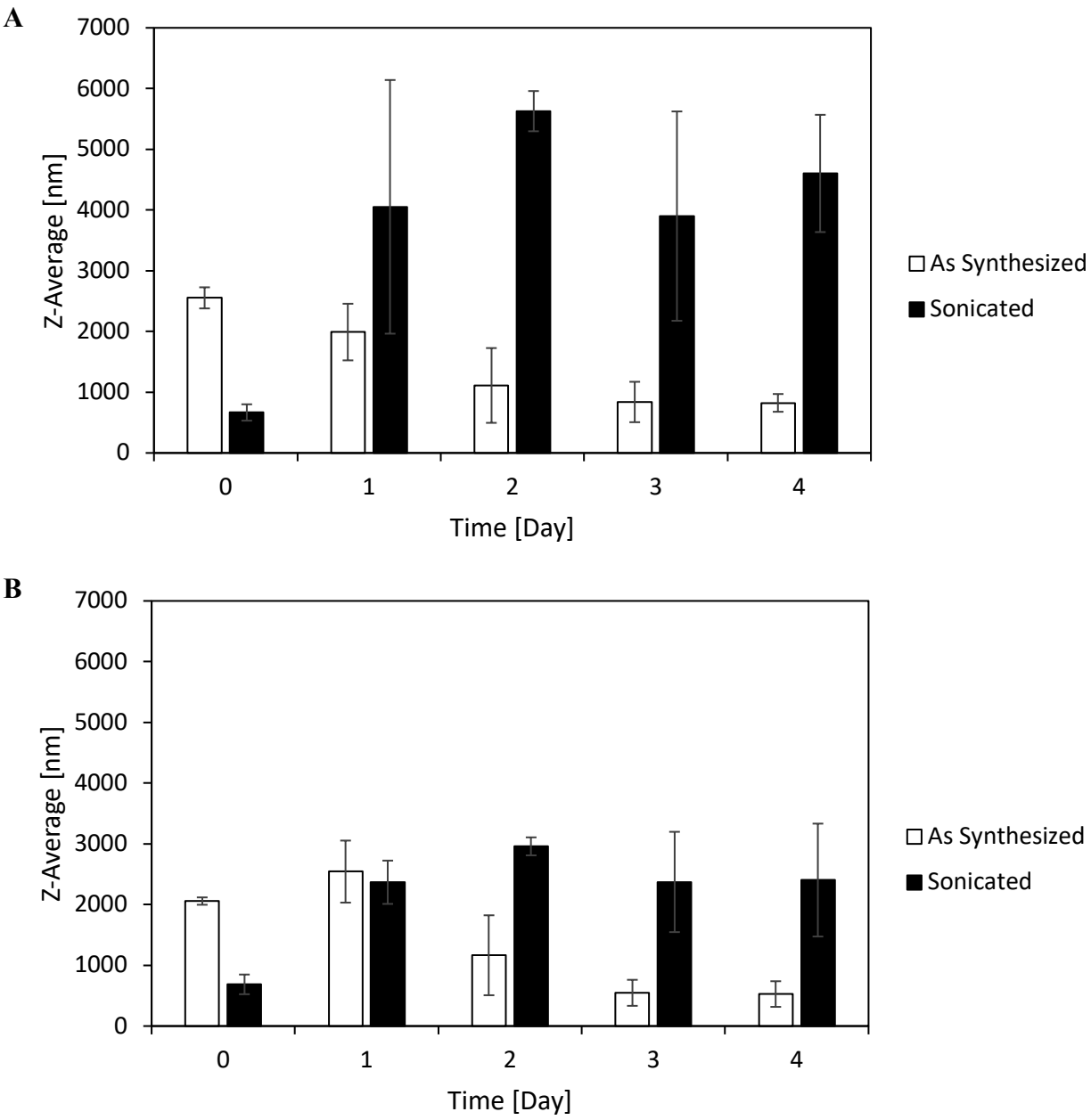

Supplementary Figure 2 – Size of polyP-based particles in synovial fluid. PolyP-based particle size was measured by DLS in 10% synovial fluid for **(A)** Ca-polyP and **(B)** Sr-polyP particles. Measurements were performed every day for 4 days to assess size stability. Data are presented as averages ± standard deviation for n = 3 experiments.

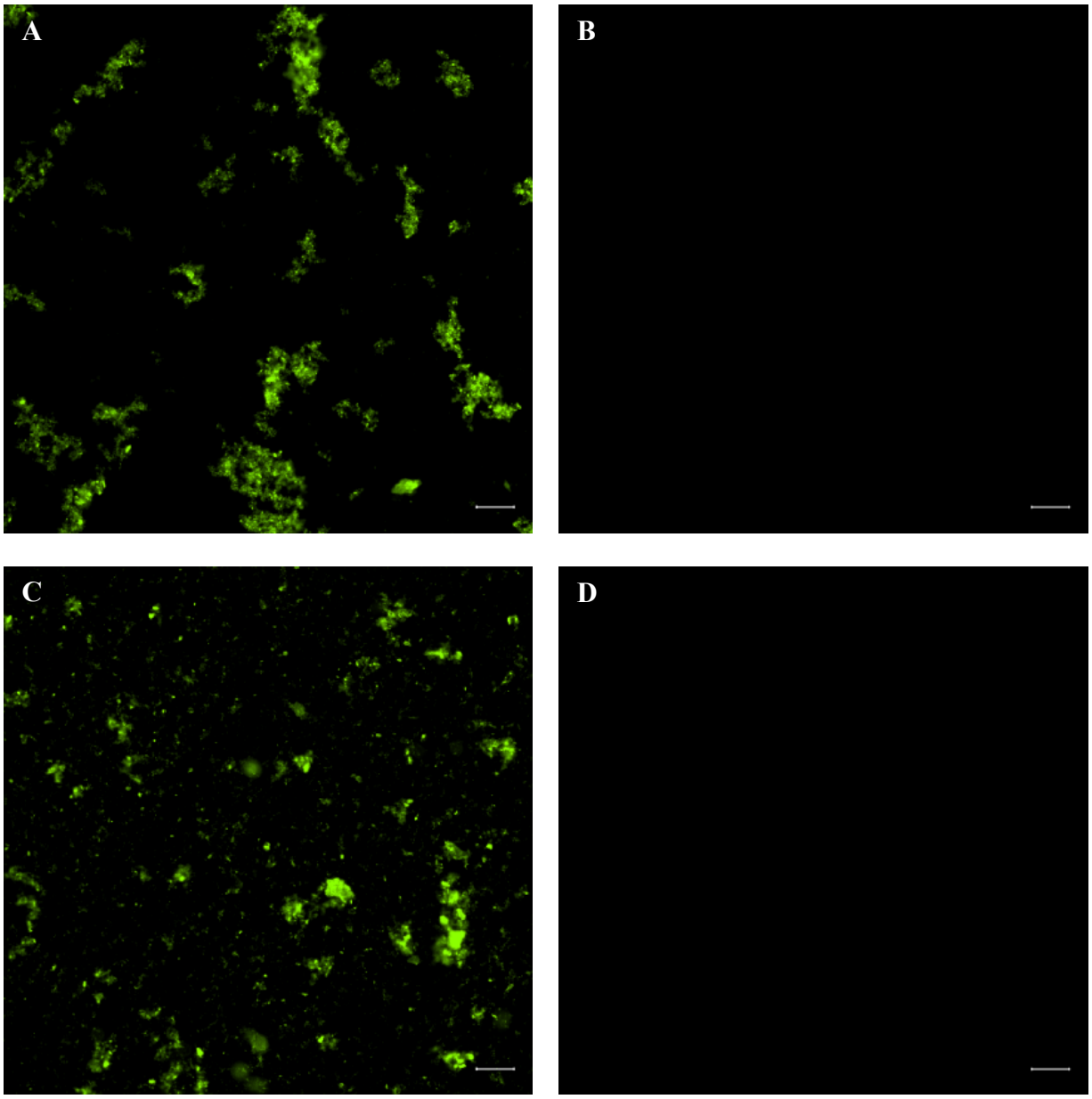

Supplementary Figure 3 – Trypan blue quenching of DAPI-stained polyP-based particles. DAPI-stained (green), as synthesized **(A)** Ca-polyP and **(B)** Ca-polyP with 0.1% trypan blue along with **(C)** Sr-polyP and **(D)** Sr-polyP with 0.1% trypan blue were imaged under fluorescent microscopy. Scale bar = 100 μm.

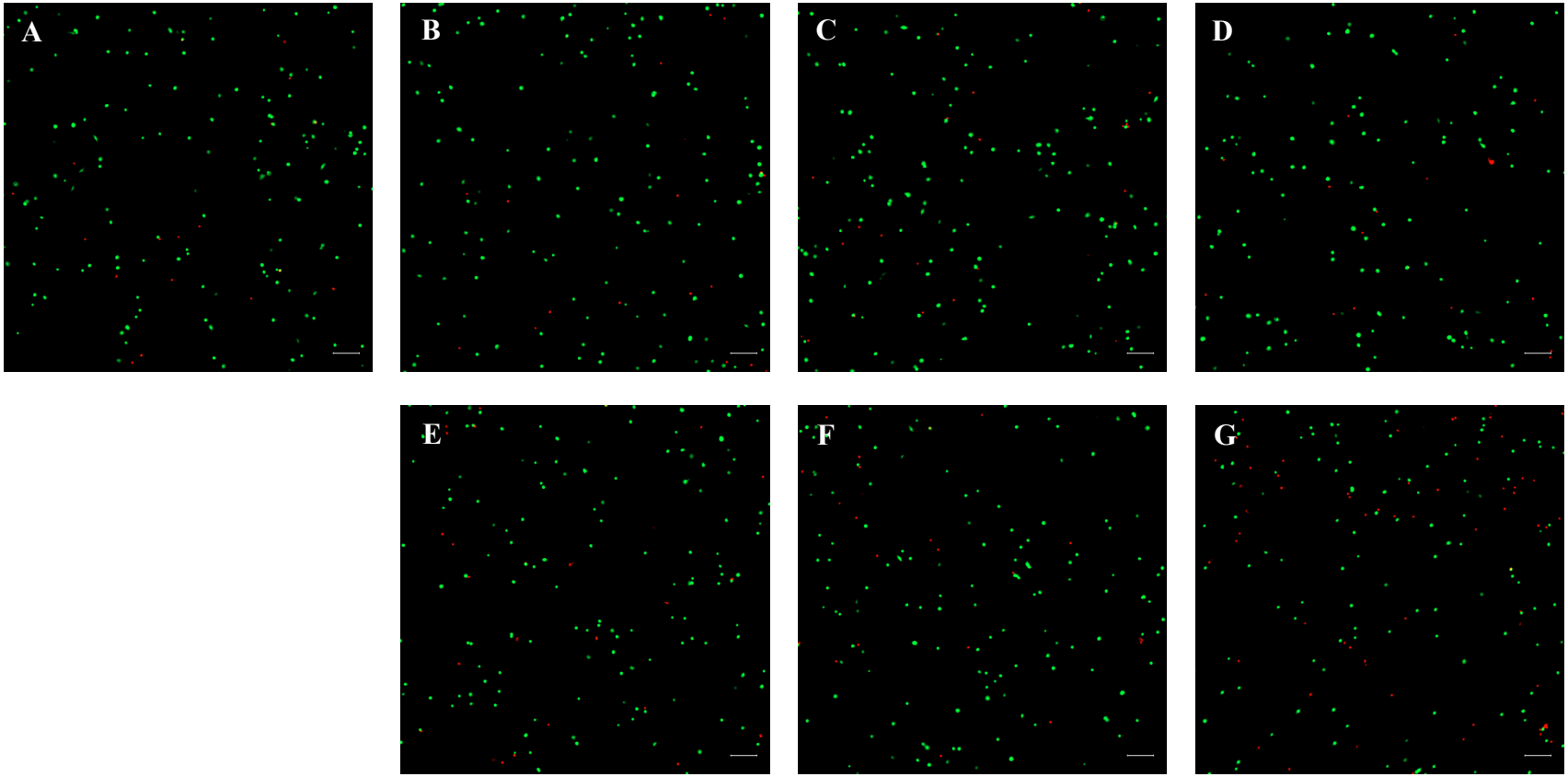

Supplementary Figure 4 – Representative images of live-dead assays on chondrocytes treated with Ca-polyP particles. Primary bovine chondrocytes were treated with **(A)** no particles as the control, Ca-polyP as synthesized at **(B)** 1 ng/cell, **(C)** 2 ng/cell, and **(D)** 4 ng/cell respectively, or sonicated Ca-polyP at a concentration of **(E)** 1 ng/cell, **(F)** 2 ng/cell, and **(G)** 4 ng/cell respectively for 24 hours. Chondrocytes were incubated with both calcein-AM and EthD-1 to stain live (green) and dead (red) cells respectively. Scale bar = 100 μm.

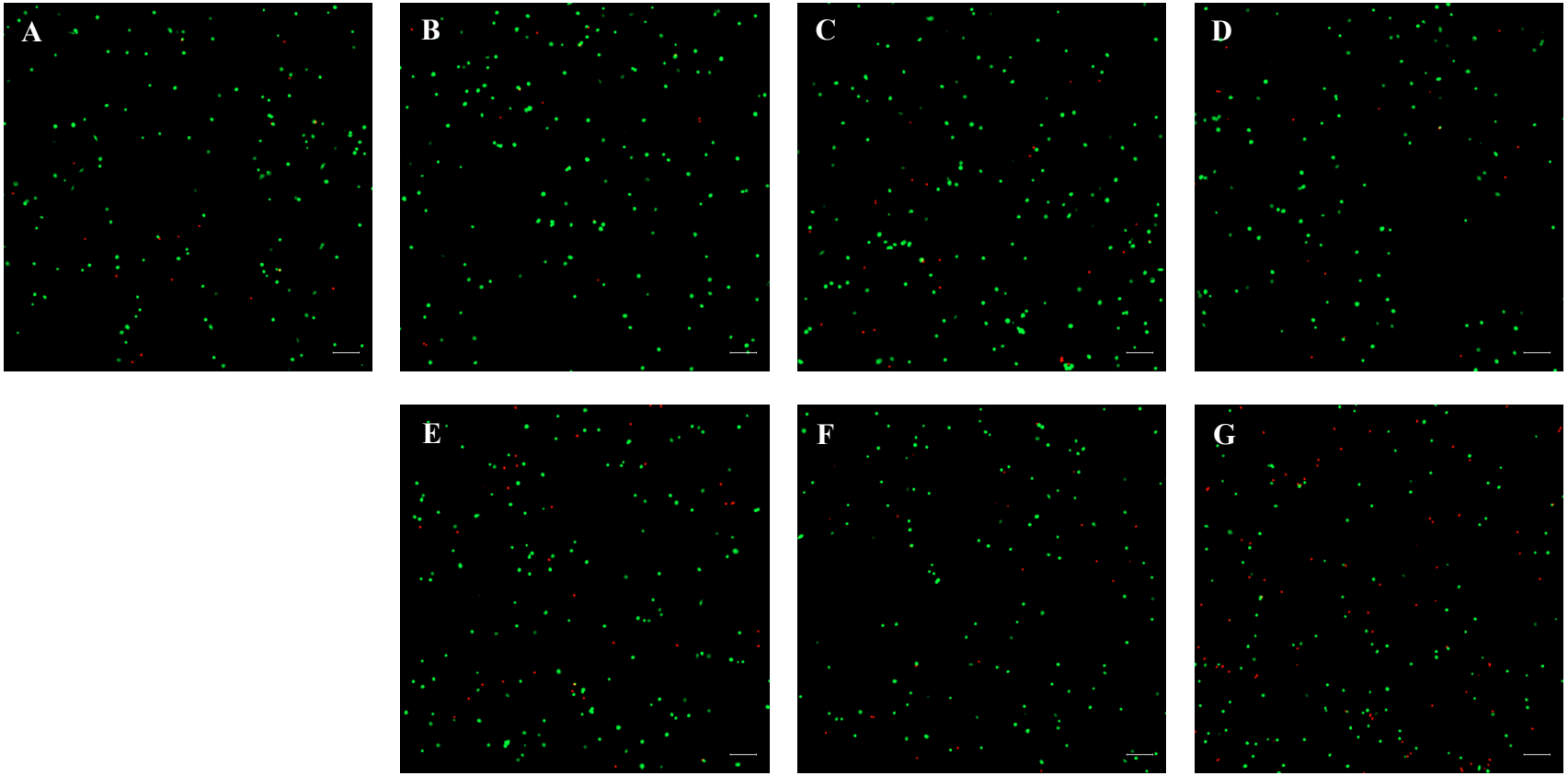

Supplementary Figure 5 – Representative images of live-dead assays on chondrocytes treated with Sr-polyP particles. Primary bovine chondrocytes were treated with **(A)** no particles as the control, Sr-polyP as synthesized at **(B)** 1 ng/cell, **(C)** 2 ng/cell, and **(D)** 4 ng/cell respectively, or sonicated Sr-polyP at a concentration of **(E)** 1 ng/cell, **(F)** 2 ng/cell, and **(G)** 4 ng/cell respectively for 24 hours. Chondrocytes were incubated with both calcein-AM and EthD-1 to stain live (green) and dead (red) cells respectively. Scale bar = 100 μm.

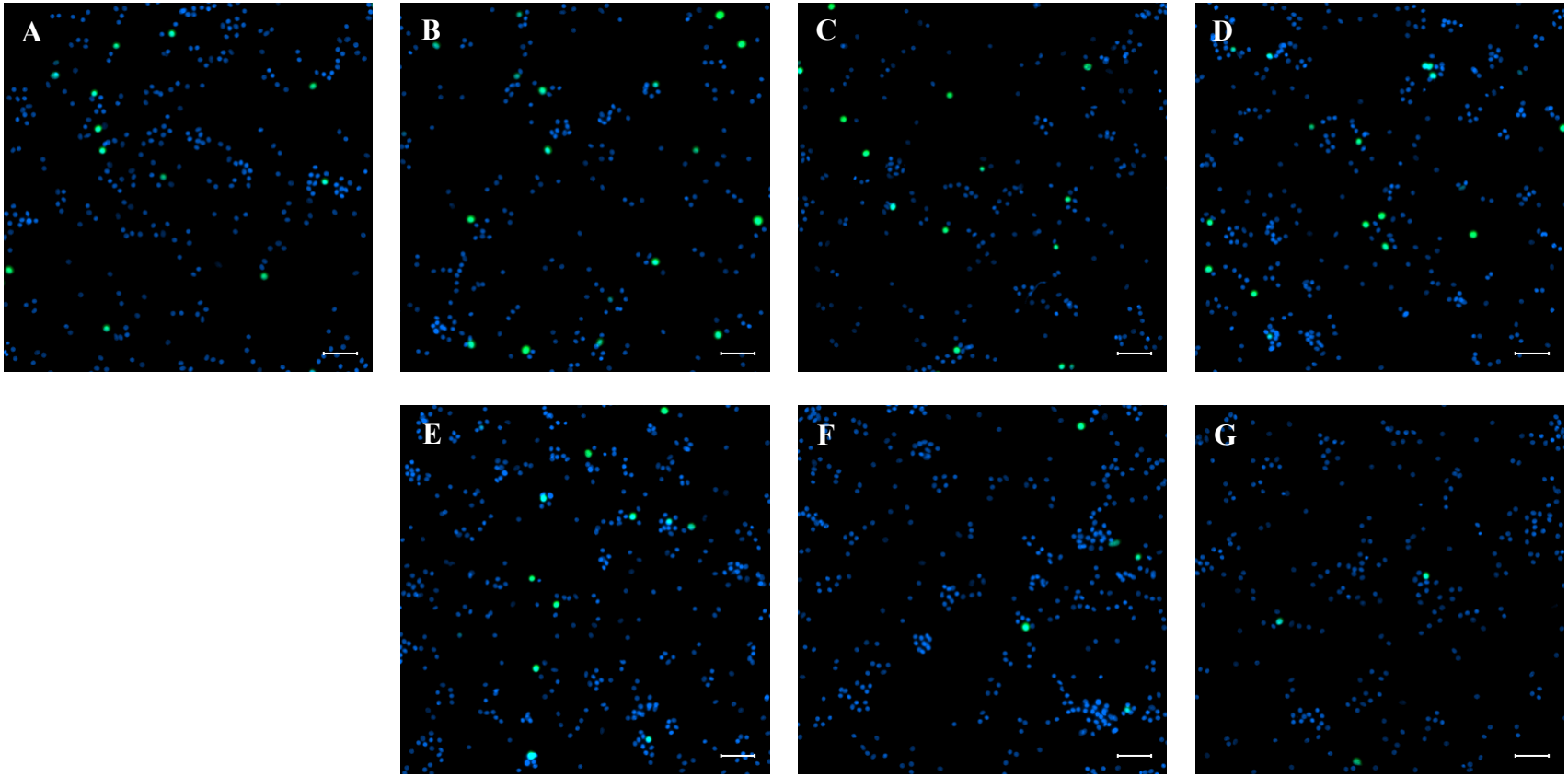

Supplementary Figure 6 – Representative images of EdU proliferation assays on chondrocytes treated with Ca-polyP. Primary bovine chondrocytes were treated with **(A)** no particles as the control, Ca-polyP as synthesized at a concentration of **(B)** 25 µg/mL, **(C)** 50 µg/mL, and **(D)** 100 µg/mL respectively, or sonicated Ca-polyP at a concentration of **(E)** 25 µg/mL, **(F)** 50 µg/mL, and **(G)** 100 µg/mL respectively for 24 hours. Proliferating cells were labelled with an Alexa Fluor 488 azide (green) and nuclei were stained with Hoechst 33342 (blue). Scale bar = 50 µm.

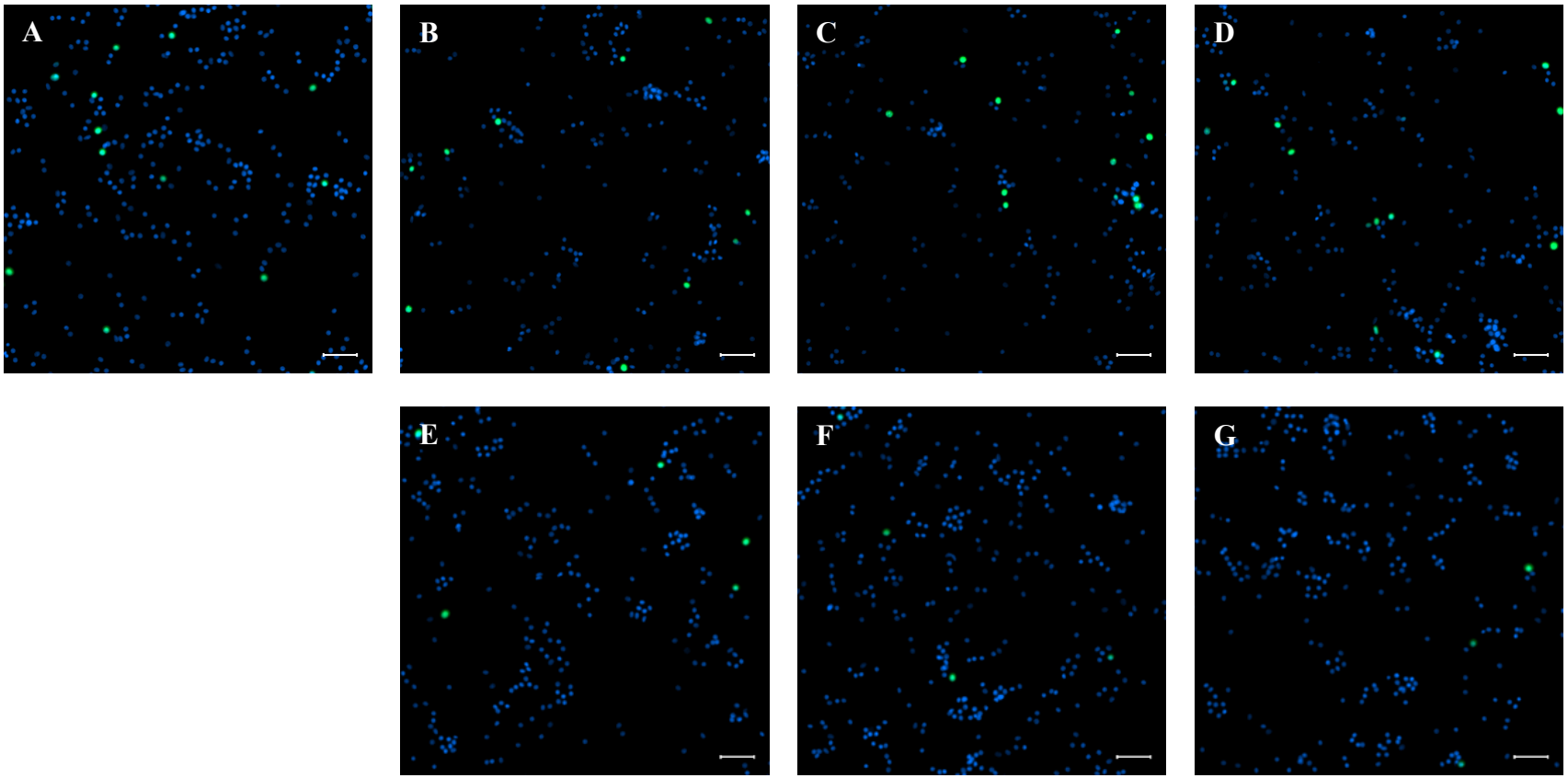

Supplementary Figure 7 – Representative images of EdU proliferation assays on chondrocytes treated with Sr-polyP. Primary bovine chondrocytes were treated with **(A)** no particles as the control, Sr-polyP as synthesized at a concentration of **(B)** 25 μg/mL, **(C)** 50 μg/mL, and **(D)** 100 μg/mL respectively, or sonicated Sr-polyP at a concentration of **(E)** 25 μg/mL, **(F)** 50 μg/mL, and **(G)** 100 μg/mL respectively for 24 hours. Proliferating cells were labelled with an Alexa Fluor 488 azide (green) and nuclei were stained with Hoechst 33342 (blue). Scale bar = 50 μm.

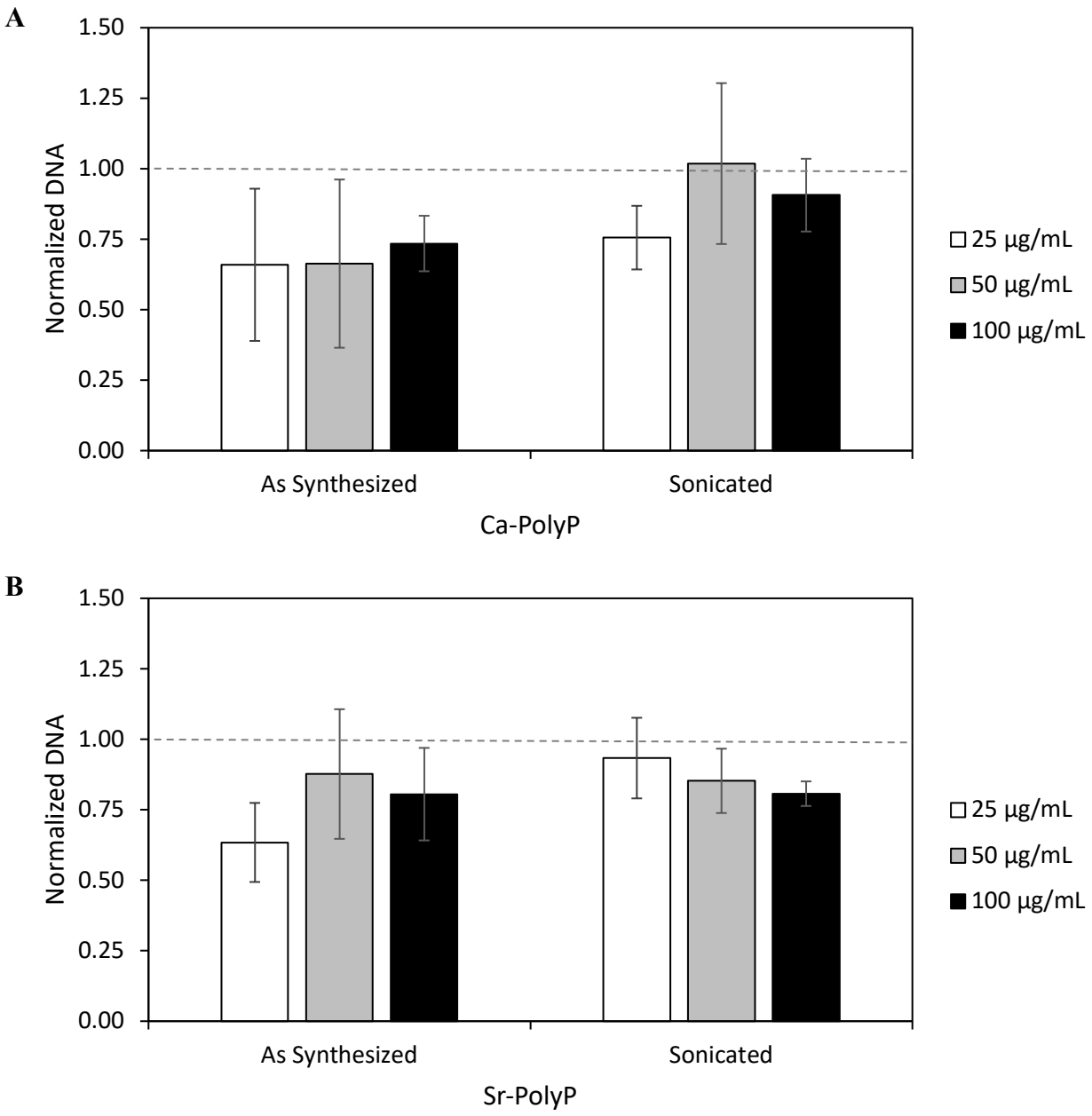

Supplementary Figure 8 – DNA content in response to incubation with polyP-based particles. Primary bovine chondrocytes were treated with **(A)** Ca-polyP and **(B)** Sr-polyP as synthesized or sonicated at varying concentrations for 24 hours. The cells were lysed and digested, and DNA was subsequently quantified from the cell digests. Values were normalized to the control samples cultured in the absence of particles, represented by the dotted lines. Data are presented as averages ± standard deviation for n = 3 biological replicates.

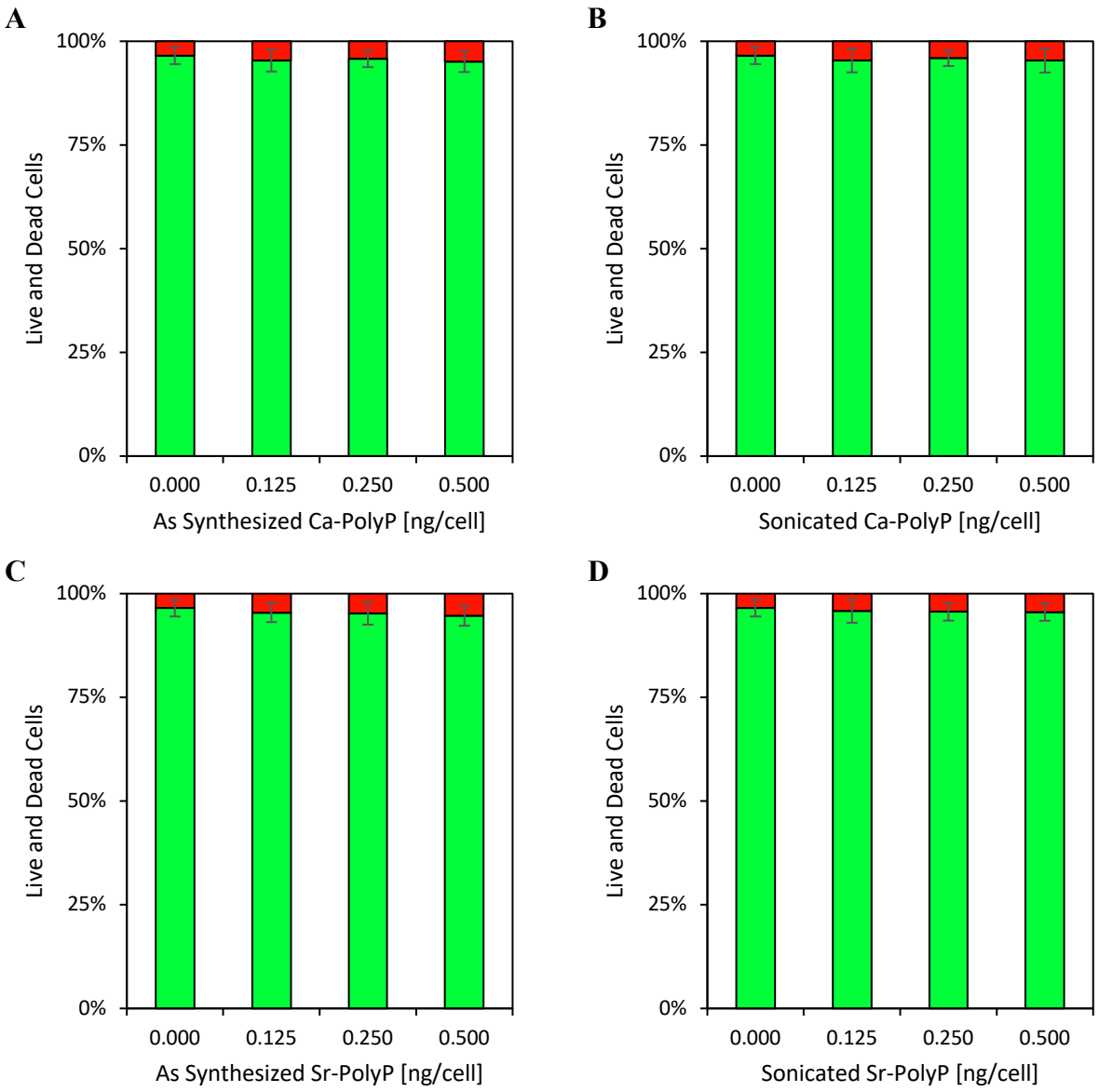

Supplementary Figure 9 – Live-dead assay under identical culture conditions of MTT and EdU assays. Primary bovine chondrocytes were treated with **(A)** Ca-polyP as synthesized or **(B)** sonicated and **(C)** Sr-polyP as synthesized or **(D)** sonicated at varying concentrations for 24 hours. Chondrocytes were incubated with calcein-AM (green) and EthD-1 (red) to stain live and dead cells respectively and imaged under fluorescent microscopy. Data are presented as averages ± standard deviation for n = 4 biological replicates.

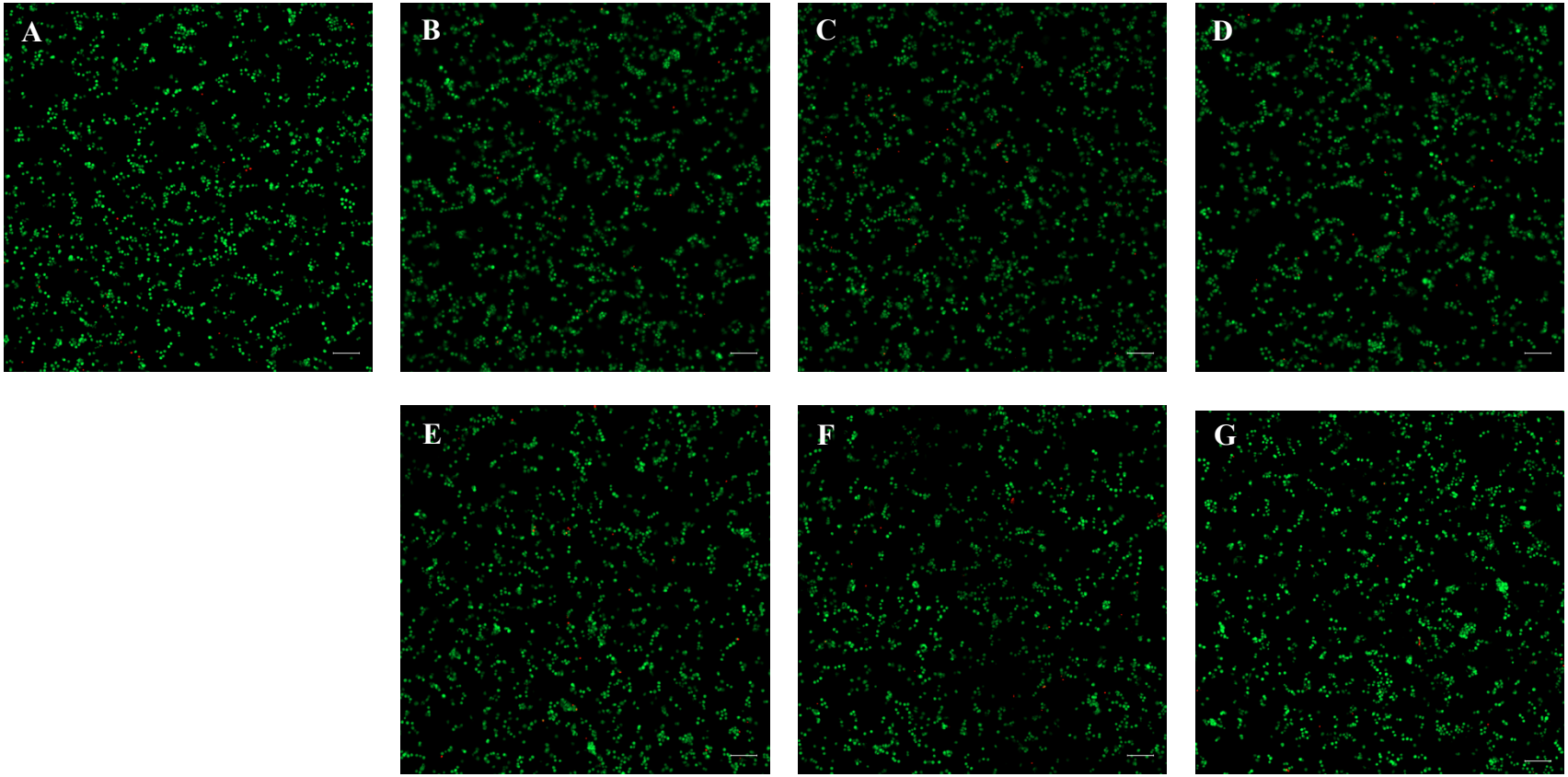

Supplementary Figure 10 – Representative images of live-dead assays on chondrocytes treated with Ca-polyP under identical culture conditions of MTT and EdU assays. Primary bovine chondrocytes were treated with **(A)** no particles as the control, Ca-polyP as synthesized at **(B)** 0.125 ng/cell, **(C)** 0.25 ng/cell, and **(D)** 0.5 ng/cell respectively, or sonicated Ca-polyP at a concentration of **(E)** 0.125 ng/cell, **(F)** 0.25 ng/cell, and **(G)** 0.5 ng/cell respectively for 24 hours. Chondrocytes were incubated with both calcein-AM and EthD-1 to stain live (green) and dead (red) cells respectively. Scale bar = 100 μm.

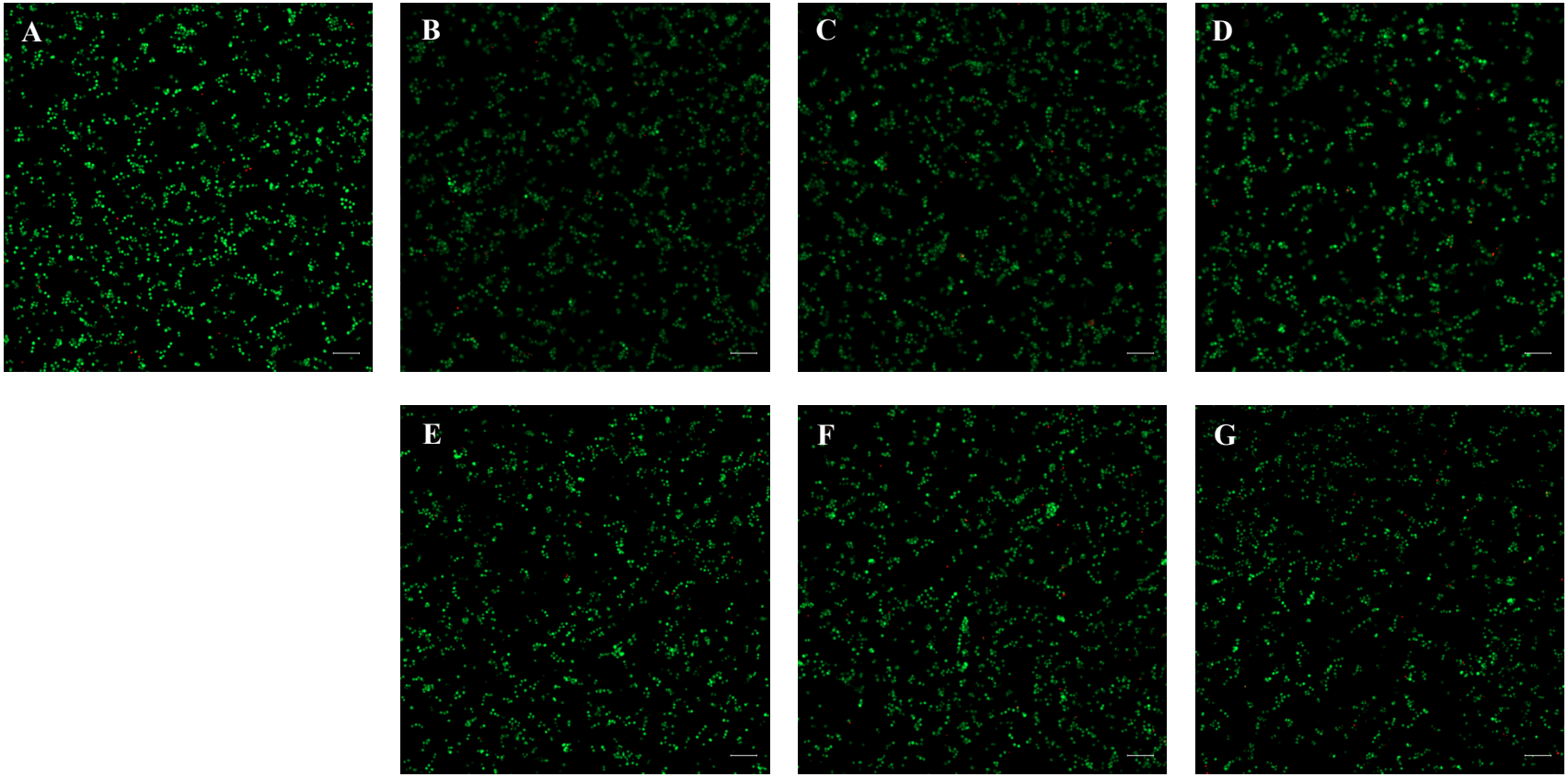

Supplementary Figure 11 – Representative images of live-dead assays on chondrocytes treated with Sr-polyP under identical culture conditions of MTT and EdU assays. Primary bovine chondrocytes were treated with **(A)** no particles as the control, Sr-polyP as synthesized at **(B)** 0.125 ng/cell, **(C)** 0.25 ng/cell, and **(D)** 0.5 ng/cell respectively, or sonicated Sr-polyP at a concentration of **(E)** 0.125 ng/cell, **(F)** 0.25 ng/cell, and **(G)** 0.5 ng/cell respectively for 24 hours. Chondrocytes were incubated with both calcein-AM and EthD-1 to stain live (green) and dead (red) cells respectively. Scale bar = 100 μm.

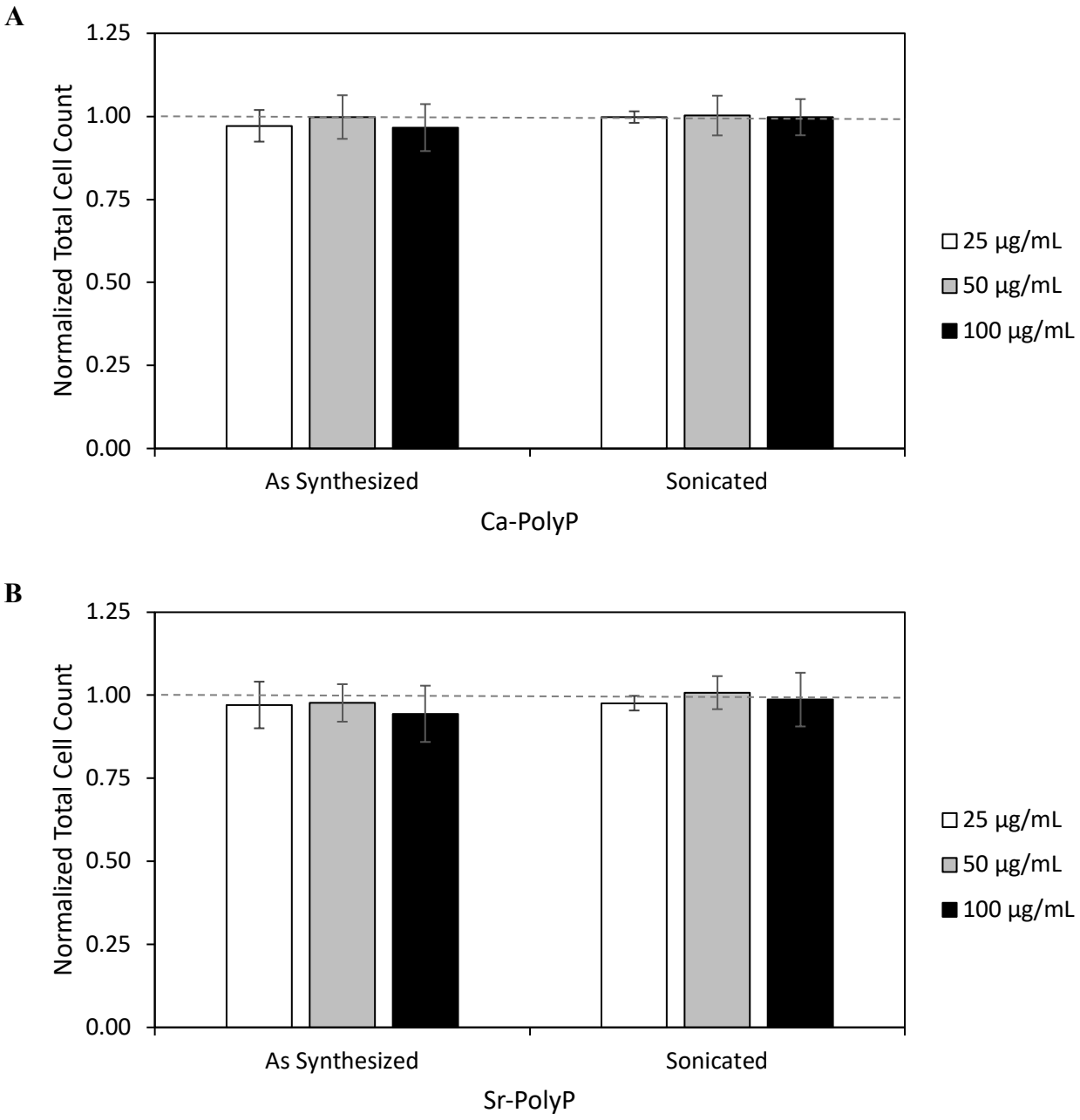

Supplementary Figure 12 – Total cells counts from EdU assays. Primary bovine chondrocytes were treated with **(A)** Ca-polyP and **(B)** Sr-polyP as synthesized or sonicated at varying concentrations for 24 hours. Cells were fixed and nuclei were stained with Hoechst 33342 (blue) and imaged under fluorescent microscopy. Values were normalized to the control samples cultured in the absence of particles, represented by the dotted lines. Data are presented as averages ± standard deviation for n = 4 biological replicates.

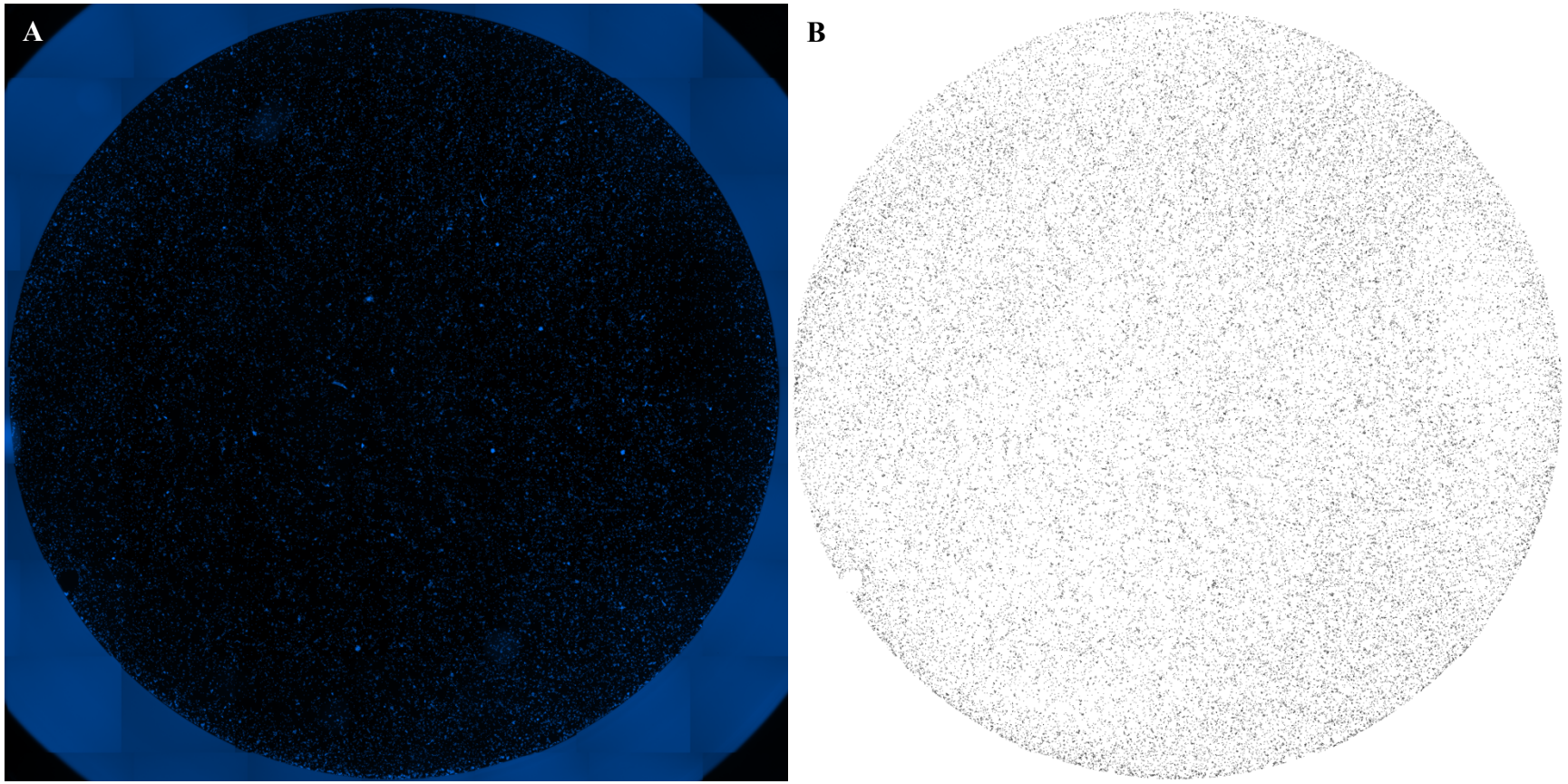

Supplementary Figure 13 – Representative whole-well image for total cell counting. (A) A whole-well image from the EdU assay, illustrating nuclei stained with Hoechst 33342 (blue). **(B)** Processed image utilized for cell counting, where nuclei are indicated as black dots.

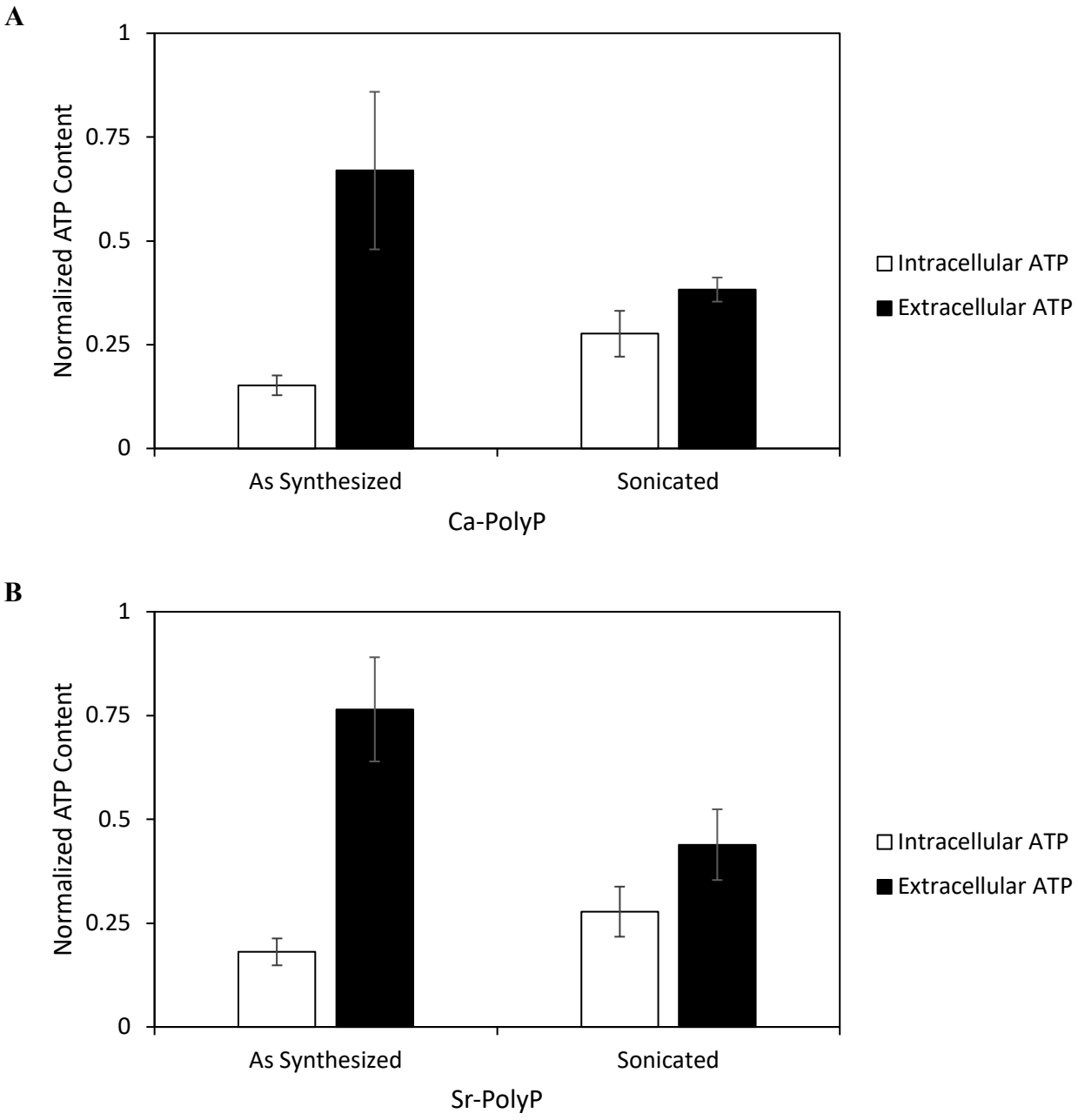

Supplementary Figure 14 – ATP levels in response to incubation with polyP-based particles. Primary bovine chondrocytes were treated with 100 μg/mL of **(A)** Ca-polyP and **(B)** Sr-polyP as synthesized or sonicated for 24 hours. Intracellular and extracellular ATP levels were assessed using the CellTiter-Glo 2.0 ATP assay, and values were normalized to the control samples cultured in the absence of particles. Data are presented as averages ± standard deviation for n = 3 biological replicates.

Supplementary Table 2 – Wet weights of cartilage tissue explants. Data are presented as averages of 19 – 25 cartilage tissue explants ± standard deviation.

Condition	Wet Weight [mg]
Control	21.6 ± 4.4
Ca-PolyP, As Synthesized	21.0 ± 3.2
Ca-PolyP, Sonicated	21.1 ± 3.9
Sr-PolyP, As Synthesized	21.3 ± 3.3
Sr-PolyP, Sonicated	20.8 ± 4.1
Total (n = 107)	21.2 ± 3.8

A.2 Copyright Permission

SPRINGER NATURE LICENSE TERMS AND CONDITIONS

Feb 07, 2023

This Agreement between University of Ottawa -- Jordan Nhan ("You") and Springer Nature ("Springer Nature") consists of your license details and the terms and conditions provided by Springer Nature and Copyright Clearance Center.

License Number	5483780616420
License date	Feb 07, 2023
Licensed Content Publisher	Springer Nature
Licensed Content Publication	Nature Reviews Rheumatology
Licensed Content Title	Repair and tissue engineering techniques for articular cartilage
Licensed Content Author	Eleftherios A. Makris et al
Licensed Content Date	Sep 23, 2014
Type of Use	Thesis/Dissertation
Requestor type	academic/university or research institute
Format	electronic
Portion	figures/tables/illustrations
Number of figures/tables/illustrations	1
High-res required	no
Will you be translating?	no
Circulation/distribution	1 - 29
Author of this Springer Nature content	no
Title	Development of Inorganic Polyphosphate-Based Nanoparticles for Drug Delivery into Articular Cartilage
Institution name	University of Ottawa
Expected presentation date	Apr 2023
Portions	Figure 1

ELSEVIER LICENSE TERMS AND CONDITIONS

Feb 07, 2023

This Agreement between University of Ottawa -- Jordan Nhan ("You") and Elsevier ("Elsevier") consists of your license details and the terms and conditions provided by Elsevier and Copyright Clearance Center.

License Number	5483780800061
License date	Feb 07, 2023
Licensed Content Publisher	Elsevier
Licensed Content Publication	The Lancet
Licensed Content Title	Osteoarthritis
Licensed Content Author	David J Hunter,Sita Bierma-Zeinstra
Licensed Content Date	27 April–3 May 2019
Licensed Content Volume	393
Licensed Content Issue	10182
Licensed Content Pages	15
Start Page	1745
End Page	1759
Type of Use	reuse in a thesis/dissertation
Portion	figures/tables/illustrations
Number of figures/tables/illustrations	1
Format	electronic
Are you the author of this Elsevier article?	No
Will you be translating?	No
Title	Development of Inorganic Polyphosphate-Based Nanoparticles for Drug Delivery into Articular Cartilage
Institution name	University of Ottawa
Expected presentation date	Apr 2023
Portions	Figure 2

SPRINGER NATURE LICENSE TERMS AND CONDITIONS

Feb 07, 2023

This Agreement between University of Ottawa -- Jordan Nhan ("You") and Springer Nature ("Springer Nature") consists of your license details and the terms and conditions provided by Springer Nature and Copyright Clearance Center.

License Number	5483780105949
License date	Feb 07, 2023
Licensed Content Publisher	Springer Nature
Licensed Content Publication	Nature Reviews Rheumatology
Licensed Content Title	Molecular transport in articular cartilage — what have we learned from the past 50 years?
Licensed Content Author	Chris D. DiDomenico et al
Licensed Content Date	Jun 13, 2018
Type of Use	Thesis/Dissertation
Requestor type	academic/university or research institute
Format	electronic
Portion	figures/tables/illustrations
Number of figures/tables/illustrations	2
High-res required	no
Will you be translating?	no
Circulation/distribution	1 - 29
Author of this Springer Nature content	no
Title	Development of Inorganic Polyphosphate-Based Nanoparticles for Drug Delivery into Articular Cartilage
Institution name	University of Ottawa
Expected presentation date	Apr 2023
Portions	Fig. 1, Fig. 3